

UNCLASSIFIED

AD NUMBER

ADB015785

LIMITATION CHANGES

TO:

Approved for public release; distribution is unlimited.

FROM:

Distribution authorized to U.S. Gov't. agencies only; Test and Evaluation; DEC 1975. Other requests shall be referred to Air Force Avionics Laboratory, AFAL/DHO, Wright-Patterson AFB, OH 45433.

AUTHORITY

afal ltr, 12 sep 1977

THIS PAGE IS UNCLASSIFIED

THIS REPORT HAS BEEN DELIMITED
AND CLEARED FOR PUBLIC RELEASE
UNDER DOD DIRECTIVE 5200.20 AND
NO RESTRICTIONS ARE IMPOSED UPON
ITS USE AND DISCLOSURE,

DISTRIBUTION STATEMENT A

APPROVED FOR PUBLIC RELEASE;
DISTRIBUTION UNLIMITED.

AFAL-TR-75-123

PK2

C.W. GaAs DIODE LASER

TEXAS INSTRUMENTS INCORPORATED
P.O. BOX 5012
DALLAS, TEXAS 75222

DECEMBER 1975

AD No. —
DDC FILE COPY



DDC
RECEIVED
DEC 28 1976
A

TECHNICAL REPORT AFAL-TR-75-123

FINAL REPORT FOR PERIOD 1 DECEMBER 1973 — 2 DECEMBER 1974

Distribution limited to U.S. Government agencies only; test and evaluation results reported; July 1975. Other requests for this document must be referred to the Air Force Avionics Laboratory (AFAL/DHO), Wright-Patterson AFB, Ohio 45433.

AIR FORCE AVIONICS LABORATORY
AIR FORCE WRIGHT AERONAUTICAL LABORATORIES
Air Force Systems Command
Wright-Patterson Air Force Base, Ohio 45433

NOTICE

When Government drawings, specifications, or other data are used for any purpose other than in connection with a definitely related Government procurement operation, the United States Government thereby incurs no responsibility nor any obligation whatsoever; and the fact that the government may have formulated, furnished, or in any way supplied the said drawings, specifications, or other data, is not to be regarded by implication or otherwise as in any manner licensing the holder or any other person or corporation, or conveying any rights or permission to manufacture, use, or sell any patented invention that may in any way be related thereto.

This technical report has been reviewed and is approved for publication.

| | |
|---------------------------------|--|
| ACCESSION NO. | |
| RTS | DTIC Series <input type="checkbox"/> |
| DDC | DDC Series <input checked="" type="checkbox"/> |
| UNANNOUNCED | |
| JUSTIFICATION | |
| BY..... | |
| DISTRIBUTION/AVAILABILITY CODES | |
| Dist. | AVAIL. and/or SPECIAL |
| B | |

Richard L. Remski

Richard L. Remski
Project Engineer

Stanley E. Wagner

Stanley E. Wagner, Chief
Electro-Optics Technology Branch

Copies of this report should not be returned unless return is required by security considerations, contractual obligations, or notice on a specific document.

UNCLASSIFIED

SECURITY CLASSIFICATION OF THIS PAGE (When Data Entered)

| 19 REPORT DOCUMENTATION PAGE | | READ INSTRUCTIONS BEFORE COMPLETING FORM | |
|---|---|--|--------------------------|
| 18 REPORT NUMBER AFAL TR-75-123 | 2 GOVT ACCESSION NO. | 3 RECIPIENT'S CATALOG NUMBER | |
| 4 TITLE (and Subtitle) CW GaAs DIODE LASER | 5 TYPE OF REPORT & PERIOD COVERED Final rept. 1 December 1973 - 2 December 1974 | 6 PERFORMING ORG. REPORT NUMBER TI-83-75-26 | |
| 7 AUTHOR(s) Eugene G. Dierschke | 8 CONTRACT OR GRANT NUMBER(s) F33615-74-C-1006 | 9 PROGRAM ELEMENT, PROJECT, TASK AREA & WORK UNIT NUMBERS Proj. No. 2881 62204F Task No. 01 Work unit 11 | |
| 9. PERFORMING ORGANIZATION NAME AND ADDRESS Texas Instruments Incorporated P.O. Box 5012 Dallas, Texas 75222 | 10 CONTROLLING OFFICE NAME AND ADDRESS Air Force Avionics Laboratory Air Force Systems Command Wright-Patterson Air Force Base, Ohio 45433 | 11 REPORT DATE December 1975 | 12 NUMBER OF PAGES 93 |
| 14 MONITORING AGENCY NAME & ADDRESS (if different from Controlling Office) 12 97p. | 15 SECURITY CLASS. (of this report) Unclassified | 15a. DECLASSIFICATION/DOWNGRADING SCHEDULE | |
| 16. DISTRIBUTION STATEMENT (of this Report) Distribution limited to U.S. Government agencies only; test and evaluation results reported; July 1975. Other requests for this document must be referred to the Air Force Avionics Laboratory (AFAL/DHO), Wright-Patterson AFB, Ohio 45433. | | | |
| 17. DISTRIBUTION STATEMENT (of the abstract entered in Block 20, if different from Report) | | | |
| 18. SUPPLEMENTARY NOTES | | | |
| 19. KEY WORDS (Continue on reverse side if necessary and identify by block number) Semiconductor Lasers Beryllium Oxide Gallium Arsenide Liquid-Phase Epitaxy Gallium Aluminum Arsenide Vapor-Phase Epitaxy | | | |
| 20. ABSTRACT (Continue on reverse side if necessary and identify by block number) Techniques for improving the performance of CW laser diodes at 780 nm were investigated. Work concentrated on the single heterostructure laser. The liquid-phase epitaxial growth procedure, the doping concentrations, and the active recombination region thickness were optimized to achieve low threshold currents, high slope efficiencies, and narrow emission beams. A double-sided copper heat sink design incorporating intermediate submounts was used. The submounts were used for improved control during mounting of the laser and to reduce thermal | | | |

DD FORM 1 JAN 73 1473 EDITION OF 1 NOV 65 IS OBSOLETE

UNCLASSIFIED

SECURITY CLASSIFICATION OF THIS PAGE (When Data Entered)

407454-
LB

cont

UNCLASSIFIED

SECURITY CLASSIFICATION OF THIS PAGE (When Data Entered)

20. resistance by use of high thermal conductivity materials. A suitable assembly process was established after the solution of various problems.

X The highest CW optical output power achieved was 690 milliwatts at 3A with a 13% power efficiency. This was obtained using a double-sided heat sink incorporating rectangular copper submounts. The best thermal characteristics were achieved with a double-sided heat sink incorporating single-crystal BeO submounts.

A theoretical analysis of the single heterostructure laser mounted in a double-sided heat sink was performed. The results of the theoretical analysis and the experimental results indicate that further optimization of this approach should result in CW output powers of greater than 2 W for copper submounts and greater than 4 W for single-crystal BeO submounts.

A minor portion of the program was devoted to investigating the feasibility of an integral GaAs laser diode - BeO heat sink design in which the laser structure is grown directly on a single-crystal BeO substrate. The potential advantage is decreased thermal resistance for the laser. The optimum conditions for the growth of uniform single heterostructure epitaxial layers were established. However, the material does not appear to be of sufficiently good quality to achieve high-performance lasers.

↑

UNCLASSIFIED

SECURITY CLASSIFICATION OF THIS PAGE (When Data Entered)

FOREWORD

This document constitutes the Final Technical Report under Air Force Contract No. F33615-74-C-1006, "C. W. GaAs Diode Laser." The project number was 2001, task number 01. The contract was sponsored by Air Force Avionics Laboratory, Air Force Systems Command, Air Force Wright Aeronautical Laboratory, United States Air Force, Wright-Patterson Air Force Base, Ohio. The Air Force program monitor was Mr. Richard L. Remski (AFAL/TEO-1).

The investigation was conducted between December 1, 1973 and December 2, 1974 by the Semiconductor Group, Texas Instruments Incorporated, Dallas, Texas. The program manager was Dr. Eugene G. Dierschke. The other principal contributors and their areas of responsibility were Mr. David M. Blacknall, liquid-phase epitaxial materials growth, and Mr. Ronald L. Carroll, laser fabrication, assembly, and evaluation. The principal personnel responsible for the BeO materials effort at Rockwell International were Dr. Ralph P. Ruth and Mr. S. B. Austerman.

This technical report was submitted by the author May 20, 1975 and has been assigned Texas Instruments Report No. 03-75-26.

TABLE OF CONTENTS

| <i>Section</i> | <i>Title</i> | <i>Page</i> |
|----------------|--|-------------|
| I. | INTRODUCTION | 1 |
| II. | MATERIAL AND DEVICE TECHNOLOGY | 3 |
| | 1. INTRODUCTION | 3 |
| | 2. SINGLE HETEROSTRUCTURE LASERS | 4 |
| | 3. LIQUID-PHASE EPITAXIAL GROWTH. | 4 |
| | 4. DEVICE FABRICATION AND EVALUATION | 10 |
| | 5. ROOM TEMPERATURE LASER CHARACTERISTICS. | 11 |
| III. | HEAT SINK ASSEMBLY TECHNOLOGY | 15 |
| | 1. INTRODUCTION | 15 |
| | 2. LASER HEAT SINK DESIGN. | 15 |
| | 3. HEAT SINK ASSEMBLY PROCEDURE. | 21 |
| | 4. LIQUID NITROGEN DEWAR | 23 |
| | 5. SINGLE-CRYSTAL BeO SUBMOUNTS | 28 |
| IV. | CW LASER DIODE CHARACTERISTICS | 33 |
| | 1. EVALUATION PROCEDURE | 33 |
| | 2. CHARACTERISTICS OF DELIVERED CW LASER DIODES | 34 |
| | 3. HEAT SINKS WITH BeO SUBMOUNTS. | 38 |
| V. | THEORETICAL ANALYSIS | 45 |
| | 1. INTRODUCTION | 45 |
| | 2. DOUBLE-SIDED HEAT SINK DESIGN | 46 |
| | 3. THERMAL RESISTANCE ANALYSIS | 48 |
| | 4. CW LASER OPERATION | 54 |
| | 5. COMPARISON OF SUBMOUNT DESIGNS | 58 |
| | 6. LENGTH DEPENDENCE OF CHARACTERISTICS | 62 |
| VI. | INTEGRAL GaAs LASER DIODE - BeO HEAT SINK DESIGN | 71 |
| | 1. INTRODUCTION | 71 |
| | 2. GaAs METALORGANIC-CVD GROWTH PROCESS | 73 |
| | 3. PREPARATION OF GaAs/BeO COMPOSITE SAMPLES | 75 |
| | 4. LIQUID-PHASE EPITAXIAL GROWTH. | 83 |
| | 5. SUMMARY | 85 |
| VII. | SUMMARY AND CONCLUSIONS | 87 |

LIST OF ILLUSTRATIONS

| <i>Figure</i> | <i>Title</i> | <i>Page</i> |
|---------------|--|-------------|
| 1. | Zinc-Diffused Single Heterostructure Laser Diode | 5 |
| 2. | Cross Section of Single Heterostructure Laser Diode | 5 |
| 3. | Sliding-Boat Solution Growth System | 6 |
| 4. | Solubility of GaAs versus Al Concentration in a Ga-Al Melt | 8 |
| 5. | Radiation Pattern Perpendicular to Junction Plane | 13 |
| 6. | Final Double-Sided Laser Heat Sink Design (Type II) | 16 |
| 7. | Assembled Double-Sided Heat Sink (Type II) | 17 |
| 8. | Cross Section of Stripline | 18 |
| 9. | Initial Double-Sided Heat Sink Design (Type I) | 19 |
| 10. | Assembled Double-Sided Heat Sink (Type I) | 20 |
| 11. | Liquid Nitrogen Dewar Design | 24 |
| 12. | Heat-Transfer Rate versus Temperature Difference Across Liquid-Nitrogen/Metal Interface | 25 |
| 13. | Assembled Liquid Nitrogen Dewar | 26 |
| 14. | Liquid-Nitrogen Dewar with Bottom Portion Removed | 27 |
| 15. | Metallization Patterns on BeO Heat Sinks | 31 |
| 16. | Metallized BeO Heat Sink | 32 |
| 17. | Wavelength Increase versus Temperature for GaAs Lasers | 34 |
| 18. | CW Characteristics of Single Heterostructure Lasers | 37 |
| 19. | CW Power Efficiency versus DC Diode Current | 38 |
| 20. | Lasing Wavelength versus DC Diode Current | 39 |
| 21. | Junction Temperature Increase versus DC Electrical Input Power | 40 |
| 22. | CW Characteristics of Single Heterostructure Lasers | 41 |
| 23. | Lasing Wavelength versus DC Diode Current | 42 |
| 24. | Lasing Wavelength versus DC Diode Current (Diode 279-1, No. 2) | 43 |
| 25. | Double-Sided Heat Sink Design | 47 |
| 26. | Thermal Conductivity as a Function of Temperature | 49 |
| 27. | Thermal Resistance as a Function of Temperature | 51 |
| 28. | Junction Temperature as a Function of Input Power | 52 |
| 29. | Wavelength Increase versus DC Diode Current | 53 |
| 30. | Temperature Dependence of Laser Optical Properties | 56 |
| 31. | Temperature Dependence of Threshold Conditions | 57 |
| 32. | Threshold Current versus Temperature for Single Heterostructure Lasers | 59 |

LIST OF ILLUSTRATIONS (Continued)

| <i>Figure</i> | <i>Title</i> | <i>Page</i> |
|---------------|--|-------------|
| 33. | Slope Efficiency versus Temperature for Single Heterostructure Lasers | 60 |
| 34. | Calculated CW Output Power versus Current for Single Heterostructure Lasers with Diamond Heat Sinks | 61 |
| 35. | Calculated CW Power Efficiency versus Current for Single Heterostructure Lasers with Diamond Heat Sinks | 62 |
| 36. | Calculated CW Output Power versus Current for Single Heterostructure Lasers Mounted Directly on Copper | 63 |
| 37. | Dependence on Thermal Resistance of Direct Current to Yield 150°K Junction Temperature | 64 |
| 38. | Calculated CW Output Power versus Thermal Resistance for Junction Temperature of 150°K | 64 |
| 39. | Calculated Threshold Current Density versus Length for Single Heterostructure Laser | 66 |
| 40. | Calculated Threshold Current versus Length for Single Heterostructure Laser | 67 |
| 41. | Calculated Slope Efficiency versus Length for Single Heterostructure Laser | 68 |
| 42. | Comparison of Optical Parameters at 300°K and 77°K | 69 |
| 43. | Integral GaAs Laser Diode-Heat Sink Design | 72 |
| 44. | Processing Steps for Integral Laser-Heat Sink Design | 73 |
| 45. | Expected and Observed Orientation Relationships Along (112X) Zone | 78 |
| 46. | Additional Observed Orientation Relationships for GaAs/BeO | 79 |
| 47. | Polished GaAs-BeO Composite Substrate (GaAs#9-20-A-4/BeO#AN262-1~(1122)-4) | 81 |
| 48. | Cross Section of Liquid-Phase Epitaxial Layers on GaAs-BeO Composite Substrates | 85 |

LIST OF TABLES

| <i>Table</i> | <i>Title</i> | <i>Page</i> |
|--------------|---|-------------|
| I. | Typical Compositions of Melts | 7 |
| II. | Optical, Electrical, and Thermal Characteristics of Delivered CW Laser Diodes | 35 |
| III. | Thermal Characteristics of Components of Mounted Laser Diode at 77° K | 50 |
| IV. | Thermal Resistance of Various Heat Sink Configurations at 150° K | 65 |
| V. | Calculated CW Output Power of Various Heat Sink Configurations at 150° K | 65 |
| VI. | Properties of First Group of GaAs/BeO Composite Samples | 77 |
| VII. | Properties of GaAs Films Grown by Metal-organic CVD on BeO Substrates | 80 |
| VIII. | Properties of Second Group of GaAs/BeO Composite Samples Delivered to TI | 82 |

SECTION I

INTRODUCTION

The objective of this program was to investigate techniques to improve the performance of CW laser diodes. The goal was to achieve 4-watt, 0.012-inch wide CW GaAs laser diodes at 77° K. The overall program effort consisted of three principal areas.

The first area was the optimization of the semiconductor growth and laser fabrication techniques to achieve lasers with low threshold currents and high slope efficiencies. Previous work on 77° K CW lasers concentrated on diffused homostructure lasers.¹ In this program, work concentrated on single heterostructure lasers because of the smaller temperature dependence of the threshold current and slope efficiency as compared to diffused homostructure lasers. Details of the material and device technology for single heterostructure lasers are described in Section II.

The second major effort was the design, assembly, and evaluation of the dewar and the laser package for efficient heat-sinking. The primary factor limiting the CW output power of injection lasers is removal of heat from the junction area. With increasing temperature, the thermal conductivities of the laser and heat-sink materials decrease, the laser's threshold current increases, and the laser's slope efficiency decreases. The combined effect of these factors is to quench the CW laser operation at high diode currents, due to heating. The primary double-sided heat-sink materials which were investigated were copper and single-crystal BeO. Details of the heat-sinking designs are described in Section III. The testing procedure and evaluation results for CW laser diodes are described in Section IV.

A theoretical analysis of the effect of various design parameters on the expected CW laser performance is given in Section V. The results of these calculations were used to guide the laser-diode and heat-sink designs.

The third area of activity was the evaluation of an integral laser — heat-sink design in which the P-N junction is formed in GaAs epitaxial material grown directly on single-crystal BeO substrates. The potential advantage of this design is that the heat can spread over a larger area before any high thermal resistance interfaces are reached. The details of this approach are described in Section VI.

SECTION II

MATERIAL AND DEVICE TECHNOLOGY

1. INTRODUCTION

The GaAs single heterostructure laser was used for this program. Threshold current and slope efficiency are much less temperature dependent for the single heterostructure laser than for the conventional zinc-diffused homostructure.²⁻¹⁰ At 77°K, the performance of both types of lasers is approximately equal. The temperature dependence of the characteristics is important because the primary limit in CW laser diode performance is junction heating.

Two other types of lasers which also have a relatively small temperature dependence were not used for the following reasons. Low-power CW laser operation at room temperature has been achieved with double heterostructure lasers.¹¹⁻¹⁴ Low room-temperature threshold current densities are achieved by using a narrow GaAs active layer width. This results in increased beam divergence, reduced threshold for catastrophic degradation, and increased epitaxial growth difficulties. Since the requirement for this program was high-power, narrow-beam-angle lasers, the double heterostructure laser offers no advantage over the single heterostructure laser. For equivalent active region widths ($\approx 2 \mu\text{m}$), the single heterostructure and double heterostructure lasers have essentially identical threshold current densities and temperature variations below 200°K.¹⁴

The conventional large-optical-cavity laser¹⁵⁻¹⁸ was not used because of its wide emission beam angle. This results because of the higher order optical modes which are present due to the asymmetrical structure of the conventional large-optical-cavity laser. This type of laser is usually designed with very wide cavity widths to achieve large peak power densities. Since catastrophic degradation is not a limitation and since narrow beam angles are required, the conventional large-optical-cavity laser offers no advantage over the single heterostructure laser for this application.

An important aspect of the program was the development of the material and device technology for the fabrication of single heterostructure lasers with low threshold currents and high slope efficiencies. The details of this activity are discussed in this section.

2. SINGLE HETEROSTRUCTURE LASERS

The principal materials activity concentrated on the growth of the single heterostructure laser structure shown schematically in Figure 1(a). The structure requires the growth of three liquid-phase epitaxial layers. The first layer is heavily doped N-type GaAs grown on an N-type GaAs substrate. The second layer is heavily doped P-type GaAlAs. The third layer is heavily doped P-type GaAs for achieving good contacts with a low specific contact resistance. This is common practice for most heterostructure lasers. The P-N junction is formed by zinc out-diffusion from the GaAlAs P-type layer into the GaAs N-type layer. Typical thicknesses for the N-type GaAs, P-type GaAlAs, and P-type GaAs epitaxial layers are 6 to 8 μm , 2 to 3 μm , and 3 to 6 μm , respectively. The zinc out-diffusion into the N-type GaAs layer is typically 1.7 to 2.0 μm . A photograph of an angle-lapped cross section of a grown single heterostructure laser is shown in Figure 2.

The bandgap energy profile of the single heterostructure laser is shown in Figure 1(b). The index of refraction at the laser emission wavelength ($\approx 9030 \text{ \AA}$ at 300°K and $\approx 8530 \text{ \AA}$ at 77°K) decreases with increasing bandgap energy. The composition of the P-type GaAlAs layer is generally maintained at $\text{Ga}_{0.77}\text{Al}_{0.23}\text{As}$, corresponding to a bandgap energy discontinuity of 0.3 eV at the P-type GaAs–P-type GaAlAs heterojunction. This discontinuity acts as a barrier to confine injected electrons. The recombination region and the optical cavity are defined by the N-type GaAs–P-type GaAs junction and the P-type GaAs–P-type GaAlAs heterojunction. The effective bandgap energy of the compensated active P-type GaAs region is decreased slightly due to band tailing. The refractive index steps at the boundaries of the active region serve to confine the stimulated radiation. Thus, both electron and optical confinement are achieved in the single heterostructure lasers.

Some single heterostructure lasers were also fabricated by growing the P-type GaAlAs layer directly onto the N-type GaAs substrate. The evaluation results indicate that under optimum conditions similar room temperature laser performance could be achieved with both approaches. There were two reasons for investigating lasers with a grown N-type GaAs layer. Such a structure was required for the integral GaAs diode-BeO heat-sink design discussed in Section VI. Also, there can be large variations of doping concentration and quality from substrates within one ingot, and from ingot to ingot. Therefore, the epitaxial growth of N-type material should result in much better control and reproducibility of doping concentration and crystal quality and purity. A few laser slices were also fabricated in which the P-type GaAs recombination region was a separately grown epitaxial layer. Similar room-temperature laser performance could be achieved with this approach.

3. LIQUID-PHASE EPITAXIAL GROWTH

The multilayer laser structures were grown by the liquid-phase epitaxial growth process in a multimelt graphite sliding boat system shown in Figure 3. The graphite felt wipers can be used to

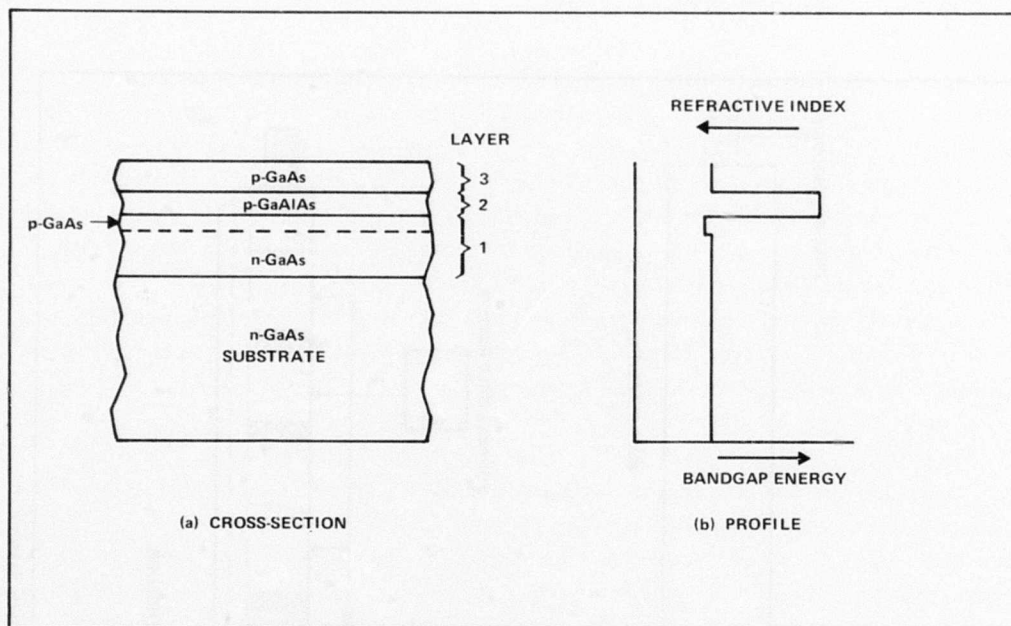


Figure 1. Zinc-Diffused Single Heterostructure Laser Diode

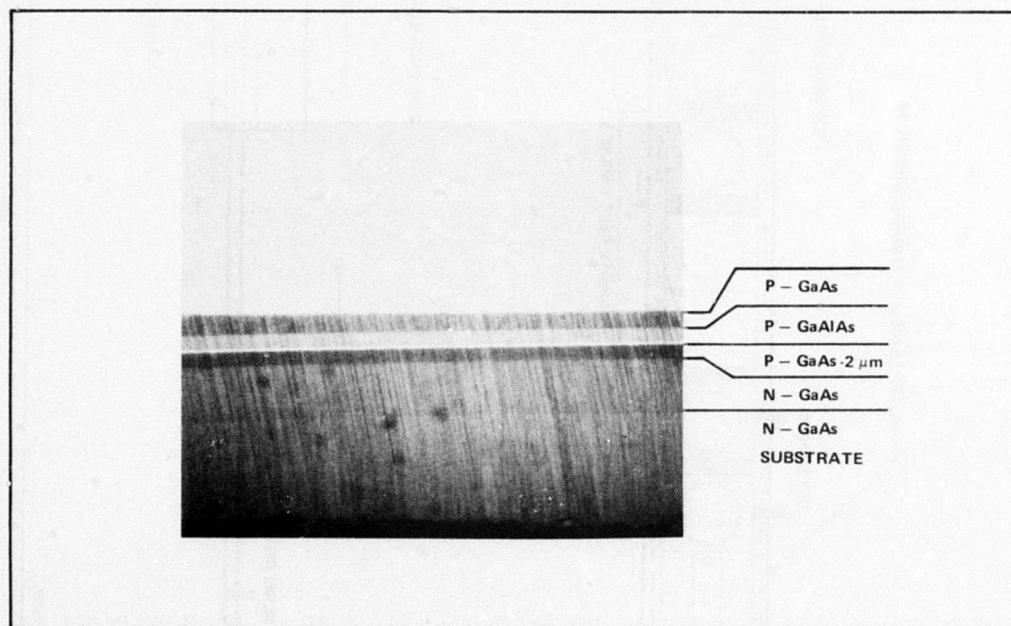


Figure 2. Cross Section of Single Heterostructure Laser Diode

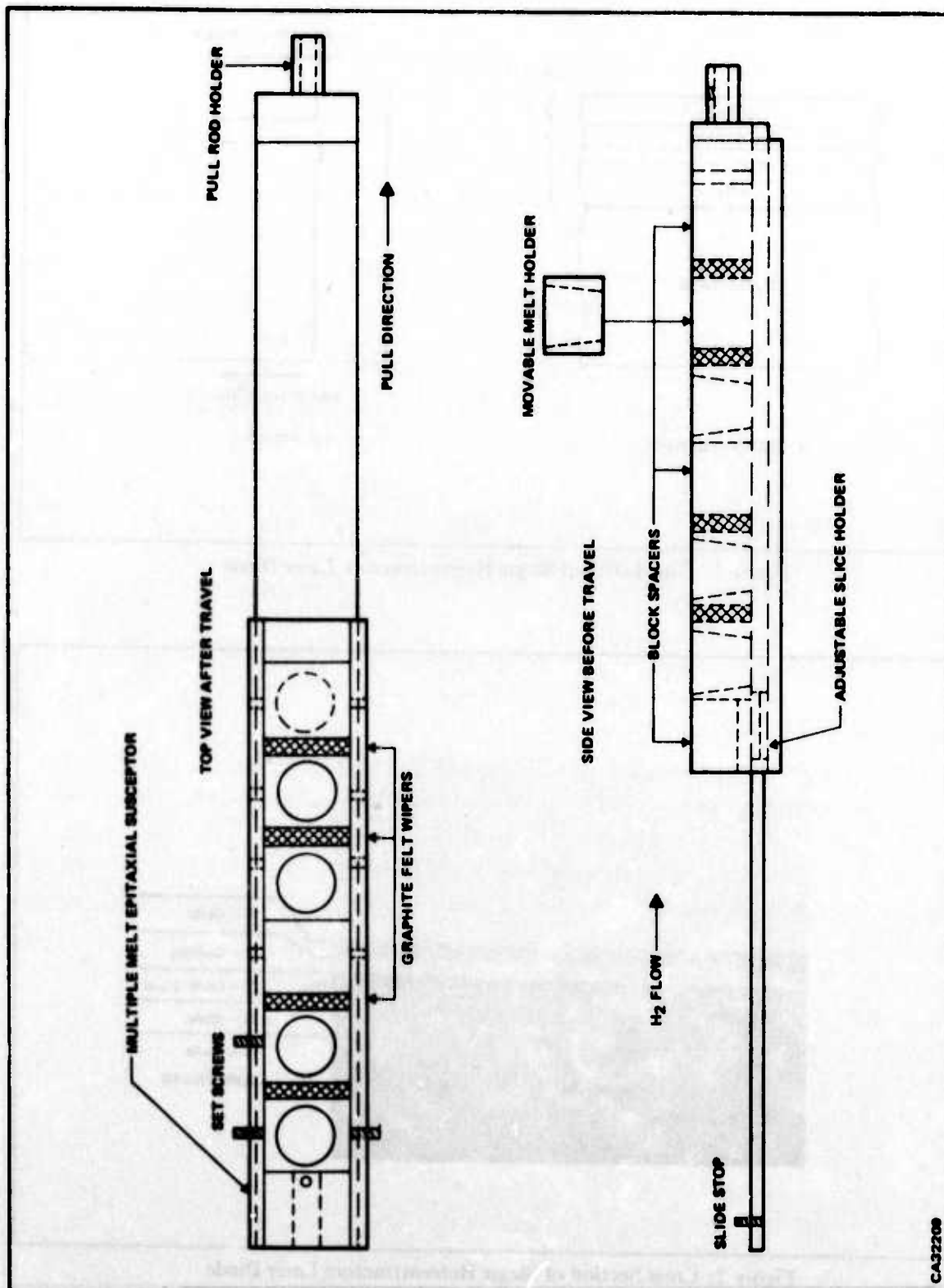


Figure 3. Sliding-Boat Solution Growth System

remove the Ga as the slice moves from one melt to the next melt. For the growth of single heterostructures, generally only one was used for the removal of the Ga after the growth of the last layer. The boat is placed in a quartz tube in a three-zone diffusion furnace which is adjusted to achieve a flat temperature profile. In addition, an isothermal "heat-pipe" furnace liner is used to minimize any remaining horizontal thermal gradient. The reactor system is vacuum-tight and is pumped down and backfilled with forming gas several times prior to each run to ensure removal of all air. Pd-diffused hydrogen is used during all temperature cycles.

The Ga and GaAs are homogenized at $\approx 950^{\circ}\text{C}$ for several hours in a separate run. The Al and dopants are generally added to the Ga melts just prior to the actual growth cycle. In the present growth cycle, the furnace is heated to 700°C . The boat is pushed into the hot zone and the furnace is heated to 855°C . After 30 minutes at 855°C , the furnace is then cooled at the rate of $0.33^{\circ}\text{C}/\text{min}$. The first epitaxial layer is grown starting at 835°C . After the growth of the last layer, the temperature is maintained at a constant temperature for 3 hours while the slice remains under the Ga melt. During this period zinc out-diffuses from the P-type GaAlAs layer into the N-type GaAs layer. At the end of this period the slice is removed from under the last melt and the sliding boat system is cooled to room temperature.

The melt compositions which were found to yield optimum laser performance are given in Table I. The growth procedure and melt compositions were continually refined during the program. Ten-gram Ga melts were generally used. The solubility of GaAs versus Al concentration in a Ga-Al melt has been determined at several temperatures.^{19,20} The values of solubility at 835°C and 855°C have been extrapolated from these experimental results and are shown in Figure 4. Generally, 7.5 mg of Al was added to the P-type GaAlAs melt to obtain an AlAs concentration of 23%.¹⁸ A slight excess of GaAs was generally used to ensure saturation. Typically 0.72 g and 0.55 g GaAs were added to the N-type GaAs and P-type GaAlAs 10-gram melts, respectively. A much greater oversaturation was found desirable for the P-type GaAs melt. If normal oversaturation was used, a very thick GaAs layer ($>15\mu\text{m}$) often grew during the 3-hour diffusion step at constant temperature. Apparently for large oversaturation many GaAlAs platelets form in the melt and most of the excess GaAs deposits on these platelets instead of on the slice during the 3-hour diffusion step.

TABLE I. TYPICAL COMPOSITIONS OF MELTS

| | <u>N-Type GaAs</u> | <u>P-Type GaAlAs</u> | <u>P-Type GaAs</u> | <u>Units</u> |
|------|--------------------|----------------------|--------------------|--------------|
| Ga | 10.0 | 10.0 | 10.0 | g |
| GaAs | 0.72 | 0.55 | 0.83 | g |
| Al | — | 7.5 | — | mg |
| Te | 4.5 | — | — | mg |
| Sn | 65 | — | — | mg |
| Zn | — | 350 | 500 | mg |
| Ge | — | 90 | 90 | mg |

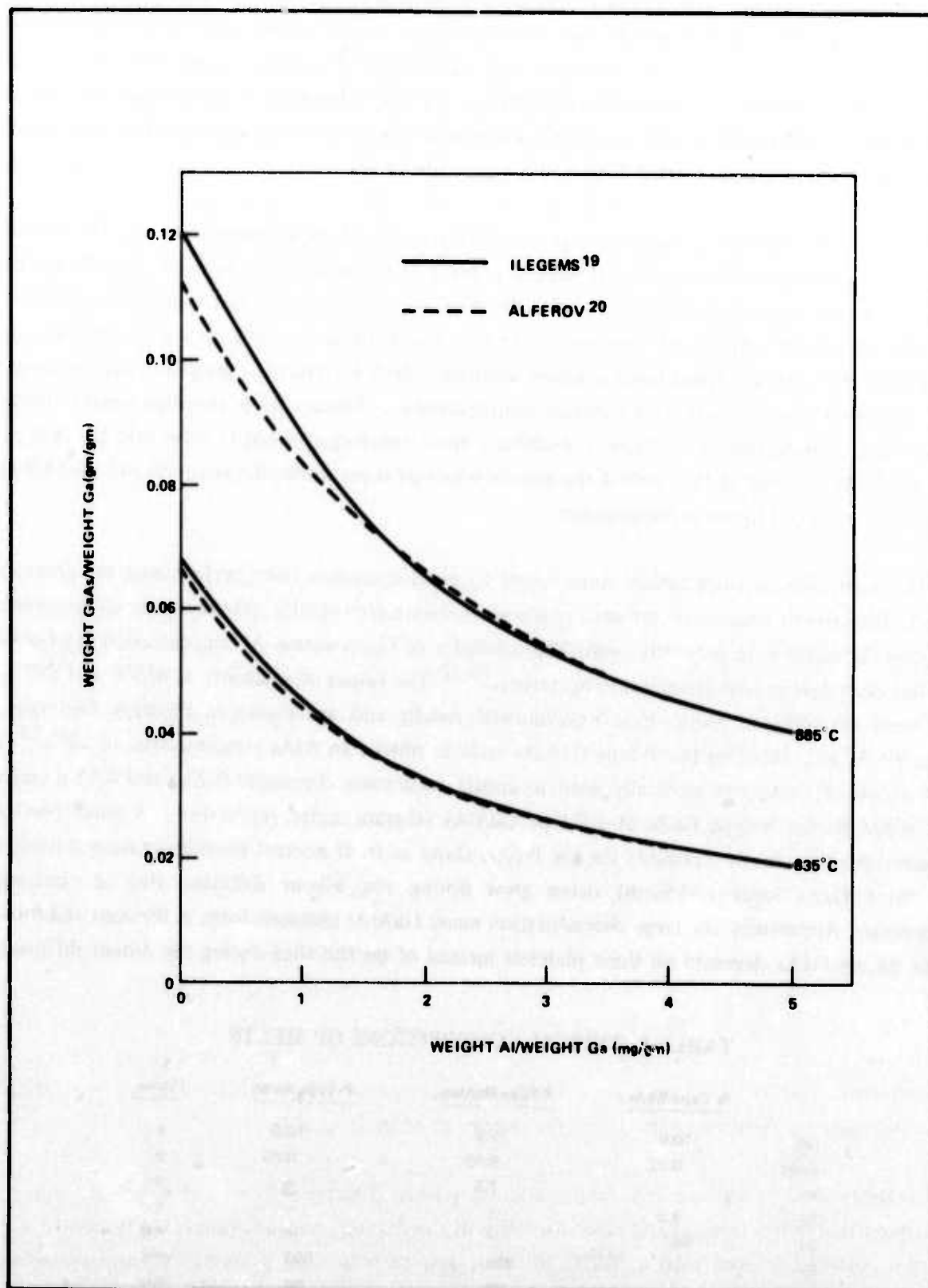


Figure 4. Solubility of GaAs versus Al Concentration in a Ga-Al Melt

The substrates used were (100) Si-doped and were 0.88-inch diameter. The hole in the graphite melt holder enables the growth of a 0.7-inch diameter area on the substrate. Typical growth rates are 1 μm per minute for a cooling rate of 0.33°C/minute.

The optimum dopant concentrations used for the Ga melts were determined by evaluation of the device performance for lasers fabricated under different conditions. A discussion of the dependence of the device characteristics on the epitaxial layer characteristics is given in Section II.5. The N-type GaAs layer is estimated to have an electron carrier concentration of $4 \times 10^{18} \text{cm}^{-3}$.¹⁸ Due to the vaporization of the zinc, the value of the hole concentration in the P-type layers is difficult to estimate but is probably in the order of 2 to $3 \times 10^{19} \text{cm}^{-3}$.

A number of modifications to the growth process and melt composition were made during the program to achieve good single heterostructure lasers. The previous development program at Texas Instruments involved the investigation of large-optical-cavity heterostructure lasers¹⁸ with zinc-diffused recombination regions. The optimum performance for these lasers was achieved for 1.5 mg Te in the 10-gram Ga melt for the N-type GaAs layer and for a zinc diffusion depth of less than 0.6 μm .

One problem initially observed during this program was a difficulty in achieving the 1.7 to 2.0 μm diffusion depth which is required for single heterostructure lasers. The basic cause was zinc vaporization during the 3-hour hold period. Increasing the growth temperature to 885°C and increasing the zinc concentration to increase the zinc diffusion coefficient resulted in only slight improvement because the zinc depletes more rapidly at higher temperatures and higher concentrations. The solution to the problem was the use of a graphite disk on the top of the Ga melt. This eliminated most of the surface area of the Ga exposed to the hydrogen atmosphere and apparently greatly decreased the zinc vaporization rate at 835°C.

A detailed investigation during the program showed that the doping concentration had to be increased to greater than 4 mg Te per 10-g Ga melt for the N-type GaAs layer to obtain good laser performance. This higher doping concentration also increased the difficulty of obtaining a deep diffusion depth. Single heterostructure lasers which have an insufficient zinc diffusion depth and/or an N-type doping concentration that is too low exhibit an anomalous behavior. This is discussed in Section II.5. Lasers with the proper N-type doping concentration but with a cavity thickness of greater than 2 μm or with too high a P-type doping concentration exhibited a broader far-field radiation patterns. Possible explanations for this are given in Section II.5.

Initially in the program, the sliding boat was pushed directly into an 855°C furnace. Later it was found that better control and reproducibility of the doping concentration could be obtained by initially putting the boat into a 700°C hot zone and then heating it to 855°C. Apparently this prevents the instantaneous vaporization of the Zn and Te while they are still in the elemental form before being diluted in the solution.

The accuracy of the orientation of the GaAs substrate was found to be much more critical for single heterostructure lasers than for large-optical-cavity lasers. All good single heterostructure lasers were grown on GaAs substrates with the surface within one-half degree of the (100) orientation.

Near the end of the program, a slight melt-back of the GaAs substrate before the growth of the first N-type GaAs layer was tried for three epitaxial growth cycles. The limited results indicated a slight improvement in laser performance and uniformity. Additional slices would have to be grown to confirm this conclusion. The melt-back was accomplished by pushing the GaAs substrate under the N-type GaAs melt at 844°C instead of at 835°C. This temperature increase was sufficient for the Ga melt to be slightly undersaturated and to melt back a few micrometers of the GaAs substrate.

The material growth and device processing procedures described here are different than have been developed for production of single heterostructure lasers.²¹ The production procedure involves growing a very thick P-type GaAlAs layer ($> 50 \mu\text{m}$) which is then lapped to reduce the thickness to 25-35 μm . In addition, the zinc out-diffusion to form the P-N junction and the optical cavity is accomplished in a separate diffusion operation in a sealed ampoule. The procedure developed during this program gives much better control of layer thicknesses and diffusion depths, enables the growth of a P-type GaAs layer for good contacting, and results in a reduction in the number of processing steps.

4. DEVICE FABRICATION AND EVALUATION

The fabrication process for laser diodes is relatively simple and permits rapid evaluation of laser material. The (100) oriented slice with the deposited epitaxial structure is lapped from the N-type substrate side to approximately 4 mils (0.004 inch) thickness. Both sides are metallized with a plated Au alloy layer which is then alloyed at high temperatures. The laser facets are formed by cleaving strips along the (110) plane with the desired laser length. The strips are sawed into individual laser diodes of the desired width.

For routine evaluation of new laser material, generally ten 10-mil by 10-mil evaluation devices are built. These evaluation devices do not have a mirror on either face. They are mounted on TO-46 coined headers, thus restricting them to pulsed, low-duty-cycle operation. The room-temperature pulsed laser performance results of the evaluation devices are used to select slices which are to be used for CW laser diodes. Laser diodes which are to be mounted on double-sided heat sinks have a mirror coating consisting of a SiO-Cr-Au-Cr-SiO composite structure evaporated onto the cleaved facet opposite the emission facet.

The SiO-Cr-Au-Cr-SiO composite mirror structure for the reflective coating was deposited during a single pumpdown in an evaporator using multi-sources which could be activated

independently. The first SiO layer provides electrical isolation between the laser diode and the Au mirror. A thin layer of Cr is used on both sides of the Au to obtain good adhesion to the SiO. The final SiO layer protects the mirror from scratches during handling and from the solder during assembly. The use of anti-reflective coatings on the front emitting facet was not investigated in this program, although their use should provide improved performance for high-power CW laser diodes. Although an anti-reflecting coating increases the slope efficiency, it also increases the threshold current. Therefore, a significant improvement in performance will be achieved only for lasers operating far above threshold.

For the pulsed evaluation of the laser diodes, a Velonex Model 380 High Power Pulse Generator with a Model 380-13 Plug-in was used. The current was monitored using a Tektronix CT-2 Current Transformer and a Tektronix Type 546 Oscilloscope with a Type 1A1 Dual-Trace Plug-in Unit. The pulsed optical output power was measured with a calibrated ITT-F 4000 Photodiode. The wavelength was determined using a Jarrell-Ash Model 82-020 Spectrometer.

For the evaluation of the CW laser diodes, a Power Design Model 1210-S Regulated DC Power Supply was used. The CW optical output power was measured with a calibrated 0.75-inch diameter silicon photodiode. A calibrated neutral density filter was used for high CW laser output powers.

5. ROOM TEMPERATURE LASER CHARACTERISTICS

The doping concentrations of the epitaxial layers were varied during the program. The room temperature laser characteristics indicate that the doping concentration and diffusion depth are critical for good laser performance. Single heterostructure lasers which have an insufficient zinc diffusion depth and/or an N-type doping concentration that is too low exhibit an anomalous behavior. The laser output power quenches above a certain current level. The result is that for a gaussian-type current pulse with a high peak current, the output power consists of two pulses, one at the leading edge and one at the trailing edge of the current pulse. A characteristic observed when the P-type doping concentration was too high was a broader optical far-field pattern, generally consisting of two principal lobes. The melt compositions which were shown in Table I were found to be optimum for achieving low threshold current, high slope efficiency, high peak power, narrow emission beam laser diodes at room temperature.

The general room temperature evaluation procedure was to measure the optical output power as a function of current to 40 A using 150-200 ns pulse widths at low duty cycle. The threshold current and slope efficiency were determined by a straight line drawn through the experimental points. The unmirrored 10-mil by 10-mil evaluation lasers from the properly grown slices generally had threshold currents of 10 A which corresponds to a threshold current density of $15,000 \text{ A/cm}^2$. Slope efficiencies of 0.5 W/A were obtained, although selected lasers had slope efficiencies of greater than 0.7 W/A.

The emission beam patterns perpendicular and parallel to the junction plane were measured. The half-intensity, full-angle beamwidth perpendicular to the junction varied from 14 degrees to 20 degrees. An example is shown in Figure 5. The beamwidth in the plane of the junction is generally slightly smaller. The laser emission wavelength is typically 9030 Å at room temperature.

The anomalous behavior described above in which certain lasers exhibit a quenching of the output power above a critical current density during a current pulse has been reported previously.²² However, only very recently has a reasonable model for this quenching effect been developed.²³ Basically the explanation is a loss of optical confinement attributed to a reduction in the refractive index discontinuity at the N-type GaAs-P-type GaAs junction. The reduction is caused by the reduction of the refractive index in the active region as a result of the injected carriers.^{23,24}

The initial refractive index discontinuity is smaller for lower N-type doping concentration and thus the threshold for loss of optical confinement will occur at a lower current density. For narrow cavity thicknesses, the threshold for loss of optical confinement is reduced because a certain current density results in a greater injected carrier concentration, that is, the same number of carriers in a smaller volume. For devices far from the optimum design, the threshold for loss of confinement may be below the normal threshold current of the laser. In this case lasing may not be achieved or only at very high currents. This general model explains the laser characteristics observed early in the program, before the doping concentration and active region thickness were optimized.

The model is also consistent with the recent results of Minden and Premo²⁵ for GaAs single heterostructures with separately grown P-type GaAs active regions. For a constant P-type layer doping concentration, improved high-temperature laser performance was achieved as the doping concentration of the N-type layer was increased, thus increasing the refractive index discontinuity and the optical confinement.

An H-pulsing effect in which short light pulses are superimposed on the beginning and end of a steady laser emission for a rectangular current input has recently been observed and described by Grundorfer, et al.²⁶ for single heterostructure lasers. The double pulses observed for non-optimum lasers in this program are not believed to be related to this effect because of the relatively slow current rise times which are used.

A second characteristic observed for some non-optimum lasers was a broad far-field radiation pattern perpendicular to the junction plane, usually consisting of two principal lobes. This behavior was observed only in lasers with an N-type doping concentration equal to or greater than the optimum value and with either a cavity thickness of greater than 2.0 micrometers, or a higher than optimum P-type doping concentration. The broader radiation pattern is attributed to higher-order transverse modes. Possible explanations for why the higher-order modes may be favored over the

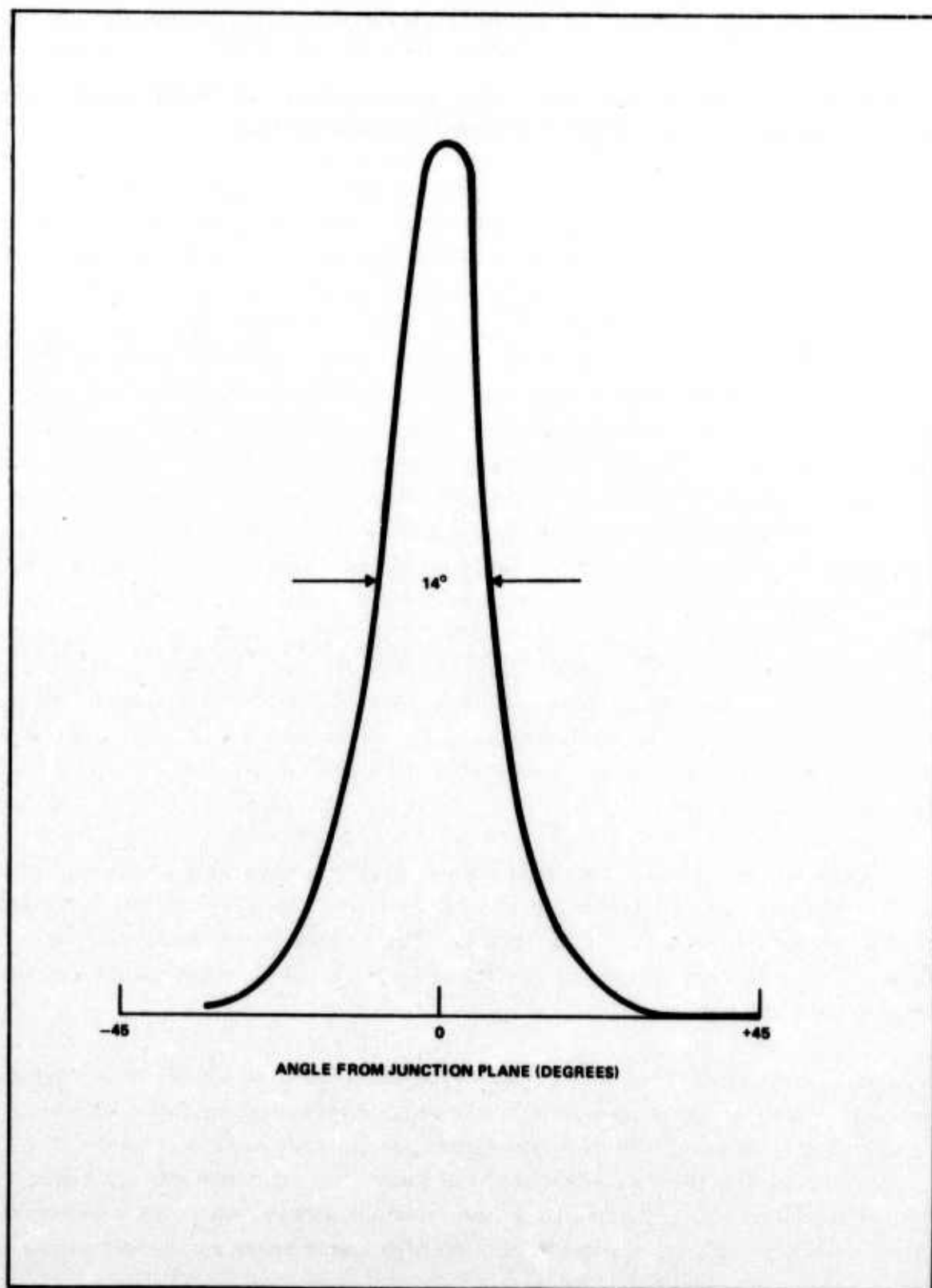
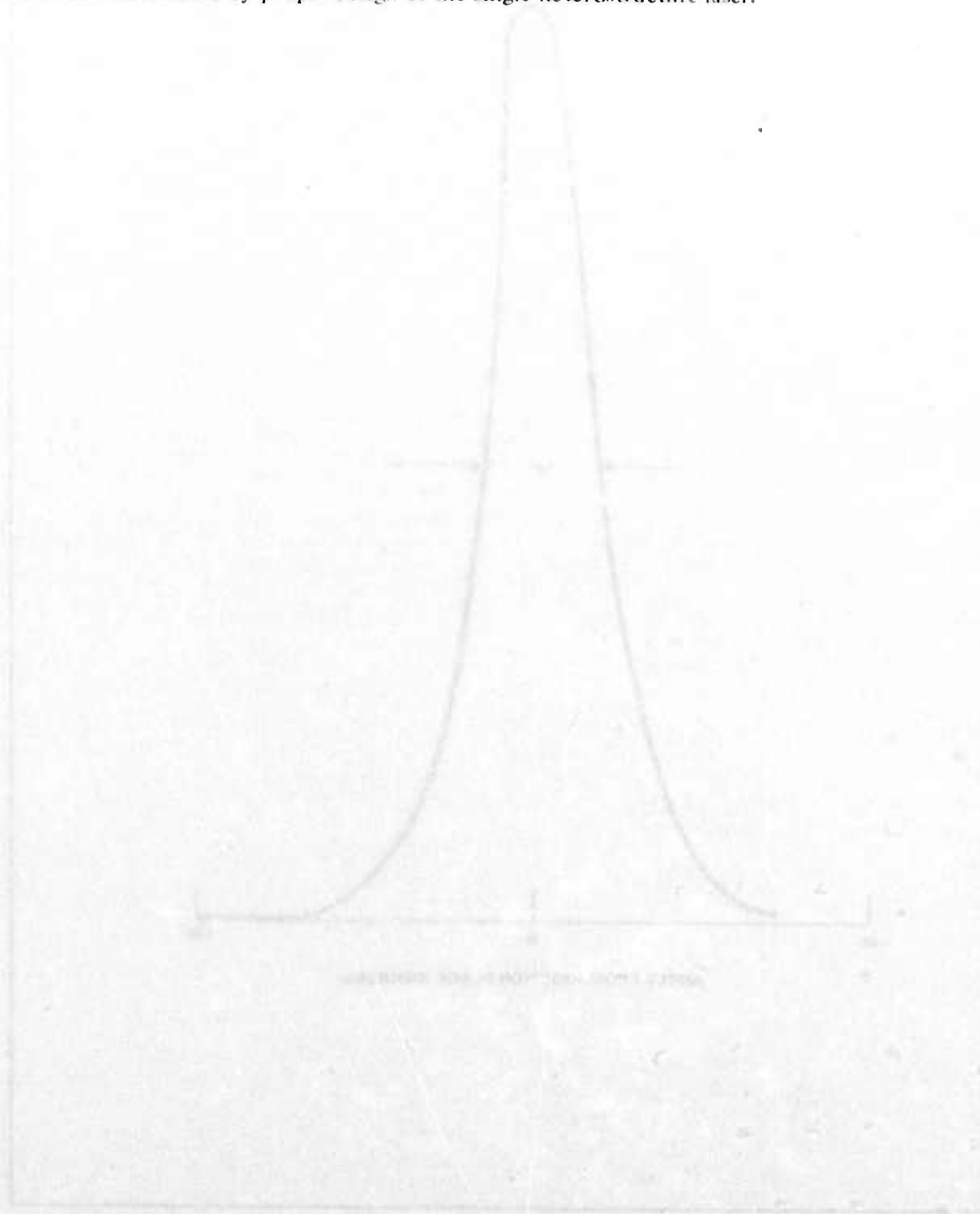


Figure 5. Radiation Pattern Perpendicular to Junction Plane

fundamental mode are: first, asymmetrical excitation due to excessive and nonuniform zinc doping concentrations and a wide cavity thickness, and second, sufficiently large refractive-index discontinuity and cavity thickness to permit higher-order modes to propagate with low loss.

Both the quenching effect of lasers at high currents and the wide far-field radiation pattern have been eliminated by proper design of the single heterostructure laser.



SECTION III

HEAT SINK ASSEMBLY TECHNOLOGY

1. INTRODUCTION

The achievement of high-power CW laser diodes depends on two principal factors, high-performance laser diodes and low thermal resistance to minimize junction heating. The heat-sink assembly technology developed on this program will be discussed in this section.

2. LASER HEAT SINK DESIGN

The double-sided laser heat sink design which was used for most of the program is shown in Figure 6. The body of the heat sink consists of two pieces of high thermal conductivity copper. Intermediate submounts between the laser and the copper were used. The principal submount materials which were investigated were copper and single-crystal BeO. A detailed description of the BeO submounts is given in Section III.5. The BeO submounts were $0.3 \times 0.3 \times 0.08$ inch³ and had a Ti-W-Au metallization. The Cu submounts were rectangular bars $0.4 \times 0.13 \times 0.06$ inch³. The long dimension of the Cu submount was parallel to the laser emitting facet. A photograph of an assembled double-sided heat sink with Cu submounts is shown in Figure 7.

The laser diode is generally mounted with the P-side toward the L-shaped Cu piece of the heat sink, thus making this part the anode of the package. The laser is mounted in this way since the thickness of P-type GaAs material is much less than that of the N-type GaAs material. Thus, it is desirable to have the majority of the heat come out the side of the heat sink which has the lowest thermal resistance.

An intermediate submount is used for two reasons. First, better control is achieved during the critical assembly step of mounting the laser when small pieces of material are used. Second, a high thermal conductivity material such as single-crystal BeO can be used for the submount to enable the heat from the laser to spread over a larger area before reaching the Cu.

A thin stripline spacer is used between the submounts to give mechanical protection to the laser diode. The cross section of the stripline used is shown in Figure 8. It consists of a 1-mil KAPTON dielectric film with a 0.7-mil (0.5-oz) copper layer on both sides. Layers of 0.5-mil thick

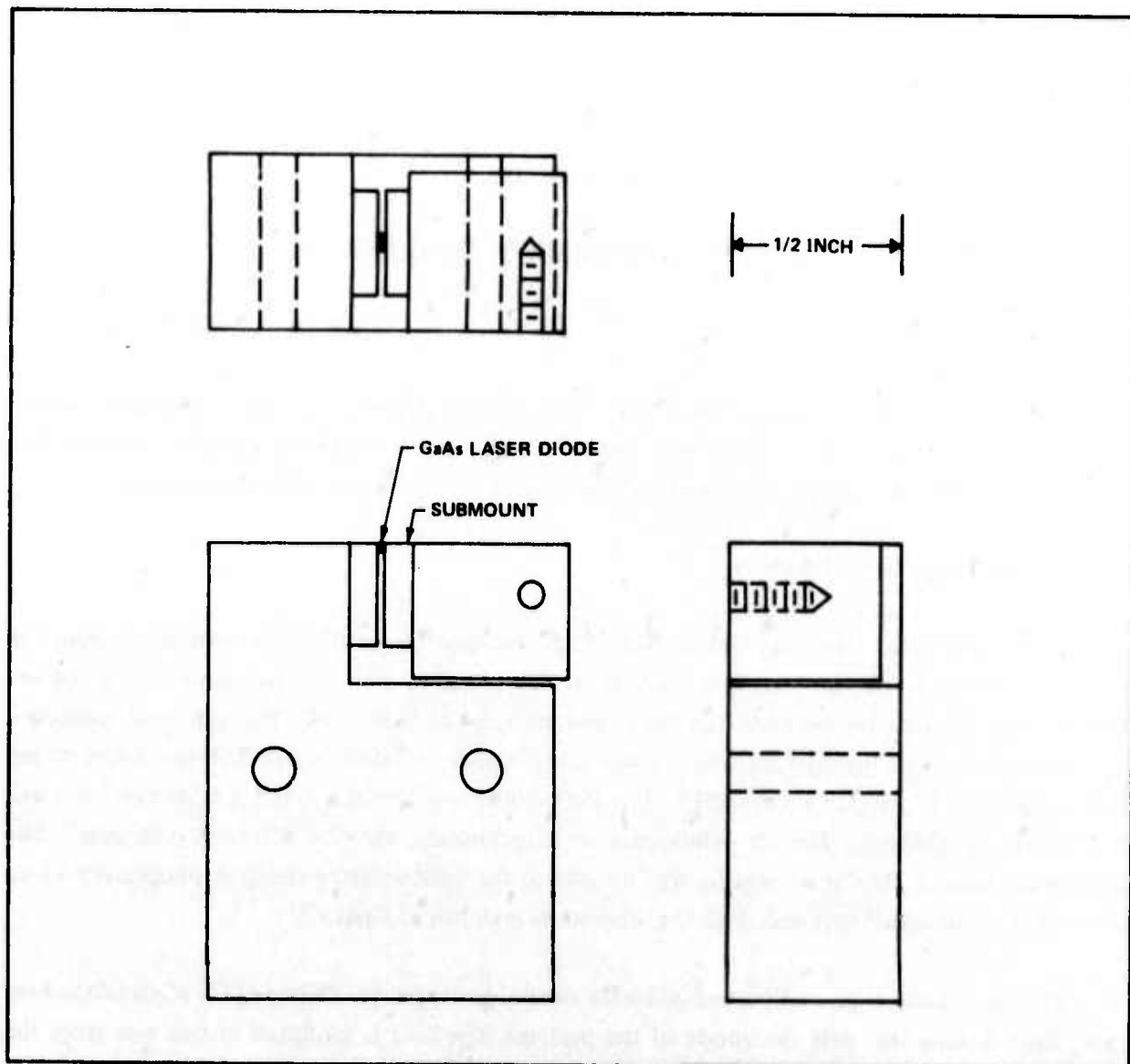


Figure 6. Final Double-Sided Laser Heat Sink Design (Type II)

adhesive are used for bonding the stripline together, for a total thickness of 3.5 ± 0.4 mils, approximately the same thickness as the laser diode. The KAPTON film has a dielectric constant of 3.0 to 3.5, a thermal conductivity of $0.002 \text{ W/cm}^2\text{K}$, a dielectric strength of 7000 volts/mil, and a linear thermal expansion coefficient of 2×10^{-5} per $^{\circ}\text{C}$. An important property of the stripline is its characteristic impedance. Wheeler²⁷ has shown that the characteristic impedance for stripline with a very wide strip is equal approximately to $360 t/W(K)^{1/2}$ where W is the width, t is the dielectric thickness, and K is the dielectric constant. The dielectric properties of the adhesive are not known. The characteristic impedance of the stripline can be approximated by assuming $W = 220$ mils, $t = 2$ mils, and $K = 3$, which yields 1.9 ohms.

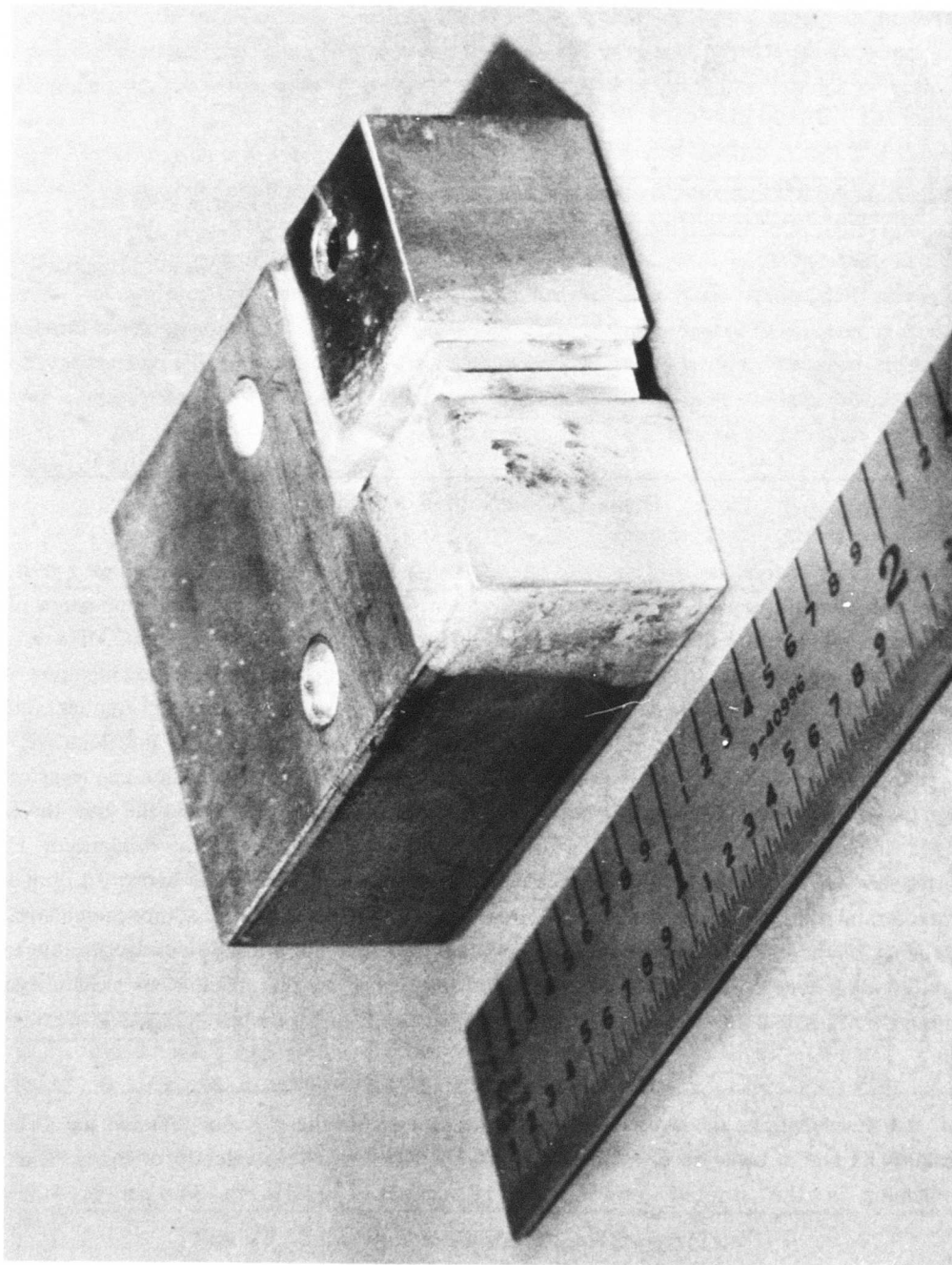


Figure 7. Assembled Double-Sided Heat Sink (Type II)

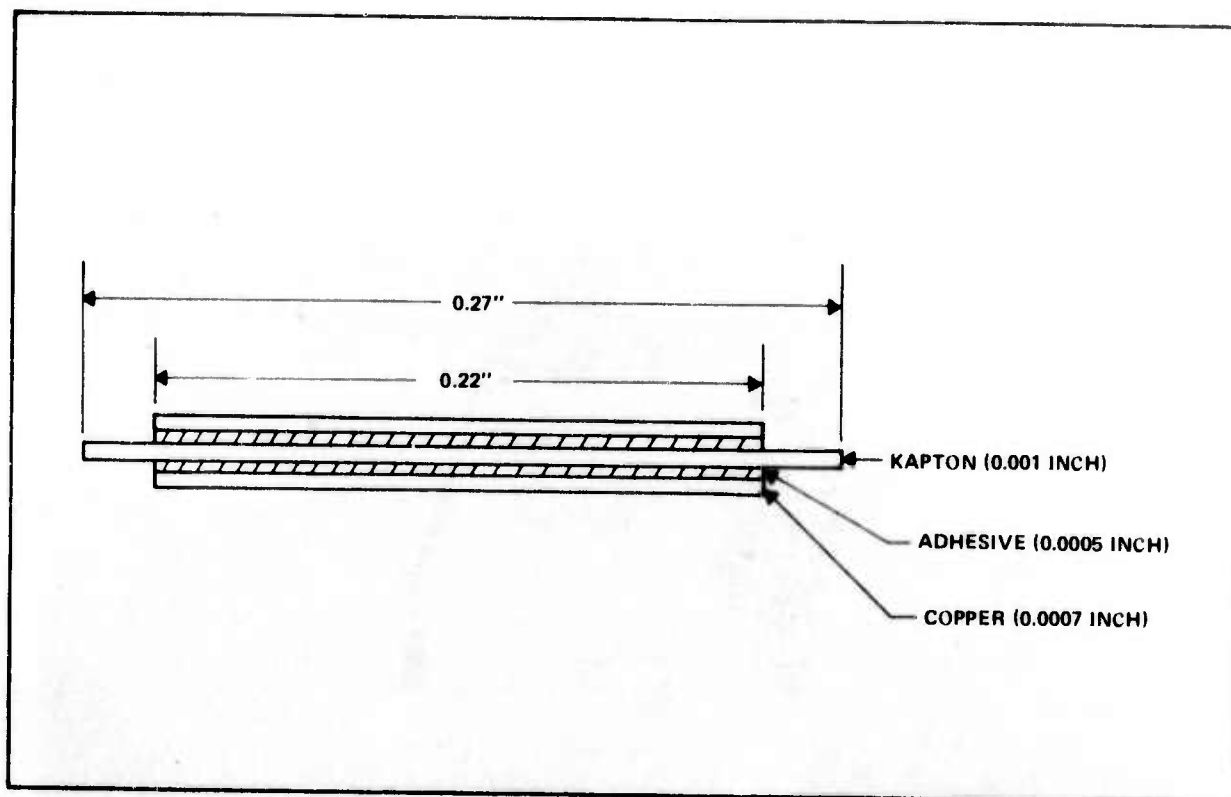


Figure 8. Cross Section of Stripline

A stripline spacer was used because one of the goals of the program was to have a heat sink design which would be compatible with high-frequency operation. An eventual application of CW laser diodes may require that a single frequency modulation within the 100 to 500 MHz range be superimposed on the output radiation of the laser. A major problem in modulating high-power CW laser diodes is the efficient transfer of the input power from a 50-ohm high-frequency signal generator to the 0.1-ohm laser diode. One approach for efficient coupling of the electrical input power to the laser diode is to use the stripline as a quarter-wavelength transmission-line transformer. Since the stripline has a characteristic impedance between that of the source and the load, the effect of the impedance mismatch between the source and the load can be minimized. For a quarter-wavelength stripline with a characteristic impedance of 1.9 ohms and with a 0.1 ohm diode on the termination, the input impedance is 36 ohms, close to the 50 ohms source impedance. The impedance of the diode in general will not be strictly resistive but will also be reactive due to the junction capacitance. This will cause the input impedance to the stripline to have a reactive component. This reactive component can be compensated for by the use of a shunt short-circuit stub.

The wavelength of the signal on the stripline depends on the frequency (f) and the dielectric constant (K) and is equal to $c/(f\sqrt{K})$ where $c = 3 \times 10^{10}$ cm/s (the velocity of light). Thus, the wavelength in the stripline varies from 173 cm at 100 MHz to 34.6 cm at 500 MHz.

Correspondingly, the length of a quarter-wavelength stripline would vary from 43.3 cm (17.0 inches) at 100 MHz to 8.7 cm (3.4 inches) at 500 MHz. Connection of the stripline to a 50-ohm signal generator would be made with an SMA flange-type connector. For high-frequency modulation, the laser would be operated with a dc bias current midway between threshold and the maximum laser current. The laser emission would be amplitude modulated simply by modulating the current through the laser. No investigation of the laser modulation characteristics was conducted during this program.

The initial double-sided heat sink design which was evaluated on the program is shown in Figure 9. A photograph of an assembled heat sink with this design is shown in Figure 10. A stripline can be used for electrical connection. Several mechanical difficulties with the design were encountered. The principal problem was maintaining the top Cu piece parallel to the bottom Cu piece so that uniform pressure could be applied to the submount-laser subassembly. Because of cumulative tolerances on the thickness of the various parts, it was necessary to make an extra spacer of critical thickness (different for each heat sink assembly) at the interface between the top and bottom copper parts. Also the overall dimensions of the heat sink were too large considering the small size of the laser diode. The large dimensions were originally chosen to minimize the thermal resistance of the Cu piece parts.

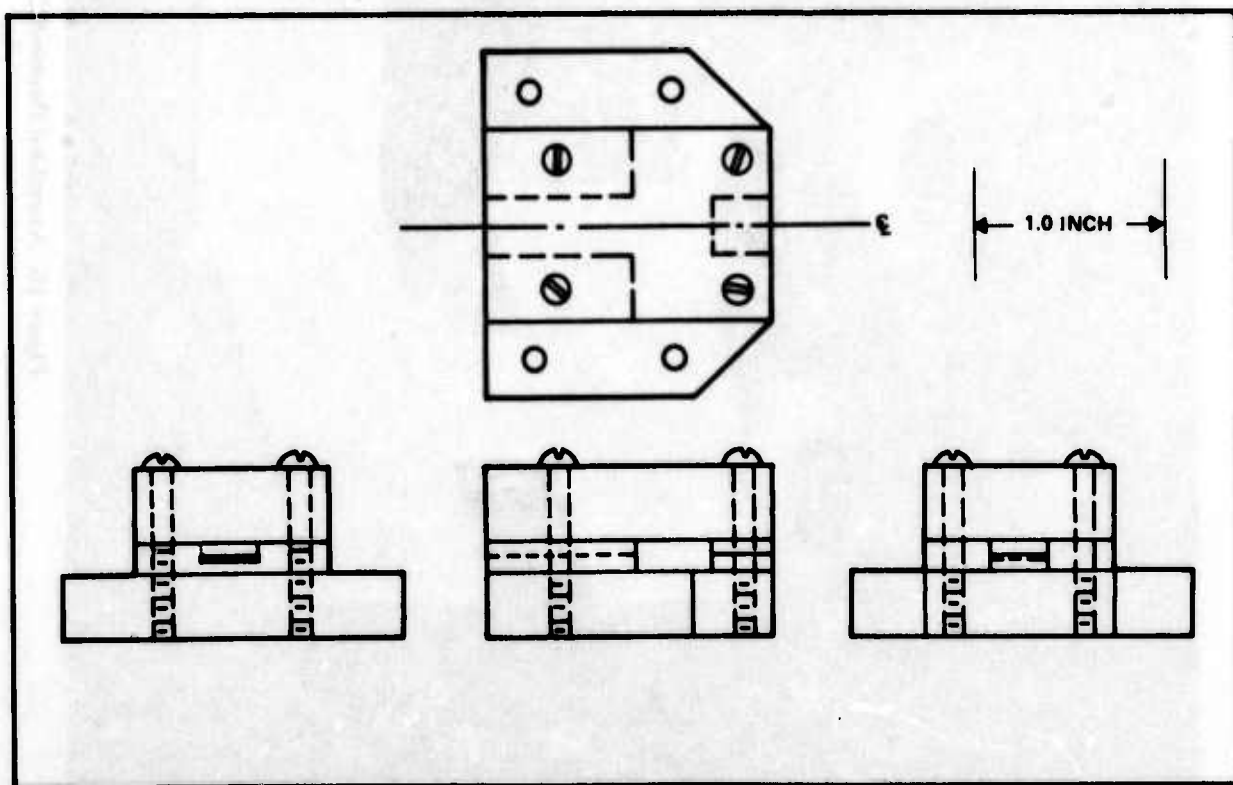


Figure 9. Initial Double-Sided Heat Sink Design (Type I)

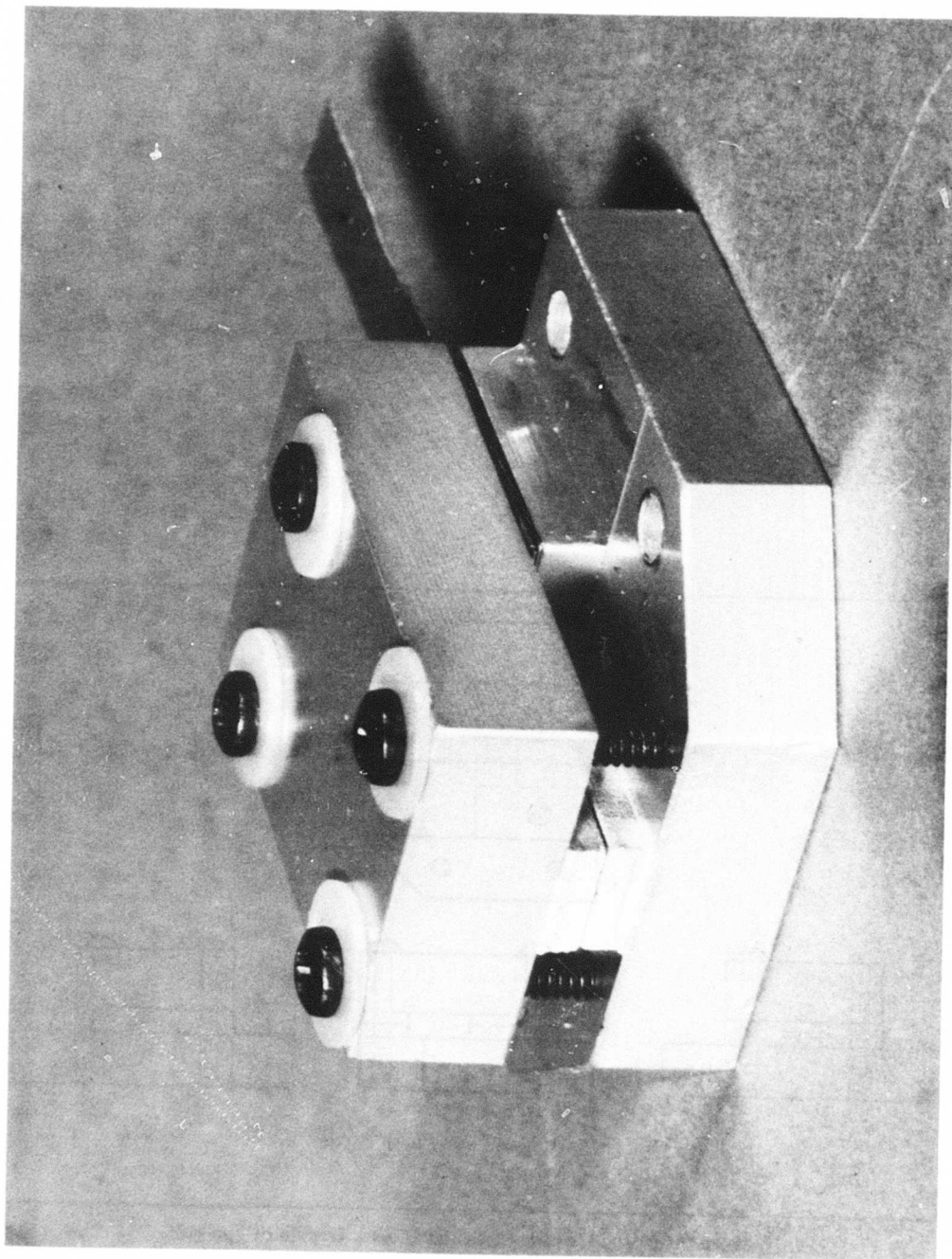


Figure 10. Assembled Double-Sided Heat Sink (Type I)

The final double-sided laser heat sink design which was shown in Figure 6 was much simpler than the initial design. The principal advantage was the elimination of the requirement for tight thickness tolerances on the submounts and the copper parts. Also, the reduced overall size made assembly easier.

3. HEAT SINK ASSEMBLY PROCEDURE

The basic assembly procedure for CW laser diodes using the final double-sided heat sink design shown in Figure 6 is as follows. Mirrored lasers are fabricated from material slices which have been evaluated as described in Section II.4. and have been found to yield high-performance lasers. Unmounted mirrored lasers are evaluated in a special fixture to determine their pulsed room temperature laser performance characteristics. The best laser diodes are selected for mounting in the double-sided heat sinks.

The first step in the actual assembly is to mount the laser diode between the two submounts. A layer of indium is plated on the submounts to enable good thermal contact to the laser. Indium is sufficiently ductile at room temperature to flow under pressure to fill any voids or to absorb minor thickness variations. A stripline is used as a mechanical spacer between the submounts to protect the laser diode from excessive pressure. The laser-submount sandwich-type subassembly is placed in a special fixture which applies uniform pressure to ensure good thermal contact. Epoxy is then applied around the edges of the laser-submount subassembly to mechanically bond it together. The epoxy is cured while the subassembly remains under pressure in the fixture. After this step, the laser is retested to ensure that it is not damaged. The most common failure at this time in the assembly is a shorted junction due to indium flowing up the side of the laser chip. However, if too little indium is used, cracked chips can result.

The laser-submount subassembly is next mounted between the two copper parts of the double-sided heat sink. The copper parts have indium plated on them, so that an In-to-In cold weld is obtained between the submount and the copper for good heat transfer. While the laser-submount subassembly is held under pressure between the two copper pieces, electrically insulating epoxy is applied into the space between the two copper pieces and is allowed to cure. After assembly of the double-sided heat sink, the pulsed laser performance is again evaluated to ensure that the device was not damaged during assembly.

The indium plating on the submounts and the copper parts was performed using an indium sulfamate plating solution produced by Indium Corporation of America. The optimum conditions for obtaining flat, dense, small-grain-size indium layers was to plate at room temperature using a sinusoidal current superimposed on a 50-mA dc current such that the current was reversed during 10 to 15% of each cycle. After plating, the indium surface was scraped lightly with a sharp, flat tool

to remove any high spots which formed during plating and to produce a final shiny surface for the formation of a good cold weld. Typical final layer thicknesses were 6 to 12 micrometers.

The epoxy used between the submounts and between the Cu parts was Abletherm 8-2 produced by Ablestik Laboratories. This epoxy had the best overall characteristics of the various epoxies studied. It has a relatively high thermal conductivity, is electrically insulating, has a low cure temperature, and has a sufficiently high viscosity to prevent flowing to the laser diode during the cure cycle. Typical temperatures and times for the cure cycle were 60 to 80°C and 2 to 3 hours, respectively. Radiant heating with a quartz-iodide lamp was used since it did not degrade the device, eliminated the need to move the assembly fixture after final alignment of the parts, and enabled laser diode current-voltage characteristics to be monitored with a curve tracer during the cure cycle.

The establishment of a suitable and reproducible assembly procedure for CW laser diodes was more difficult and time consuming than had originally been anticipated and was the primary reason that high-power CW laser diodes were not achieved until near the end of the development program. The final assembly procedure was established after the evaluation of various approaches. Modifications and improvements in the assembly process were made continually during the course of the program.

Initially, the assembly procedure was to first mount the submounts onto the copper parts and then to mount the laser between the submounts. This was done to achieve a good In-to-In cold-weld bond for low thermal resistance between the submount and the copper. This sequence of assembly steps, however, did not allow good control for the critical laser to submount bond and either cracked laser diodes resulted from excessive pressure or poor thermal characteristics resulted from too little pressure.

A degradation of the laser performance during assembly was found to be caused by the temperature cycle used for curing the epoxy. This degradation was eliminated by reducing the temperature and lengthening the cure time. Before the indium plating capability was established, epoxy was also used to bond the submounts to the copper. This approach resulted in high thermal resistance.

An initial problem with some of the BeO submounts was peeling of the metallization. The original approach was to plate an additional 8- μ m thick layer of Au onto the thin Ti-W-Au metallization supplied with the BeO submounts. Since the BeO is electrically insulating, the thick Au layer was for good electrical conduction of the large currents required for laser operation. When peeling did occur, separation generally occurred between the Ti-W and Au layers, although in some samples the separation occurred between the submount and the Ti-W-Au layers. The peeling problem was minimized by reducing the plated gold thickness to 4 micrometers. No peeling was observed when the indium was plated directly onto the evaporated Ti-W-Au layer.

4. LIQUID NITROGEN DEWAR

A liquid nitrogen dewar is required for the practical use of 77° K injection lasers. The dewar serves as a reservoir for the liquid nitrogen coolant and provides a vacuum environment around the laser to prevent heat flow from the ambient and "frosting" on the laser diode due to condensation from the atmospheric water vapor.

A special liquid nitrogen dewar was designed and built for the program. A survey of the literature from various dewar companies indicated that no standard dewar was available which would have the flexibility desired for the development program. The general limitations were: small cold plate diameter and thus limited heat dissipation capability, poor accessibility to the cold plate, and lack of readily removable electrical feedthroughs. Once a final design is defined, this flexibility will not be required and a simpler dewar can be used.

A cross-sectional outline of the final dewar design is shown in Figure 11. The diameters of the inner and outer circular stainless steel tubings are 3.5 inches and 4.0 inches respectively. The heat sink can be mounted on the cold plate either by removing the bottom plate or by removing the entire bottom assembly which allows the maximum working room. The design also enables the base plate to be surface-ground again if it becomes necessary after repeated use. There are five access holes for the assembled dewar, four symmetrical holes on the bottom assembly, and one on the upper assembly. Electrical leads and the vacuum line are presently made through the upper access hole. One of the bottom access holes is used as a window for the laser emission. The opposite access hole can be used for the electrical leads if the lengths need to be minimized such as for high-frequency operation. Because of the multiple access holes, more than one device could be evaluated on a single run, although this was not done. The diameter of the access hole is large enough so that all the laser emission can escape from the dewar without optics.

The volume of the liquid nitrogen reservoir is 53 in^3 or 865 cm^3 or 0.87 liter. One liter of liquid nitrogen weighs 1.79 pounds. Liquid nitrogen has a latent heat of vaporization of 47.6 cal/gm. This corresponds to 161 joules/cm³ or 45 watt-hours/liter. Thus for an electrical input power of 25 W, a diode could ideally operate continuously for 1.8 hours. In practice, the liquid nitrogen evaporates more rapidly because of heat conduction from the top resulting from the simplified dewar design near the top.

A relatively large cold plate is used in the dewar. One reason was to minimize any temperature difference between the cold plate and the liquid nitrogen. The maximum rate of heat extraction from a metal immersed in liquid nitrogen is 10.4 W per cm² of surface area; the temperature difference across the interface at this rate is 13.8°C. At higher heat flows, a continuous film of gas is formed on the metal surface and much larger temperature differences occur. The heat transfer rate versus temperature difference across the liquid nitrogen-metal interface is shown in Figure 12.

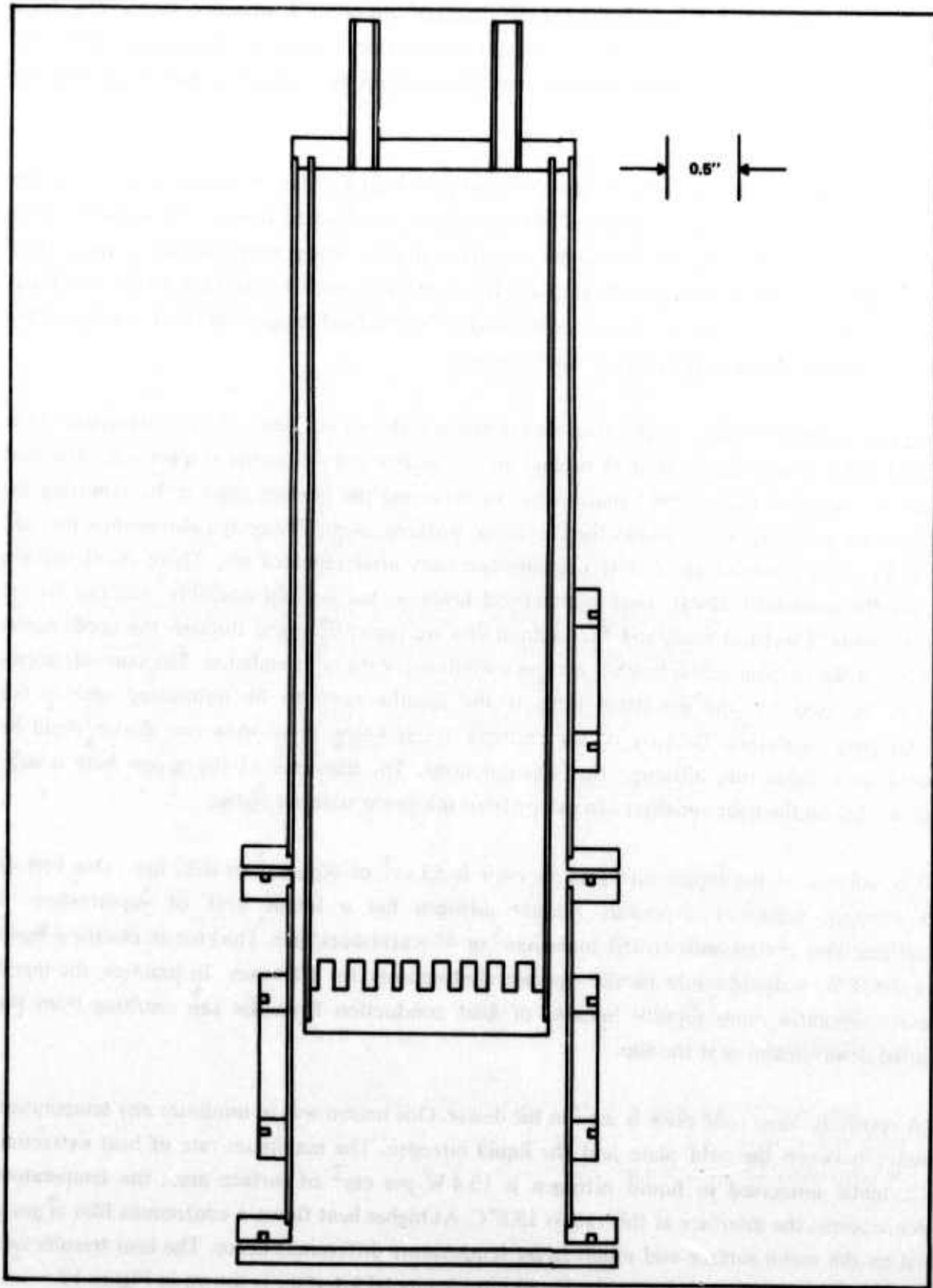
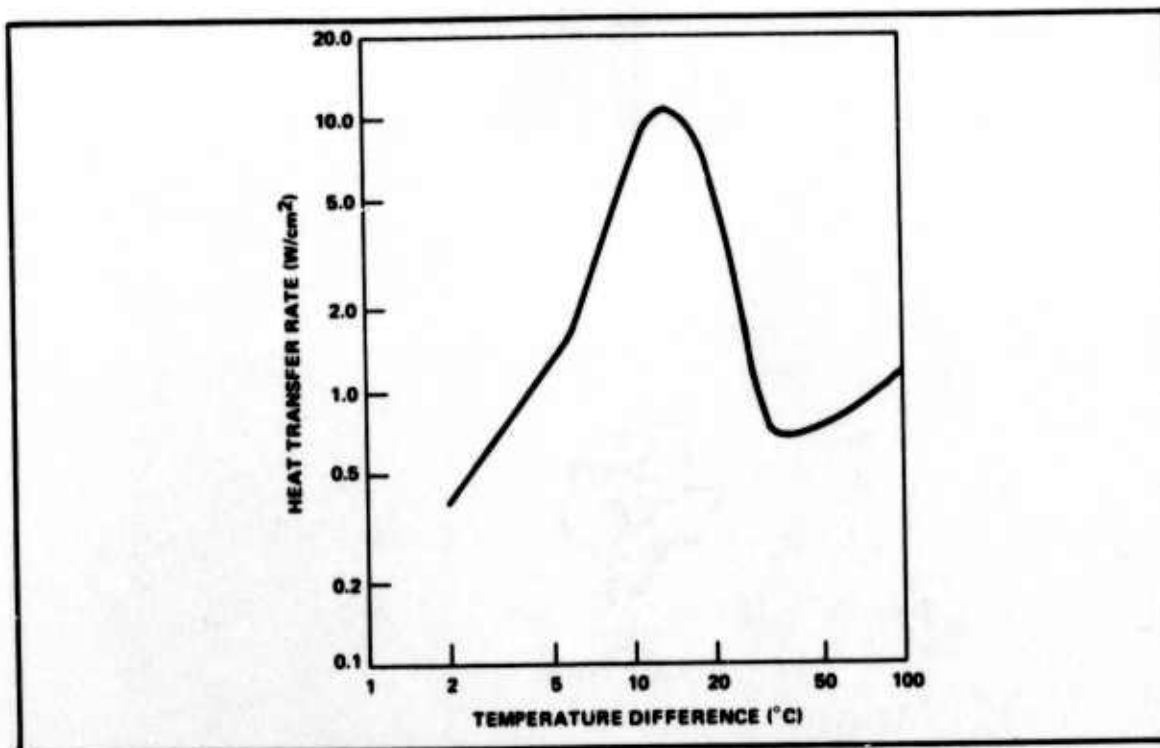


Figure 11. Liquid Nitrogen Dewar Design



**Figure 12. Heat-Transfer Rate versus Temperature Difference
Across Liquid-Nitrogen/Metal Interface**

The total area of the cold plate is 9.6 in² or 62 cm². Assuming 25 W is dissipated uniformly across the area of the cold plate, the heat transfer rate would be 0.4 W/cm² and the temperature difference should be 2°C. Actually the heat from the diode may spread only over a 2 in² or 12.9 cm² area. In this case, the heat transfer rate would be 2 W/cm² and the temperature difference would be 7°K. However, the temperature difference would probably be less since fins have been designed on the back side of the cold plate in the dewar to increase the effective surface area.

An assembled dewar is shown in Figure 13. The window has been removed so that the mounted heat sink can be seen more clearly. Figure 14 shows a double-sided heat sink mounted on the cold plate. The bottom portion of the dewar has been removed. The initial Type I double-sided heat sink design was being evaluated at the time the photographs were taken.

The double-sided heat sink was mounted onto the cold plate of the dewar with a 1 to 2 mil thick indium spacer and with a thermally conducting compound. This assembly step was found to be very critical for achieving good thermal characteristics.

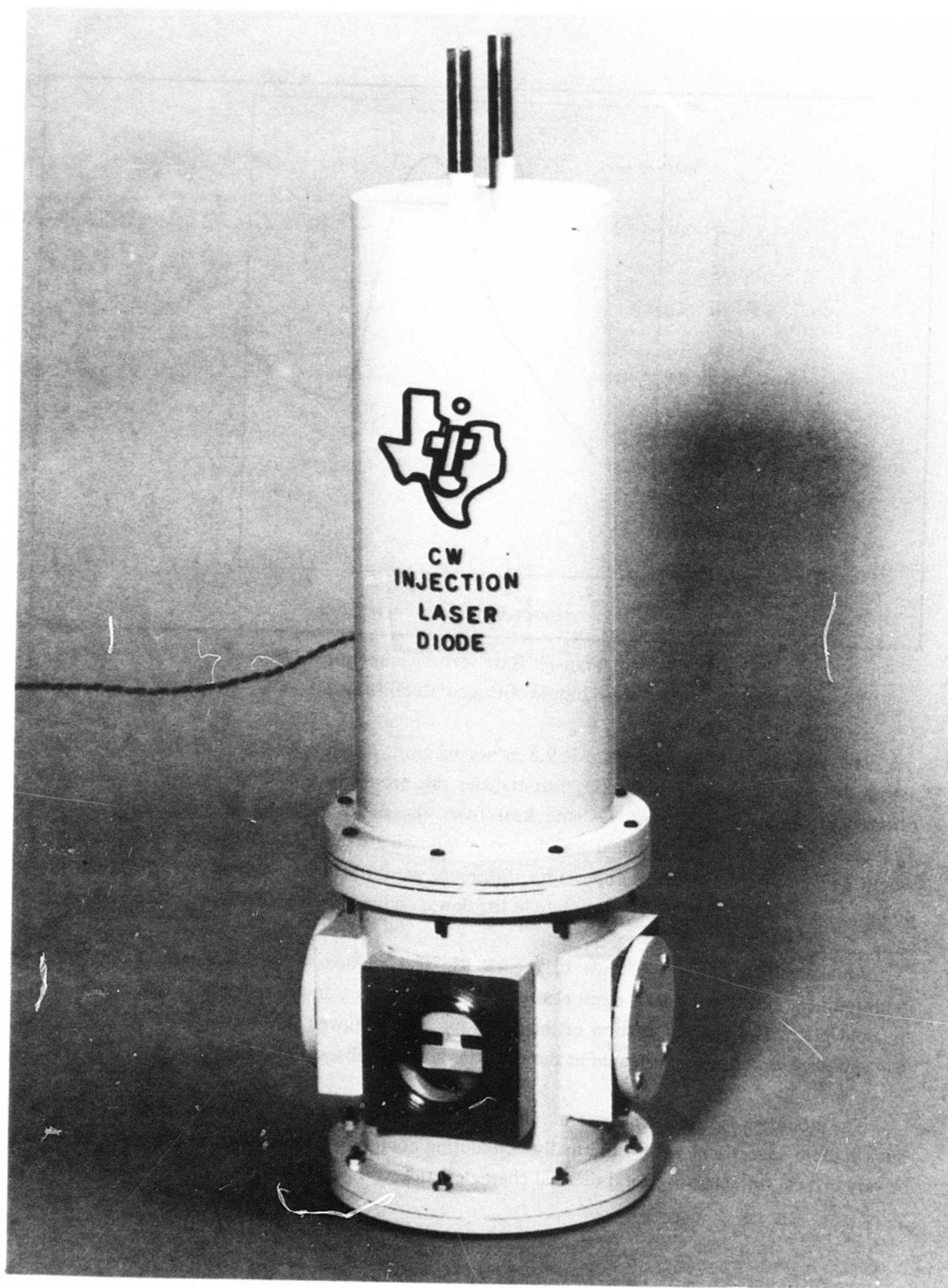


Figure 13. Assembled Liquid Nitrogen Dewar

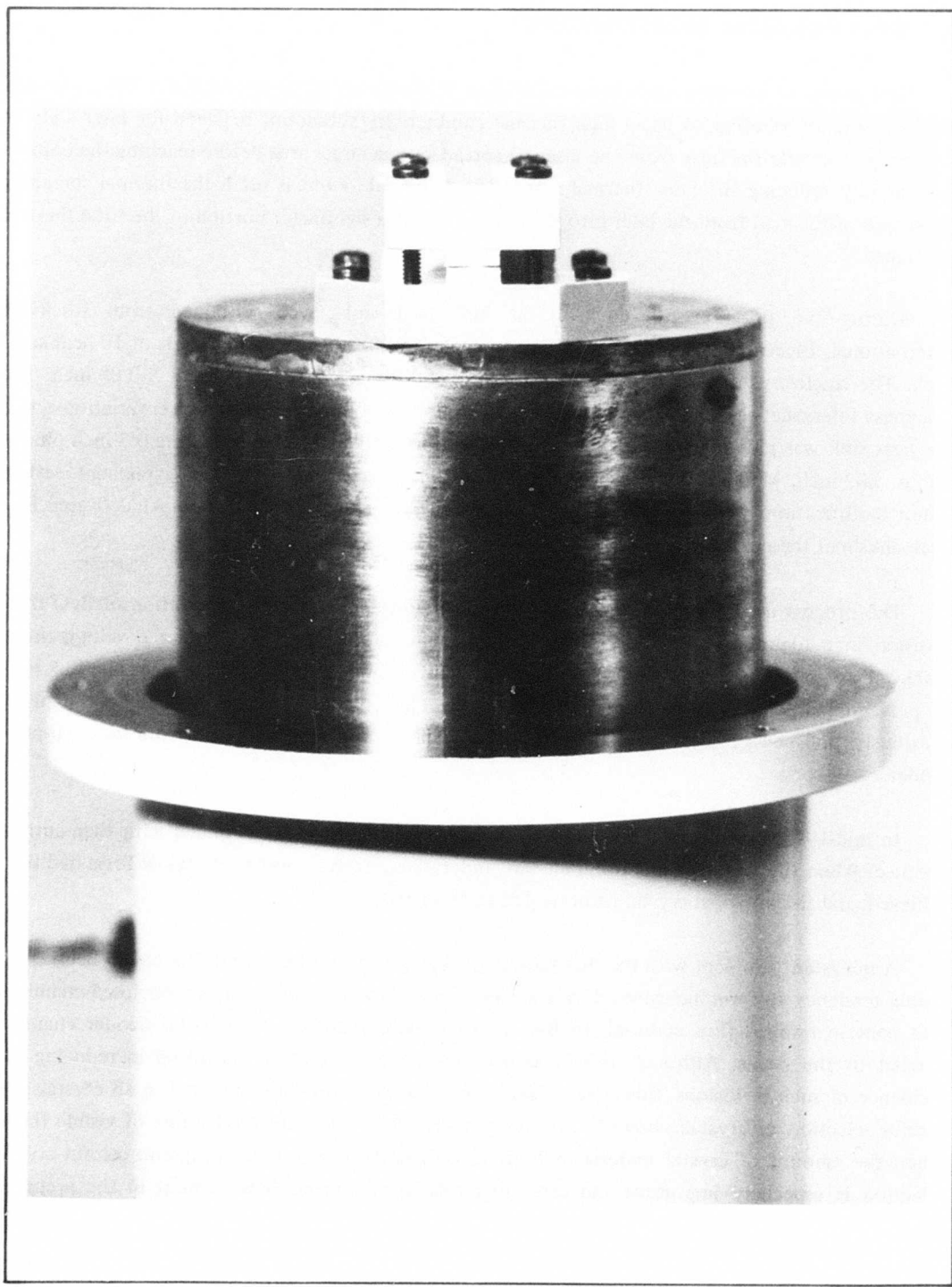


Figure 14. Liquid Nitrogen Dewar with Bottom Portion Removed

5. SINGLE-CRYSTAL BeO SUBMOUNTS

One aspect of the program was an evaluation of the use of single-crystal BeO submounts. The basic reason for wanting to use a high thermal conductivity submount between the laser and the copper is to enable the heat from the laser to spread over a larger area before reaching the copper, thus greatly reducing the laser thermal resistance. If no submount is used, the thermal spreading resistance of the heat from the laser into the copper can be a significant portion of the total thermal resistance.

During the program 50 single-crystal BeO heat sinks were obtained from Rockwell International, Electronics Research Division, Anaheim, California in five shipments of 10 heat sinks each. The single-crystal BeO rectangular heat sinks had dimensions of 0.3 X 0.3 X 0.08 inch. The thickness tolerance was 0.080 inch plus 0.005 inch minus 0.000 inch. The thickness variation across the heat sink was plus or minus 0.001 inch. The length and width tolerances were 0.3 inch plus or minus 0.02 inch. Metallization was supplied on the BeO heat sinks. By mutual agreement, several minor modifications were made to the original specifications during the program. All delivered BeO heat sinks met the purchase specifications.

The process used for BeO crystal production involves controlled precipitation of BeO from solution in a high-temperature solvent flux.^{28,29} The process has been under development at Rockwell for several years, with crystal size and quality slowly improving with time. The flux used in prevailing practice is potassium polymolybdate. The crystals are grown on BeO seed plates previously polished on the (10 $\bar{1}$ 0) crystallographic plane and mounted on a rotating seed-plate holder.

In mid-1973, crystals with the (33 $\bar{6}$ 2) crystallographic form were obtained with then-current practice. When the work on this program was undertaken, better control of crystal form had been achieved, and the principal crystal form tended to be (10 $\bar{1}$ 0).

A persistent problem with the flux-growth of crystals (including but not limited to BeO) is the strong tendency to form inclusions during growth. These inclusions generally are enclosed chambers that contain trapped flux material. In BeO crystals these chambers tend to be slender channels parallel to the c-axis. Although there has been continual progress at Rockwell in reducing the incidence of such inclusions, this type of defect has not been totally eliminated in all crystals. By careful selection of crystals, however, pieces can be cut out that are totally free of visible flaws. When the amount of crystal material is limited, as was the case for this program, careful crystal selection is especially important and can still result in minimized flaw content in the prepared samples.

A very important property of BeO, especially for the intended device application, is its high thermal conductivity. At room temperature, the thermal conductivity of BeO single crystal material has been measured to be $3.7 \text{ W/cm}^\circ\text{K}$,³⁰ a value $\sim 93\%$ that of copper. As the temperature decreases, the conductivity markedly increases to $67 \text{ W/cm}^\circ\text{K}$ at the temperature of liquid nitrogen.

Since the measurements that provided these values were made with crystals produced under the same conditions as those used in the present program, it is a reasonable assumption that the thermal conductivity is the same in the recent crystals as in the earlier (measured) crystals. For this reason, as well as the considerable expense involved in measuring the conductivity of even a few test pieces of the BeO heat sink wafers, no verification measurements of the thermal conductivity were made on the delivered heat sinks.

The crystals used for preparing the heat sinks were selected to be free or nearly free of inclusions and free of visible cracks. The selected crystals were cut with a diamond-impregnated wire saw. Each wafer was lapped on the 0.3×0.3 -inch faces to obtain the required thickness and parallelism. As work on this program was initiated the BeO crystals being grown generally had the $(10\bar{1}0)$ form. Therefore, it was most practical to cut the wafers parallel to the $(10\bar{1}0)$ face. All heat sink wafers fabricated and delivered to TI were of this orientation.

A problem not normally encountered was found with the first group of heat sinks prepared for delivery. Although cracks were not detected initially in the BeO crystals, many of the cut heat sinks had short cracks that appeared to lie in the $(10\bar{1}0)$ cleavage planes. To the extent possible the cracked pieces were eliminated by selection. This problem did not persist for the other four sample groups, even though a crack was detected occasionally in isolated samples of the other groups. The distribution of flaws was described in detail in the data sheets and photographs accompanying the groups of samples. To aid in the detailed description of the samples, each one (except for the first group delivered) had one corner beveled. This not only distinguished between opposite main faces, but also served as an index marker from which the four individual edge surfaces could be identified. The most common defect observed on the delivered BeO heat sinks were chips or microcracks along the sawed edges.

All delivered heat sinks were metallized on both main faces for subsequent electrodeposition at TI of an Au layer. The composition of the metallization and the extent of area coverage by the metallization evolved during discussions between TI and Rockwell personnel relative to preparation of the first three groups of samples. The third, fourth, and fifth groups had similar metallizations in all respects.

For all wafers, the surfaces were thoroughly cleaned prior to metallization. The final "on the bench" cleaning procedure was to boil the wafers individually in a 1:1 mixture of hydrogen peroxide and deionized water. The wafers were handled only with clean plastic tongs for placing in the evaporator. The wafers were exposed to a glow discharge in the vacuum chamber immediately prior to metallization.

Deposition of successive metal layers was done sequentially without breaking the vacuum. The thickness of each layer was monitored with an optical-reflection thickness monitor installed in the vacuum chamber.

The wafers for the first group to be delivered were coated with Ti and W, although one of the pieces also had an additional layer of Au on one face. All wafers other than the first group also were Au-coated on both main faces, on top of the Ti and W layers. The final evaporated Au layer was added because of a difficulty in plating Au directly to the Ti-W layers supplied on the first BeO heat sinks. The successive layer thicknesses were approximately as follows:

| | |
|---|-------------|
| Ti | 50-100 Å |
| W | 2600-2800 Å |
| Total thickness 3300-5500 Å, including Au | |
| (except 9300 Å on one side of the fourth group) | |

The thicknesses varied somewhat from group to group relative to the values stated here.

With each group of samples installed in the vacuum system for metallization there were several clean glass plates added to test layer adhesion. Following the deposition sequence in each case, the adhesion between metal layer and glass surface was tested by the widely-used Scotch Tape test. In no case was there any evidence of adhesion failure.

At T1 there appeared to be variable adhesion failure between the BeO surface and the metal layer after further build-up of the Au layer to 8 μ m by electrodeposition. As a result of this disclosure, further adhesion tests were made at Rockwell on the final (fifth) group of heat sinks prior to shipment. Two BeO wafers were tested by the Scotch Tape test, with no evidence of adhesion failure. At T1 the adhesion problem was later minimized by reducing the Au layer thickness.

In two other cases (on wafers not delivered) adhesion was tested by scratching with the sharp tip of an Exacto knife blade. Although the tip could be made to gouge the metal layer, again there was no evidence visible under the microscope that the metal could be chipped or peeled from the BeO surface.

The first two groups delivered were metallized while held on simple rails in the metallizing chamber. As a result, a strip along two opposing edges of each main face was masked from metallization. Thus, the metal layer extended to only two edges on each main face rather than to all four edges, as shown in Figure 15(a).

The metallization configuration was altered for the final 30 BeO heat sinks. A special holding fixture was made that would support the wafers only at the corners. This allowed the metal to extend to all four edges on each main face, as shown in Figure 15(b). This increases the probability of finding a good edge with no cracks or edge chipping for mounting the laser. Additionally, one side face was metallized to provide electrical continuity between the metallization on the two main faces, desired for the configuration of the diode mounting device used by TI. This metallization pattern was applied to all wafers in the third, fourth, and fifth groups. A photograph of a BeO heat sink with this metallization pattern is shown in Figure 16.

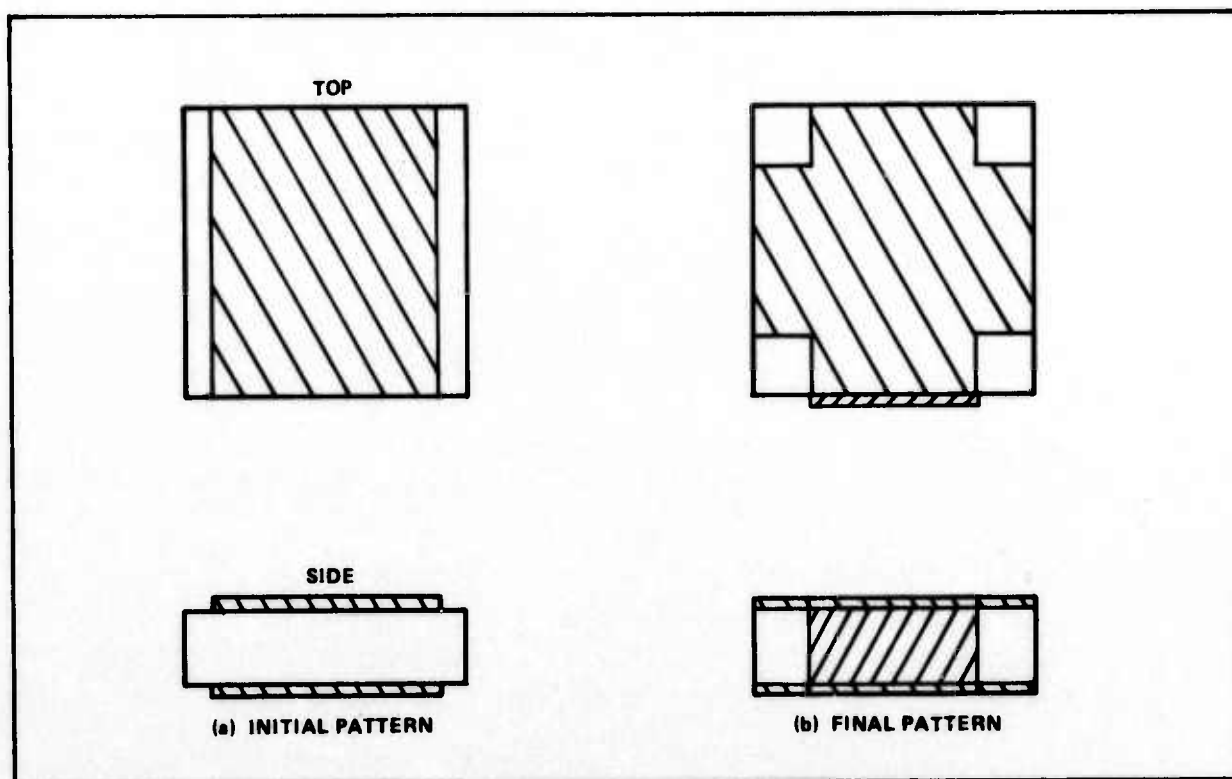


Figure 15. Metallization Patterns on BeO Heat Sinks

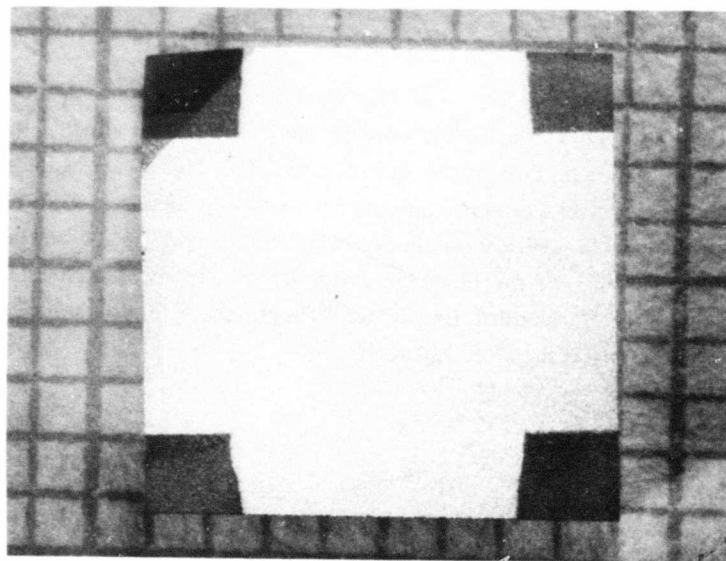


Figure 16. Metallized BeO Heat Sink

SECTION IV

CW LASER DIODE CHARACTERISTICS

1. EVALUATION PROCEDURE

An extensive series of measurements was made on each CW laser diode to determine all important electrical, optical, and thermal parameters. The sequence for the evaluation of the laser diodes was as follows. The pulsed performance of the lasers was measured after each step in the assembly sequence to determine if any degradation had occurred. Pulsed measurements of the optical output power as a function of current were measured after mounting between submounts, after mounting in double-sided heat sink, after mounting on cold plate of dewar, and after cooling to 77°K. Pulsed currents up to 30 A at 300°K and up to 10 A at 77°K were generally used. The emission spectrum was also measured under pulsed conditions to determine the lasing wavelength for no heating.

At 77°K, the CW optical output power, the diode forward voltage, and the lasing wavelength were measured as a function of dc current. The CW optical output power was measured with a calibrated 0.75-inch diameter silicon photodiode detector positioned approximately 1.0 inch from the laser. Thus, the detector measured the light emitted into an emission cone with a 35° to 40° full cone angle. The total emitted power was slightly higher since an infrared viewing scope indicated that some power was emitted beyond this cone angle. At high CW output powers, a calibrated neutral density filter was used.

The shift of the lasing wavelength with increasing dc current gives an estimate of the increased junction temperature due to heating. The variation of wavelength with temperature is non-linear and increases from 1.5 Å/°K at 77°K to 2.8 Å/°K at 300°K³¹ as shown in Figure 17. The total wavelength shift between 77°K and 300°K is 530 Å. The thermal resistance of the laser is determined by dividing the temperature increase at high currents by the electrical input power.

The total series resistance is determined from the slope of a plot of diode forward voltage versus dc diode current. The intercept of the slope line with the voltage axis typically occurred at 1.5 volts. The diode series resistance was calculated by subtracting the 0.06-ohm resistance of the electrical leads from the total series resistance.

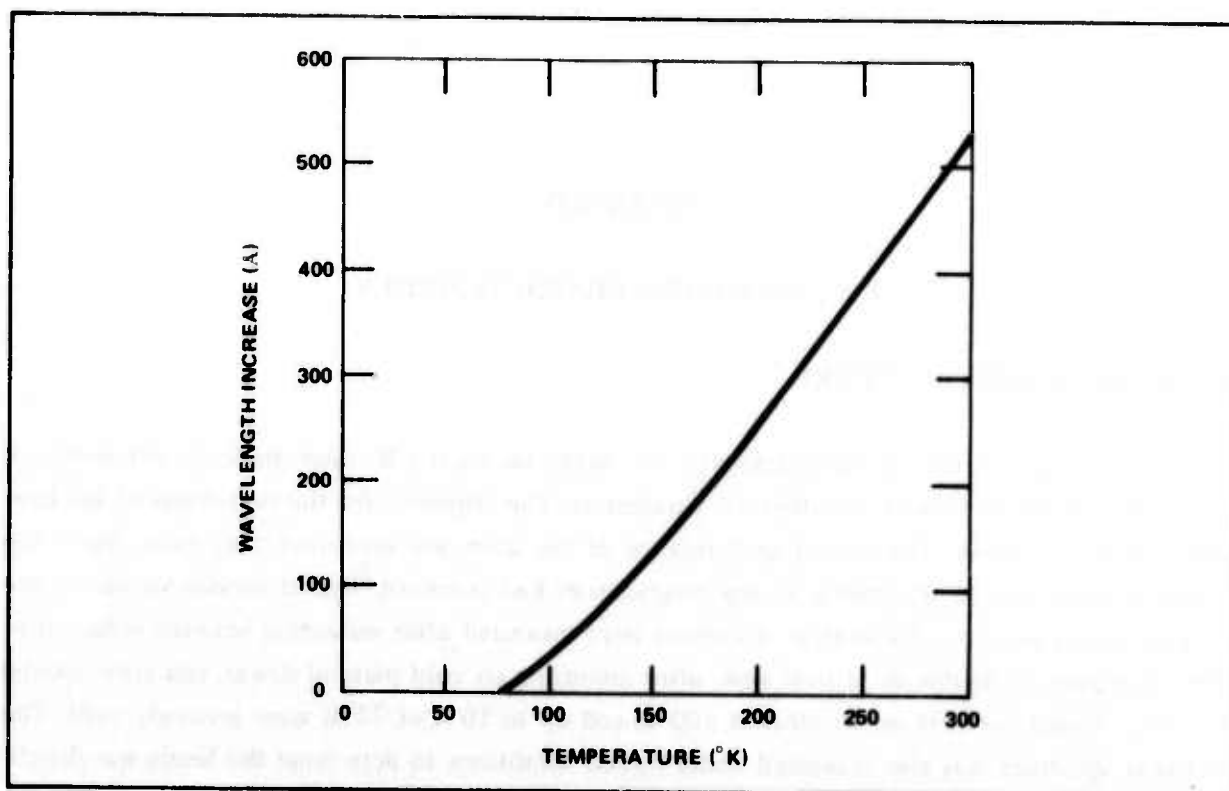


Figure 17. Wavelength Increase versus Temperature for GaAs Lasers

2. CHARACTERISTICS OF DELIVERED CW LASER DIODES

A summary of the characteristics of the ten diodes delivered at the end of the contract is shown in Table II. All laser diodes were mounted in the Type II double-sided heat sinks. Cu and BeO submounts with no bevels were used. Typical room temperature pulsed threshold current densities were 9,000 to 12,000 A/cm² with a slope efficiency of 0.3 W/A. Typical 77°K pulsed threshold current densities were 500 to 800 A/cm² with slope efficiencies of 0.5 to 0.7 W/A. These experimental values agreed well with the theoretical values predicted in Section V. The pulsed slope efficiencies of heat sinks 1314 and 1325 degraded approximately 50% during assembly. The pulsed lasing wavelengths were typically 9030 Å at 300°K and 8530 Å at 77°K.

Typical 77°K CW threshold current densities were 600 to 900 A/cm². The CW slope efficiencies ranged from 0.10 to 0.36 W/A. The values of the thermal resistance ranged from 3.7°K/W to 17°K/W. The lowest values agreed well with the theoretical values predicted in Section V. Some of the last heat sinks fabricated had the highest values of thermal resistance. This is attributed to the use of reworked heat-sink parts which resulted in non-optimum thermal contact because of uneven non-parallel surfaces. The increase of the junction temperature over the dewar cold plate temperature of 77°K ranged from 21°K to 64°K at maximum current. The specific resistance of the diodes ranged from 10 to 24 ohms-mil².

**TABLE II. OPTICAL, ELECTRICAL, AND THERMAL CHARACTERISTICS OF
DELIVERED CW LASER DIODES**

| Heat Sink Number | 1322 | 1324 | 1313 | 1329 | 1314 | 1325 | 1404 | 1331 | 1421 | 1321 |
|---|--------------|--------------|--------------|--------------|--------------|--------------|--------------|--------------|--------------|--------------|
| Laser Diode Number | 346-1 #5 | 346-1 #6 | 316B #13 | 336A #3 | 316B #4 | 316B #3 | 346-1 #1 | 346-1 #4 | 316B #2 | 344-1 #3 |
| Size (width X length) (mils ²) | 9 X 15 | 9 X 15 | 8 X 10 | 8 X 16 | 9 X 15 | 8 X 13 | 8 X 15 | 6 X 15 | 8 X 16 | 7 X 12 |
| Submount Material | Cu | Cu | Cu | Cu | Cu | Cu | 8eO | 8eO | Cu | Cu |
| 300° K Pulsed Characteristics: | | | | | | | | | | |
| Threshold Current (A) | 11.7 | 10.5 | 6.4 | 8.4 | 9.0 | 8.0 | 6.6 | 7.0 | 10.0 | 4.2 |
| Threshold Current Density (kA/cm ²) | 13.4 | 12.1 | 12.4 | 10.2 | 10.3 | 11.9 | 8.5 | 12.1 | 12.1 | 7.8 |
| Slope Efficiency (W/A) | 0.31 | 0.31 | 0.34 | 0.28 | 0.17 | 0.15 | 0.19 | 0.18 | 0.28 | 0.28 |
| Lasing Wavelength (Å) | — | 9020 | — | 9062 | — | 9055 | 9022 | 9005 | — | 9015 |
| 77° K Pulsed Characteristics: | | | | | | | | | | |
| Threshold Current (A) | ~0.60 | ~0.60 | ~0.25 | ~0.45 | ~0.40 | ~0.50 | ~0.95 | ~0.70 | ~0.45 | ~0.45 |
| Threshold Current Density (kA/cm ²) | ~0.69 | ~0.69 | ~0.48 | ~0.55 | ~0.46 | ~0.75 | ~1.23 | ~1.20 | ~0.54 | ~0.83 |
| Slope Efficiency (W/A) | 0.53 | 0.48 | 0.64 | 0.50 | 0.22 | 0.24 | 0.59 | 0.49 | 0.68 | 0.46 |
| Lasing Wavelength (Å) | 8530 | 8545 | 8558 | 8554 | 8510 | 8535 | 8550 | 8529 | 8542 | 8552 |
| 77° K CW Characteristics: | | | | | | | | | | |
| CW Output Power (mW) | 688 at 3.0 A | 664 at 3.0 A | 543 at 3.0 A | 520 at 3.0 A | 292 at 3.0 A | 179 at 3.0 A | 169 at 2.8 A | 164 at 2.8 A | 129 at 1.2 A | 104 at 1.5 A |
| Threshold Current (A) | 0.75 | 0.54 | 0.43 | 0.60 | 0.68 | 0.51 | 0.96 | 0.87 | 0.60 | 0.58 |
| Threshold Current Density (kA/cm ²) | 0.86 | 0.62 | 0.83 | 0.73 | 0.78 | 0.76 | 1.24 | 1.50 | 0.73 | 1.07 |
| Slope Efficiency (W/A) | 0.36 | 0.30 | 0.27 | 0.33 | 0.14 | 0.10 | 0.12 | 0.12 | 0.27 | 0.14 |
| Voltage Intercept (V) | 1.45 | 1.50 | 1.60 | 1.61 | 1.58 | 1.60 | 1.50 | 1.49 | 1.50 | 1.52 |
| Diode Series Resistance (ohms) | 0.13 | 0.13 | 0.12 | 0.19 | 0.10 | 0.11 | 0.20 | 0.21 | 0.18 | 0.18 |
| Specific Resistance (ohms-mils ²) | 18 | 18 | 10 | 24 | 14 | 11 | 24 | 19 | 23 | 15 |
| Wavelength Shift (Å) | 32 at 2.5 A | 26 at 2.5 A | 114 at 3.0 A | 102 at 3.0 A | 48 at 3.0 A | 55 at 3.0 A | 70 at 2.8 A | 62 at 2.8 A | 78 at 1.6 A | 94 at 1.8 A |
| Temperature Increase (°K) | 21 at 2.5 A | 17 at 2.5 A | 64 at 3.0 A | 58 at 3.0 A | 30 at 3.0 A | 34 at 3.0 A | 42 at 2.8 A | 38 at 2.8 A | 46 at 1.6 A | 56 at 1.8 A |
| Thermal Resistance (°K/W) | 4.6 | 3.7 | 10.9 | 8.9 | 5.3 | 5.9 | 7.3 | 6.0 | 16.1 | 16.9 |

The four best lasers had CW optical output powers of greater than 500 milliwatts at 3.0 A. Subsequent measurements on a larger number of diodes indicated that the lasers mounted in heat sinks 1322 and 1324 could have been safely driven to higher diode currents. Thus, these diodes had the capability for even higher CW output powers. All of the delivered CW laser diodes were assembled during the last month of the program. This was a result of the greater than expected length of time which was required to design, fabricate, and evaluate the piece parts and to develop a suitable and reproducible assembly procedure. Thus, time did not remain to retest the CW laser diode performance of these devices at higher currents.

The CW optical power is shown as a function of dc diode current in Figure 18 for the best diodes. The dc slope efficiency is defined by a straight line drawn tangent to the approximately linear portion at low currents. The CW threshold current is defined by the intercept of this straight line with the current axis. The dc slope efficiency is less than the pulsed slope efficiency and the output power begins to saturate at high currents because of junction heating. At increased junction temperature, the threshold current increases and the efficiency decreases. The power efficiency for the four best CW laser diodes is shown in Figure 19 as a function of dc diode current. The laser in heat sink 1322 had a power efficiency as high as 13%. It decreased to 12.5% at 3.0 A.

The lasing wavelength is shown as a function of dc diode current in Figure 20 for the four best CW laser diodes. The lasing wavelength for zero dc diode current is that measured under low-duty-cycle pulsed conditions to minimize heating. The lasing wavelength shifts to longer wavelengths at high dc diode currents because of junction heating. The expected shift of wavelength with temperature was shown in Figure 17. Using this curve, the increase in junction temperature is shown in Figure 21 as a function of dc electrical input power. The nonlinear characteristic indicates that the thermal resistance increases with increasing temperature. This is expected from the theoretical calculations shown in Section V since the thermal conductivity of materials decreases with temperature. The values of thermal resistance listed in Table II represent average values since they were determined by dividing the increase in junction temperature by the maximum dc electrical input power.

The CW optical output power is shown in Figure 22 as a function of dc diode current for the remaining six CW laser diodes. The lasing wavelength versus dc diode current is shown in Figure 23 for these lasers. The CW output powers of 1314 and 1325 are low because the laser performance was degraded during assembly. The CW output powers of 1321 and 1421 are low because of the high values of thermal resistance. The CW output powers of 1331 and 1404 are low because of the relatively high threshold current density ($\geq 1200 \text{ A/cm}^2$ under pulsed conditions at 77° K).

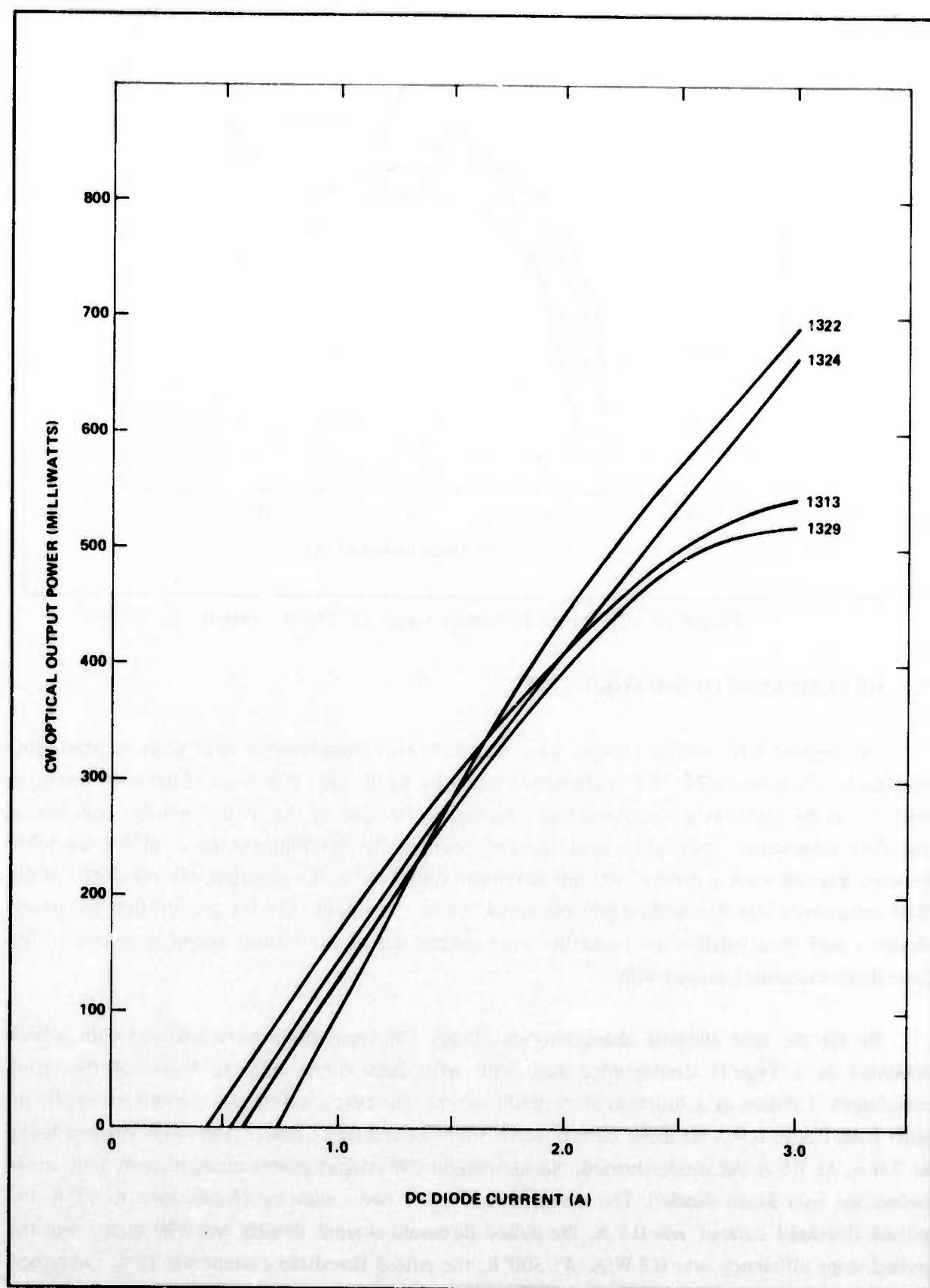


Figure 18. CW Characteristics of Single Heterostructure Lasers

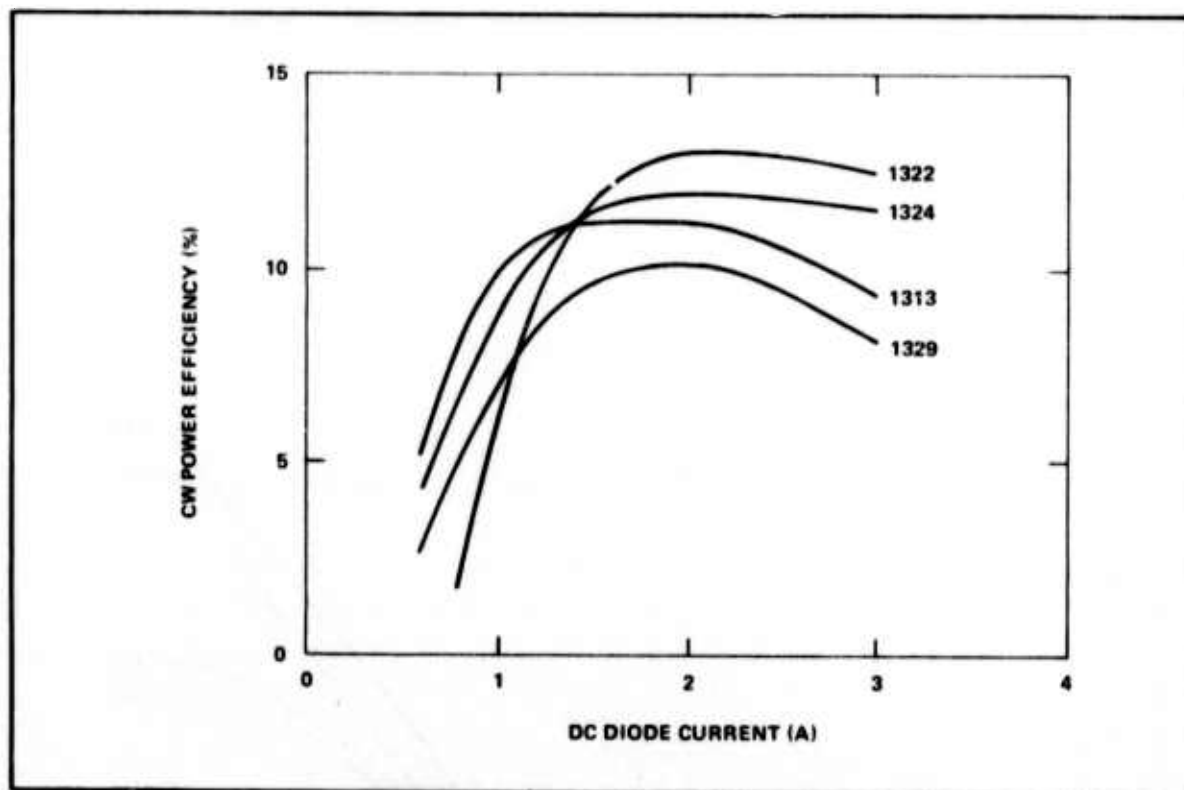


Figure 19. CW Power Efficiency versus DC Diode Current

3. HEAT SINKS WITH BeO SUBMOUNTS

The highest CW output powers were achieved with double-sided heat sinks incorporating rectangular Cu submounts. This is attributed primarily to the fact that most of the work was done with Cu as the assembly process was being developed. Because of the limited number and cost of the BeO submounts, they were used sparingly during the development of a reliable assembly process. Because such a process was not developed until late in the program, the capability of the BeO submounts was not sufficiently evaluated. An improvement over the present BeO submount design would be a smaller size to enable more control during the critical assembly process of the laser diode-submount subassembly.

By far the best thermal characteristics of any CW laser diode were achieved with a laser mounted in a Type II double-sided heat sink with BeO submounts. In Figure 24 the lasing wavelength is shown as a function of dc diode current. The lasing wavelength showed essentially no shift from 0.8 to 6.0 A dc diode current or 18.6 W electrical input power. The diode stopped lasing at 7.0 A. At 7.5 A the diode shorted. No meaningful CW output power measurements were made before the laser diode shorted. The mirrored laser was 10 mils wide by 16 mils long. At 77° K, the pulsed threshold current was 0.8 A, the pulsed threshold current density was 800 A/cm² and the pulsed slope efficiency was 0.3 W/A. At 300° K, the pulsed threshold current was 18 A, the pulsed current density was 17,000 A/cm², and the pulsed slope efficiency was 0.24 W/A.

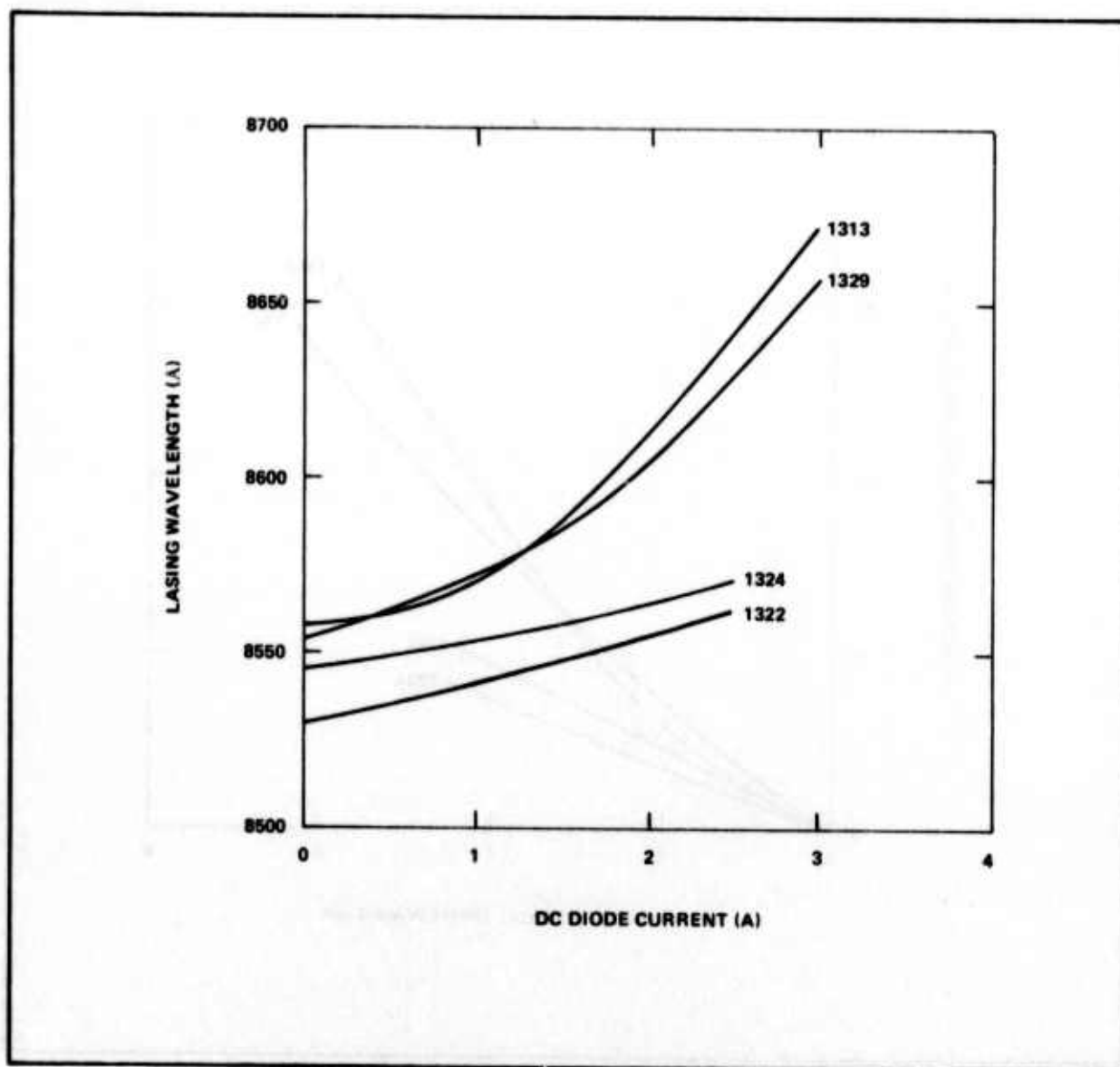


Figure 20. Lasing Wavelength versus DC Diode Current

The results on this CW laser diode indicate the potential improvement in the thermal characteristics which can be achieved with BeO submounts.

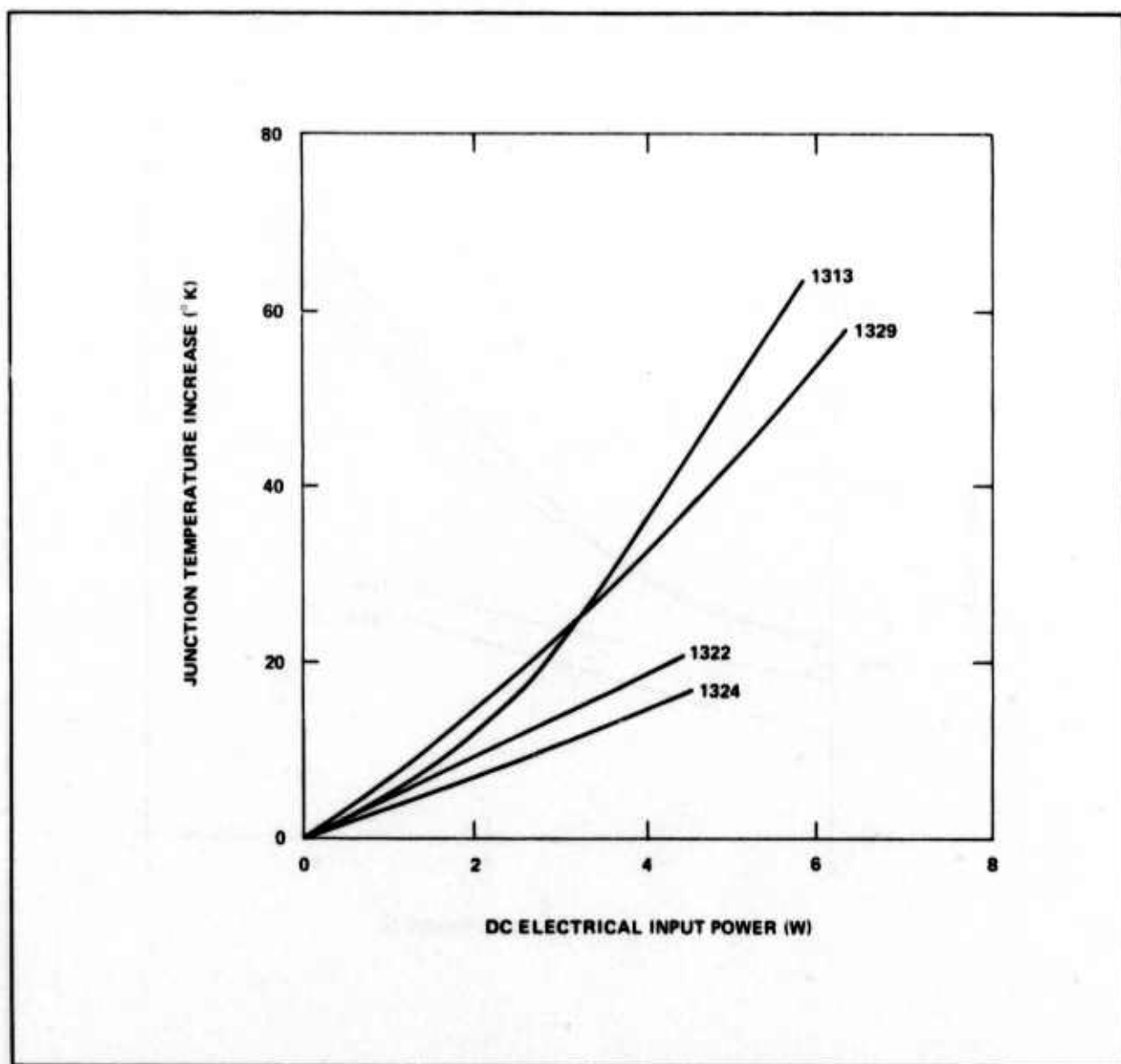


Figure 21. Junction Temperature Increase versus DC Electrical Input Power

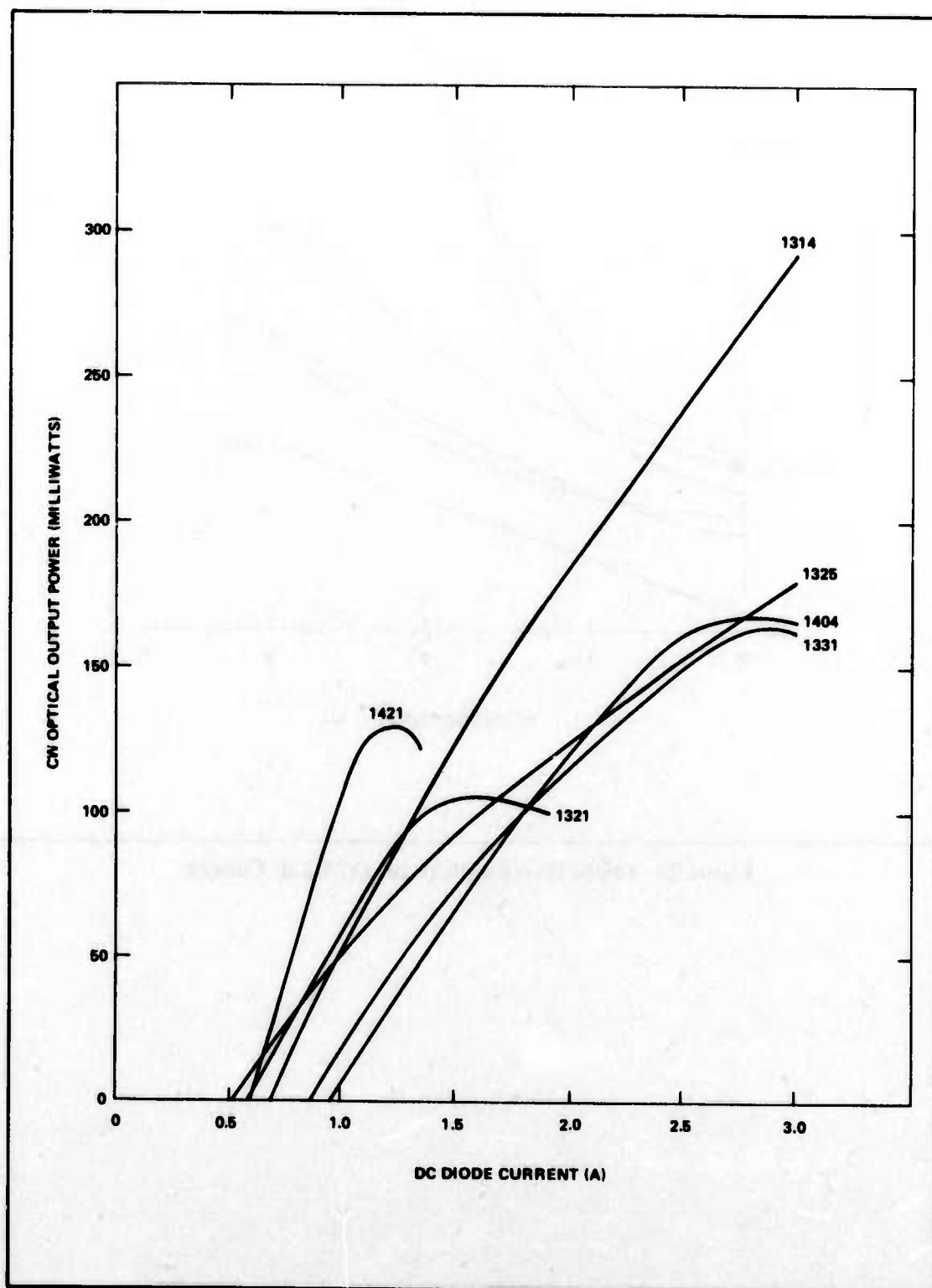


Figure 22. CW Characteristics of Single Heterostructure Lasers

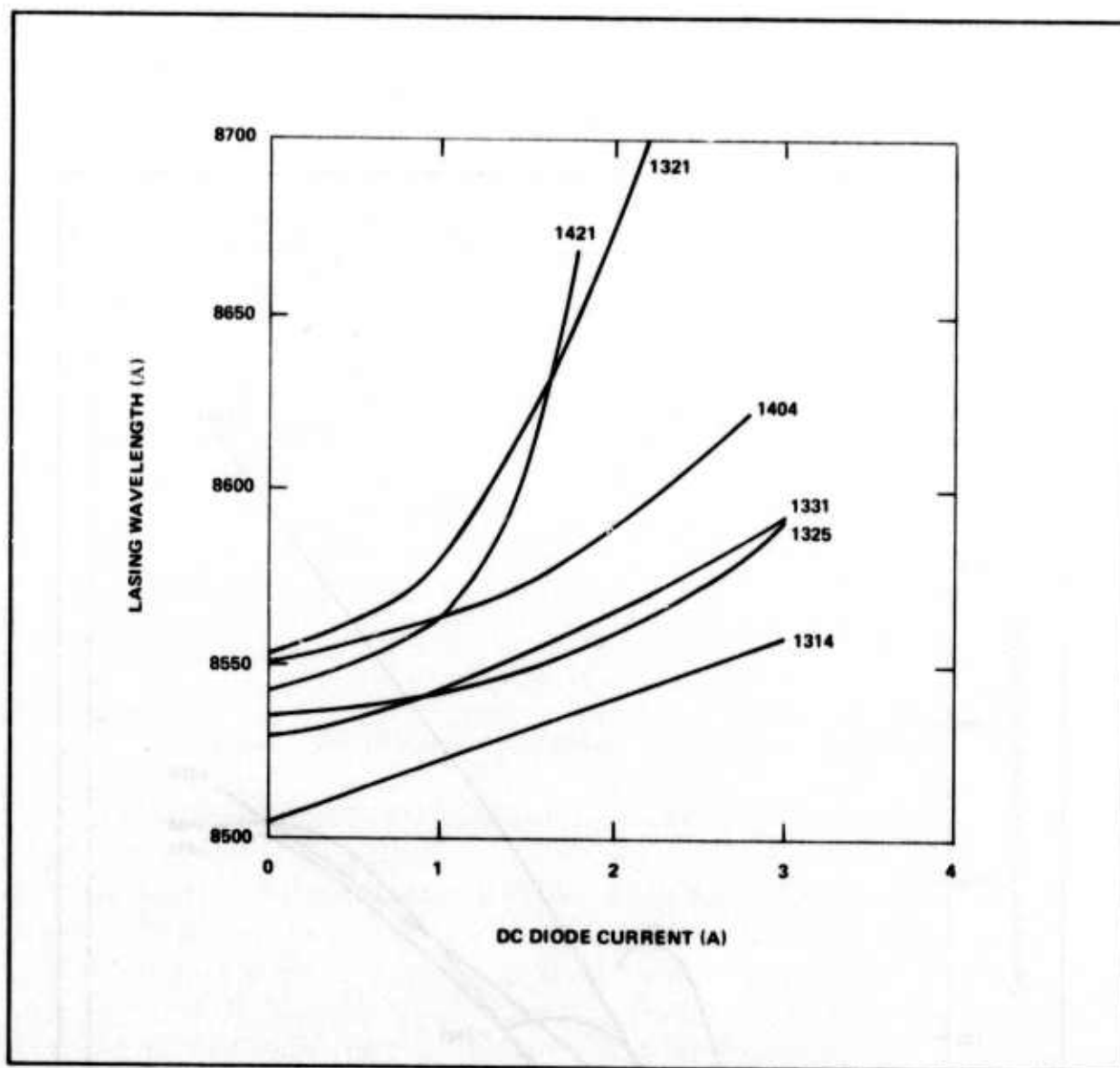


Figure 23. Lasing Wavelength versus DC Diode Current

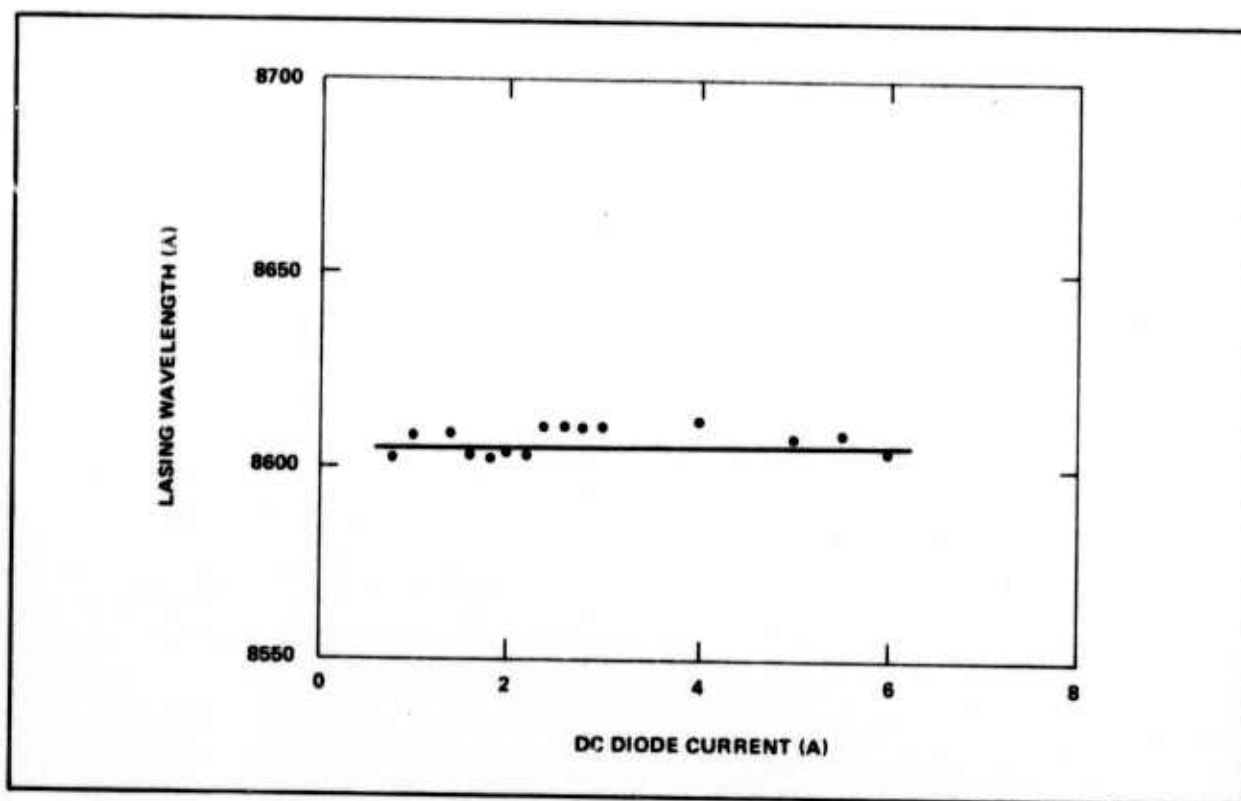


Figure 24. Lasing Wavelength versus DC Diode Current
(Diode 279-1, No. 2)

SECTION V

THEORETICAL ANALYSIS

1. INTRODUCTION

A theoretical analysis of the laser performance expected for a single heterostructure laser mounted in a double-sided heat sink is presented in this section. Because a relatively large laser-to-laser variation in CW performance is often observed for mounted lasers, a large number of devices would have to be assembled and tested to optimize the design. The results of a theoretical analysis can be used to guide the device design and to minimize the experimental work.

The expected CW optical output power is calculated for several submount materials and thicknesses and for various laser lengths. The general approach for the calculation is to first calculate the thermal resistance as a function of junction temperature, assuming all components are at the junction temperature. Then by graphical solution, the junction temperature is determined for various input powers to the diode assuming all power dissipation is at the junction. The junction temperature can then be estimated as a function of diode current. The CW output power can be estimated since the threshold current and the slope efficiency can be calculated as a function of current.

As the laser length increases, the slope efficiency decreases, the threshold current density decreases, the threshold current increases, the series resistance decreases, and the thermal resistance decreases. A careful consideration of these various factors indicates that a 12-mil-wide by 18-mil-long laser should be the optimum size for maximum CW output power with high overall power efficiency. The calculations also indicate that CW optical output powers of greater than 4 W can only be achieved by the use of high thermal conductivity submounts of diamond or single-crystal BeO.

The simplified approach used for the calculation probably gives a conservative estimate for the ultimate CW output power for several reasons. An exact calculation would require a complex iterative computer program which is not justified because the parameters are not defined with sufficient accuracy. The actual thermal resistance as a function of junction temperature is probably less because the temperature of the various heat sink materials will not be at the junction temperature but will vary in temperature from the junction temperature to 77°K. Also, the junction

temperature may not increase with current as rapidly as calculated because part of the power ($\approx 10\text{-}20\%$) is removed in the form of the laser output power and thus does not have to be dissipated as heat. The heat generated due to the series resistance occurs uniformly in the diode and thus should not increase the junction temperature as much as predicted.

There are other factors, however, which might lower the actual output power compared to the calculated values. The primary factor is temperature gradients along the junction plane. If one area of the diode were significantly higher in temperature than the rest of the diode, the band-gap energy in that region would be smaller and the absorption of the lasing wavelength would increase. This consideration gives another reason for the use of a high thermal conductivity submount material which will minimize any thermal gradients along the plane of the junction. For heat spreading into a low thermal conductivity material, the temperature near the edges may be much cooler than at the center.

2. DOUBLE-SIDED HEAT SINK DESIGN

Figure 25 shows in detail the double-sided heat sink design assumed for the calculation. The GaAs laser diode is mounted between two submounts. An intermediate submount of high thermal conductivity material between the laser and the Cu can be used to reduce the thermal resistance by enabling the heat from the laser to spread over a larger area before reaching the Cu. If a high thermal conductivity submount is not used, the thermal spreading resistance of the heat from the laser into the Cu can be a significant portion of the total thermal resistance.

The dashed lines in Figure 25 indicate the effective thermal cross section assuming the heat spreads at a 45 degree angle in the submount and in the copper and flows in one dimension in the GaAs, In, and Au. The value of the angle θ may vary from zero for no bevel to 45 degrees for a bevel on the submount edge for reduced thermal spreading resistance. The dashed line in the GaAs laser diode indicates the P-N junction. The P-type region is generally much thinner than the N-type region.

Since the submount can be an electrical insulator, a layer of Au is assumed plated onto the submount metallization for a high-current, low-resistance electrical path to the laser. A layer of In is plated on the Au layer to enable good thermal contact to the laser since In is sufficiently ductile at room temperature to flow under pressure to fill any voids or to absorb minor thickness nonuniformities. The submount is attached to the Cu with an In-to-In cold weld. Stripline with the same thickness as the laser is used as a mechanical spacer to protect the diode from excessive pressure and thus cracking. The use of stripline is one approach for coupling high electrical input power to the diode at high frequencies.

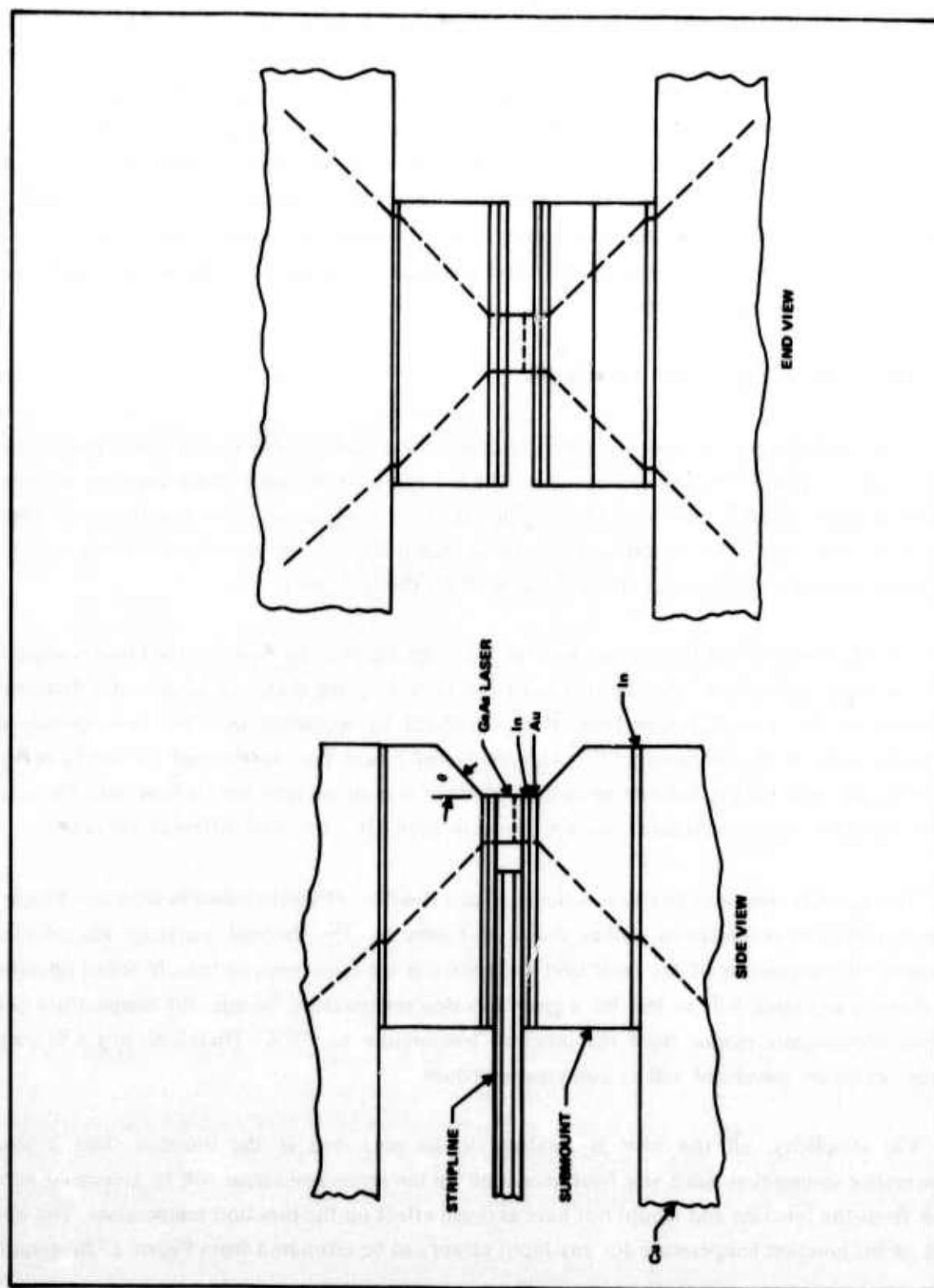


Figure 25. Double-Sided Heat Sink Design

The thermal conductivity values of various types of material which can be used for laser fabrication and assembly are shown in Figure 26 as a function of temperature between 77° K and 300° K. The values for most of the materials came from Gooch.³¹ The value for single crystal BeO was obtained from Slack and Austerman.³⁰ The thermal conductivity of GaAlAs is estimated from Afromowitz's³² work at room temperature and assuming a constant factor with respect to GaAs for lower temperatures. As shown in Figure 26, even though Cu is the best heat conductor at room temperature (except for diamond), its thermal conductivity increases only slightly at 77° K. However, the thermal conductivity of many other materials increases almost exponentially with decreasing temperature. At 77° K, diamond, BeO, Si, and Be have higher values of thermal conductivity than Cu. The junction of the laser may reach a temperature of 150° K at maximum CW output power. The submount material would then be at some intermediate temperature between 77° K and 150° K. Only single-crystal BeO and diamond could have significant reductions in the thermal resistance compared to Cu.

3. THERMAL RESISTANCE ANALYSIS

A detailed thermal analysis has been performed for a single heterostructure laser mounted in a double-sided heat sink for two cases, one in which a 1-mm (0.040-inch) thick diamond submount with a 45-degree bevel is used and one in which the laser diode is mounted directly on the edge of the copper heat sink. The materials, the thermal conductivities, the material thicknesses, and the calculated thermal resistances are listed in Table III for the two cases.

One-dimensional heat flow is assumed for the GaAs, In, and Au since the thickness is much less than the width and length. The thermal resistance caused by the diamond submount is determined primarily by the spreading resistance. It is calculated by assuming that the heat spreads at a 45 degree angle in the submount.³³⁻³⁵ One-dimensional heat flow is assumed for the In between the submount and the Cu. Infinite spreading resistance is assumed into the Cu heat sink. The results of the calculation of thermal resistance are shown in Table III for several different size lasers.

The thermal resistance has been calculated as a function of temperature as shown in Figure 27 using the thermal conductivity values shown in Figure 26. The thermal resistance was calculated assuming all components of the laser heat sinks were at the same temperature. In actual operation, the thermal resistance will be less for a given junction temperature because the temperature of the various components ranges from the junction temperature to 77° K. Therefore, any CW output powers which are calculated will be conservative values.

For simplicity, all the heat is assumed to be generated at the junction. This is also a conservative assumption since any heat generated by the series resistance will be generated mostly away from the junction and would not have as much effect on the junction temperature. The upper limit of the junction temperature for any input power can be estimated from Figure 27 by graphical

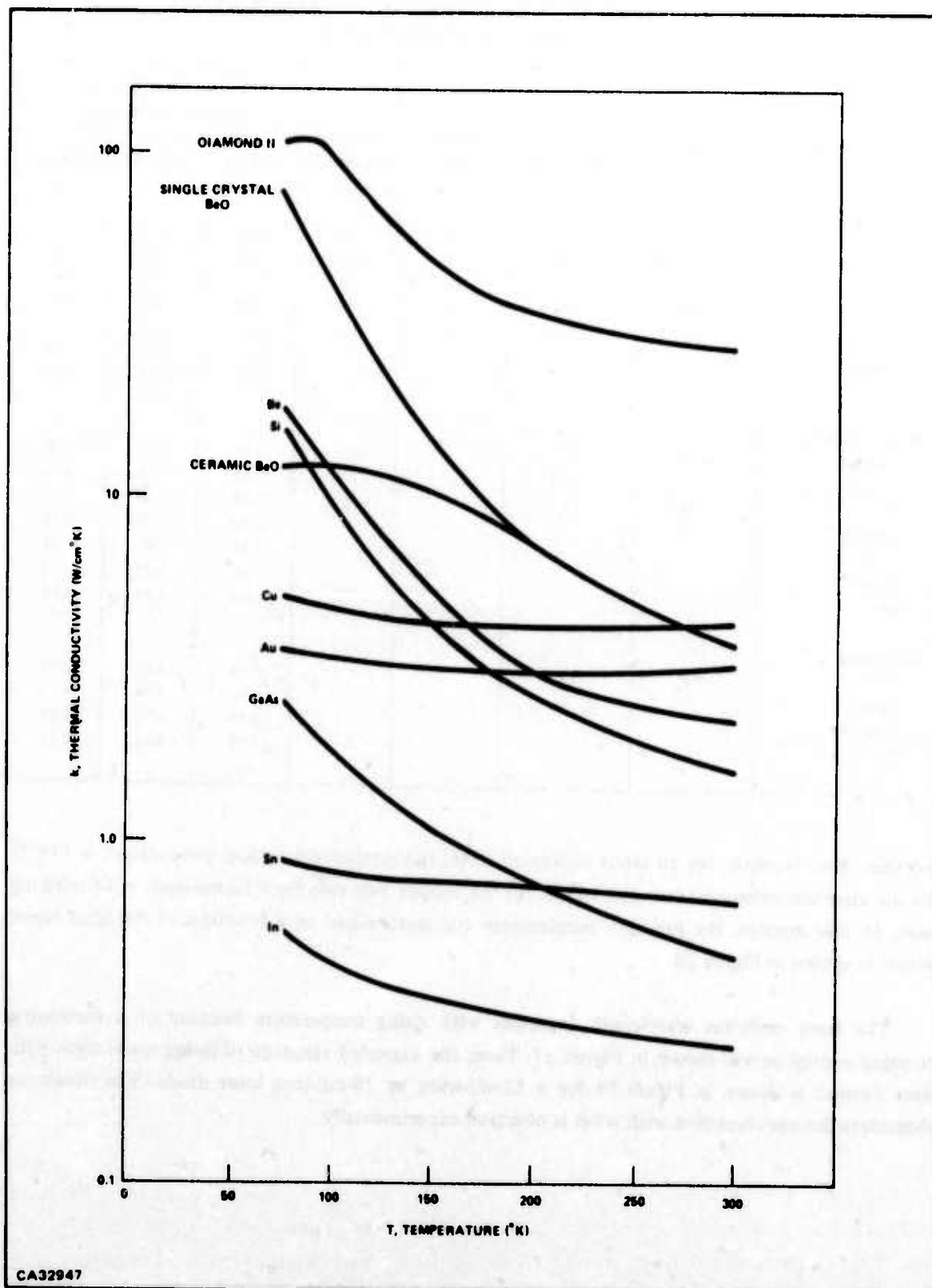


Figure 26. Thermal Conductivity as a Function of Temperature

**TABLE III. THERMAL CHARACTERISTICS OF COMPONENTS
OF MOUNTED LASER DIODE AT 77°K**

| Region Material | Thermal Conductivity (W/°K-cm) | Thermal Conductivity (mW/°K-mil) | Thickness (μ m) | Thickness (mils) | Thermal Resistance (°C/W) Width X Length (mils ²) | | |
|-------------------------|--------------------------------------|--|-------------------------|---------------------|--|---------|---------|
| | | | | | 12 X 12 | 12 X 18 | 12 X 24 |
| Laser Diode | | | | | | | |
| GaAs-P | 2.5 | 6.4 | 5 | 0.2 | 0.22 | 0.15 | 0.11 |
| GaAlAs-P | 0.8 | 2.0 | 3 | 0.12 | 0.42 | 0.28 | 0.21 |
| GaAs-N | 2.5 | 6.4 | 92 | 3.6 | 2.82 | 1.88 | 1.41 |
| In | 0.52 | 1.3 | 8 | 0.3 | 1.60 | 1.07 | 0.80 |
| Au | 3.5 | 8.9 | 8 | 0.3 | 0.24 | 0.16 | 0.12 |
| Subtotal - P | | | | | 2.48 | 1.66 | 1.24 |
| Subtotal - N | | | | | 4.66 | 3.11 | 2.33 |
| Diamond Submount | | | | | | | |
| Diamond | 108 | 274 | | 40 | 0.13 | 0.11 | 0.09 |
| Indium | 0.52 | 1.3 | | 1 | 0.09 | 0.09 | 0.08 |
| Cu | 5.0 | 13 | | ∞ | 0.58 | 0.56 | 0.53 |
| Subtotal | | | | | 0.80 | 0.76 | 0.70 |
| Total - P | | | | | 3.28 | 2.42 | 1.94 |
| Total - N | | | | | 5.46 | 3.87 | 3.03 |
| Net | | | | | 2.05 | 1.49 | 1.18 |
| Cu Directly | | | | | | | |
| Cu | 5.0 | 13 | | ∞ | 4.44 | 3.52 | 2.96 |
| Total - P | | | | | 6.92 | 5.18 | 4.20 |
| Total - N | | | | | 9.10 | 6.63 | 5.29 |
| Net | | | | | 3.92 | 2.91 | 2.34 |

solution. For example, for an input power of 20 W, the estimated junction temperature is 118°K for the diamond submount case and 163°K for the copper only case for a 12-mil-wide X 18-mil-long laser. In this manner, the junction temperature was determined as a function of electrical input power as shown in Figure 28.

The laser emission wavelength increases with rising temperature because of a decreasing bandgap energy as was shown in Figure 17. Thus, the expected variation of lasing wavelength with laser current is shown in Figure 29 for a 12-mil-wide by 18-mil-long laser diode. The nonlinear characteristics are consistent with what is observed experimentally.

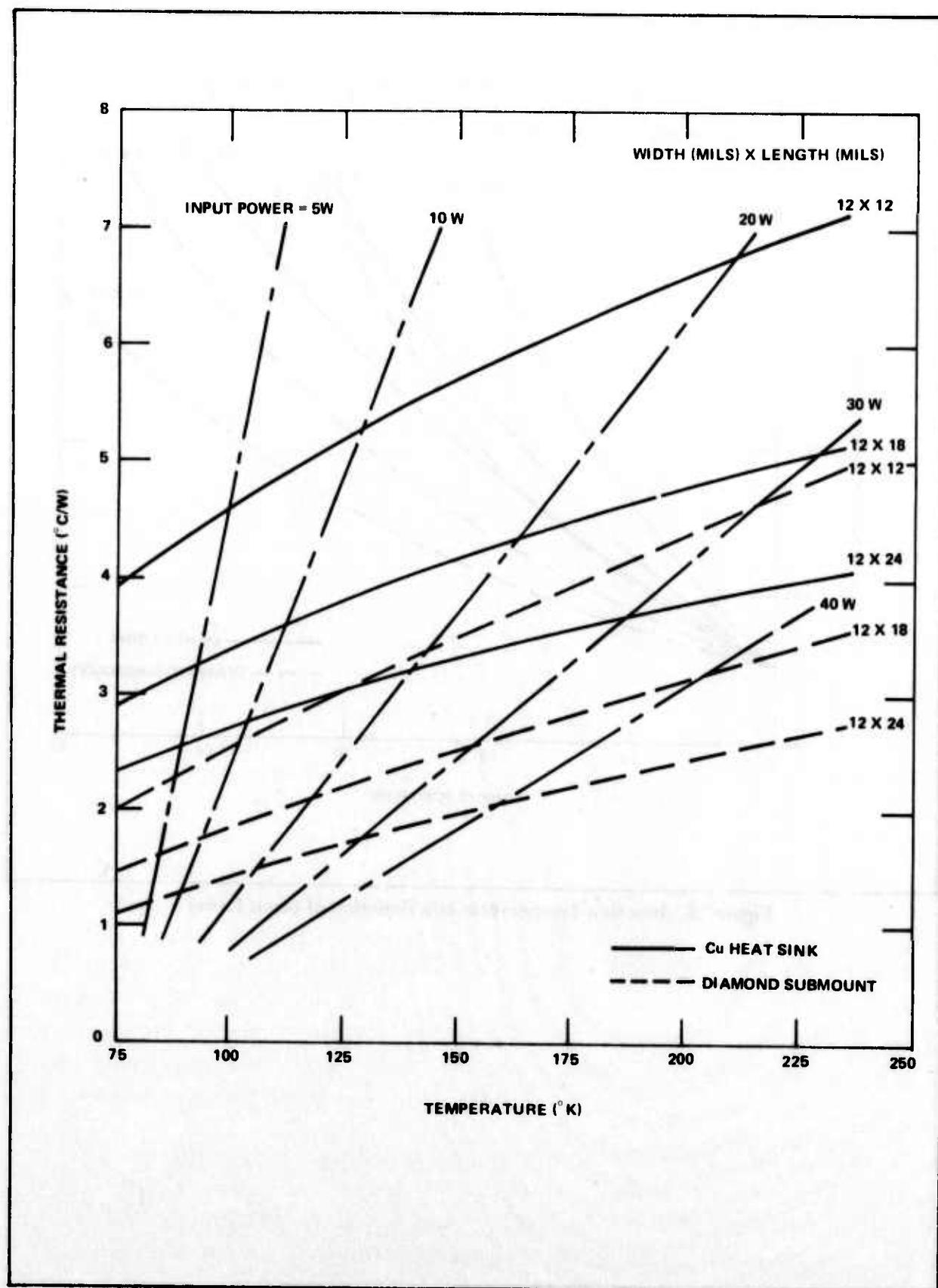


Figure 27. Thermal Resistance as a Function of Temperature

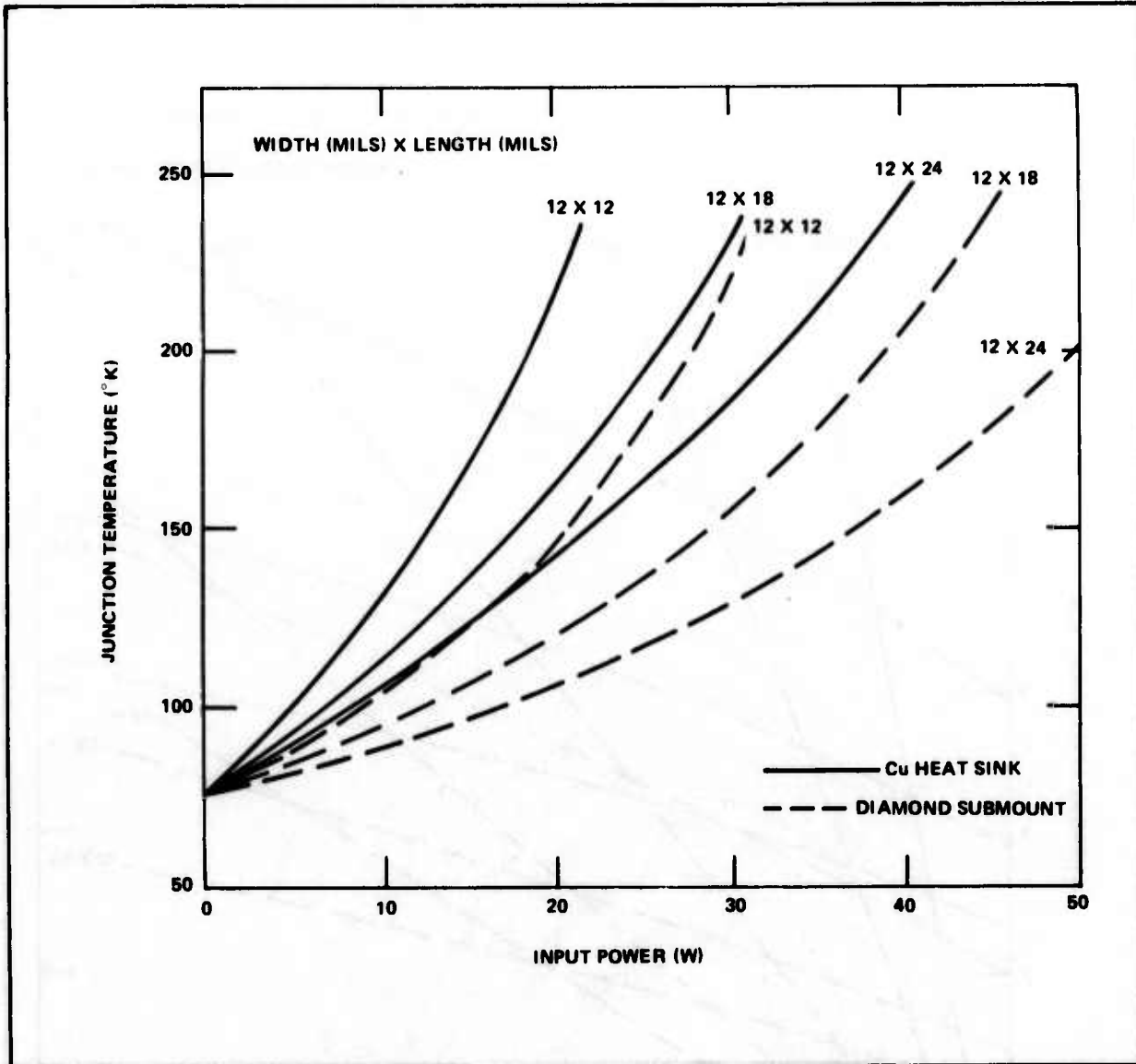


Figure 28. Junction Temperature as a Function of Input Power

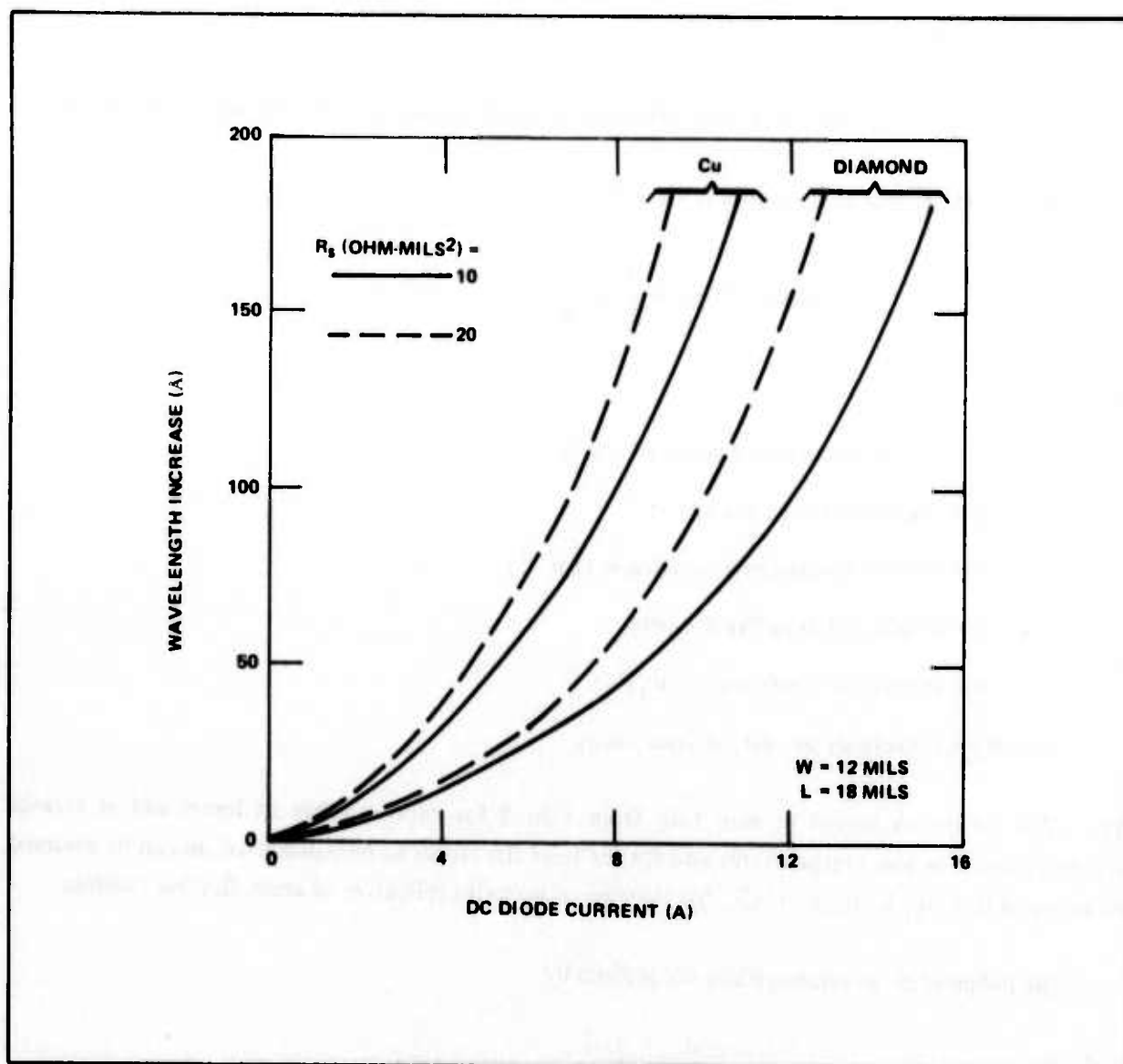


Figure 29. Wavelength Increase versus DC Diode Current

4. CW LASER OPERATION

The basic equations and parameters affecting the performance of a laser diode are discussed.

The gain coefficient at threshold is given by

$$g_t = \beta J_t^m = \alpha + \frac{1}{L} \ln \frac{1}{R} \quad (1)$$

where

J_t = threshold current density (A/cm^2)

β = gain constant (cm/kA)

α = loss (or absorption) coefficient (cm^{-1})

L = length of Fabry-Perot cavity

R = reflection coefficient = $(R_1 R_2)^{1/2}$

R_1, R_2 = reflectivity at ends of laser cavity

The value of the exponent m may vary from 1 to 3 for various types of lasers and at various temperatures. For low temperatures and for the laser structures to be considered, m can be assumed to be equal to 1. R_1 is equal to 0.32 for the case of no extra reflective or antireflective coatings.

The differential quantum efficiency is given by

$$\eta_d = \eta_i \frac{\frac{1}{L} \ln \frac{1}{R}}{\alpha + \frac{1}{L} \ln \frac{1}{R}} \quad (2)$$

where

η_i = internal quantum efficiency

The slope efficiency with units of watts per ampere is actually a more practical parameter. It is given by

$$\eta_{\Delta} = \eta_d V_p \quad (3)$$

where

V_p = equivalent voltage of a photon ($= 1.24/\lambda$ where λ is in micrometers)

The optical output power is given by

$$\begin{aligned} P_o &= \eta_{\Delta} (J - J_t) LW \\ &= \eta_{\Delta} (I - I_t) \end{aligned} \quad (4)$$

where

J = operating current density

W = width of laser cavity

I = operating current

I_t = threshold current

The power efficiency is given by

$$\eta_p = \frac{P_o}{I(V_j + R_e I)} \quad (5)$$

where

V_j = junction voltage ($= 1.5$ V)

R_e = electrical series resistance $= R_s/WL$

R_s = diode specific resistance (ohms-area)

The values of α and β are shown in Figure 30 as a function of temperature^{3,9} for three types of lasers, the conventional diffused, the epitaxial diffused, and the single heterostructure. The calculated values of threshold current are shown in Figure 31 for 12-mil-wide X 24-mil-long lasers. A comparison of the results of the various lasers indicates that the single heterostructure laser has the lowest threshold current over the entire temperature range from 77° K to 300° K.

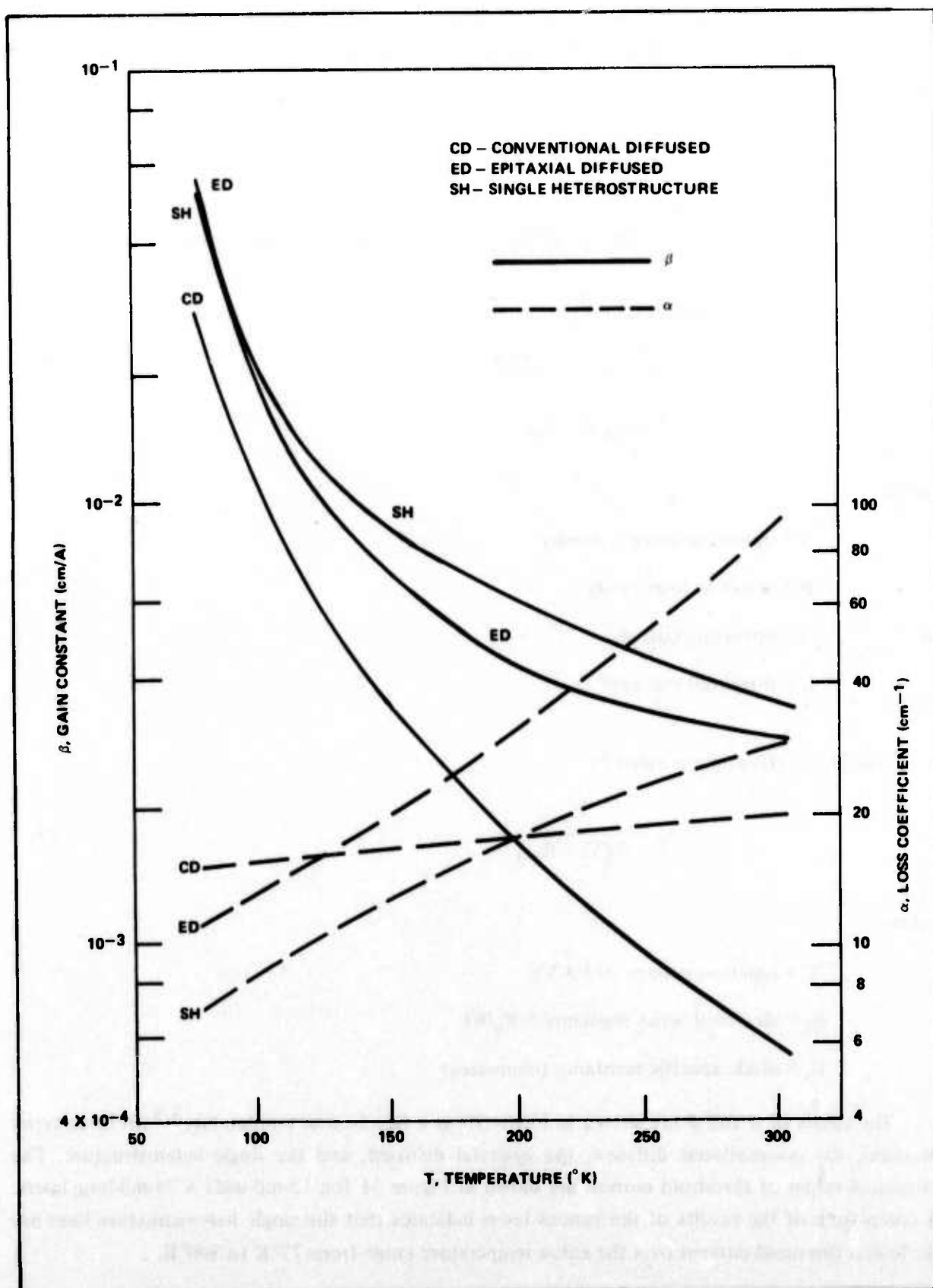


Figure 30. Temperature Dependence of Laser Optical Properties

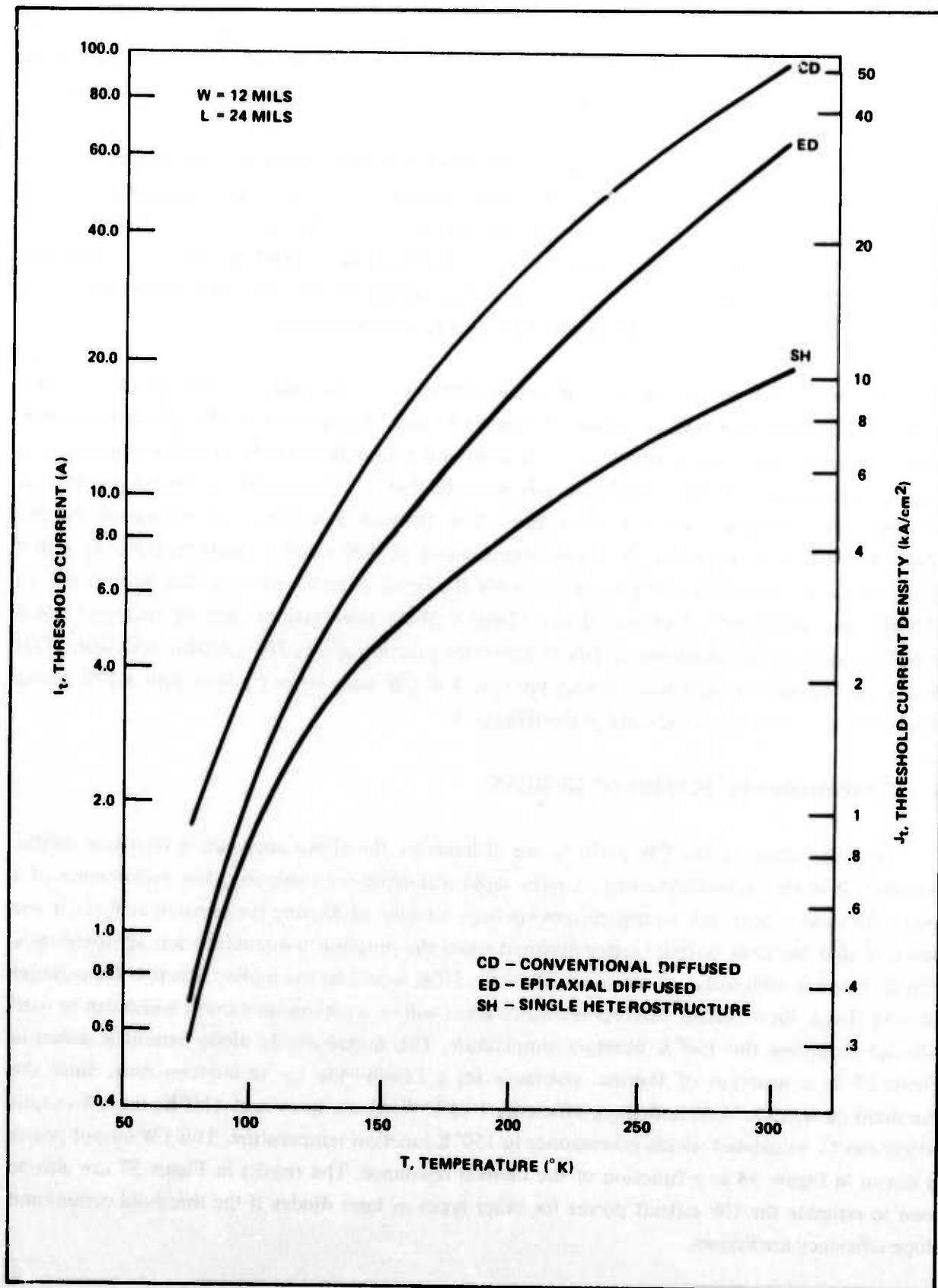


Figure 31. Temperature Dependence of Threshold Conditions

The threshold current is shown as a function of temperature for three sizes of lasers in Figure 32. The internal quantum efficiency is assumed to decrease linearly from 80% at 77° K to 50% at 300° K.^{9,10} The resulting slope efficiencies for various laser lengths are shown in Figure 33.

The basic approach for calculating the expected CW output power at a certain current is to determine the total electrical input power. From Figure 28, the junction temperature can be estimated, and knowing this temperature and the laser size, the effective threshold current can be determined from Figure 32. The output power is calculated by multiplying the slope efficiency from Figure 33 times the difference between the total current and the threshold current. The result is a family of curves for various laser lengths and specific series resistances.

The CW output power and the CW power efficiency versus direct current for the case of a diamond submount heat sink are shown in Figures 34 and 35 respectively. The CW output power versus current for the case in which the laser is mounted directly on Cu is shown in Figure 36. A careful consideration of the various factors indicate that a 12-mil-wide by 18-mil-long laser is probably the optimum size to investigate. The thermal and electrical resistances of the 12-mil X 12-mil laser are too high. Some improvement in performance could be achieved with a 12-mil by 24-mil laser but not enough to justify the larger currents which would be required. In addition, any projected advantage of the 12-mil X 24-mil laser may be lost by increased losses caused by increased temperature variations across the junction plane. The calculation indicates that at 8 A, the 12-mil X 18-mil laser should produce 4 W CW laser output power with a 27% power efficiency for a 10 ohm-mil² specific series resistance.

5. COMPARISON OF SUBMOUNT DESIGNS

The calculation of the CW performance of lasers by the above approach is relatively simple. However, it is very time-consuming. A more rapid technique for comparing the performance of a laser with various heat sink configurations has been established. During the previous analysis, it was observed that the peak output power occurred when the junction temperature was approximately 150° K. One can arbitrarily choose to specify that 150° K would be the highest junction temperature allowed. Then, for a certain thermal resistance there will be a maximum current which can be used without exceeding the 150° K junction temperature. This maximum dc diode current is shown in Figure 37 as a function of thermal resistance for a 12-mil-wide by 18-mil-long laser. Since the threshold current (3.94 A) and slope efficiency (0.492 W/A) are known at 150° K, the CW output power can be calculated which corresponds to 150° K junction temperature. This CW output power is shown in Figure 38 as a function of the thermal resistance. The results in Figure 37 can also be used to estimate the CW output power for other types of laser diodes if the threshold current and slope efficiency are known.

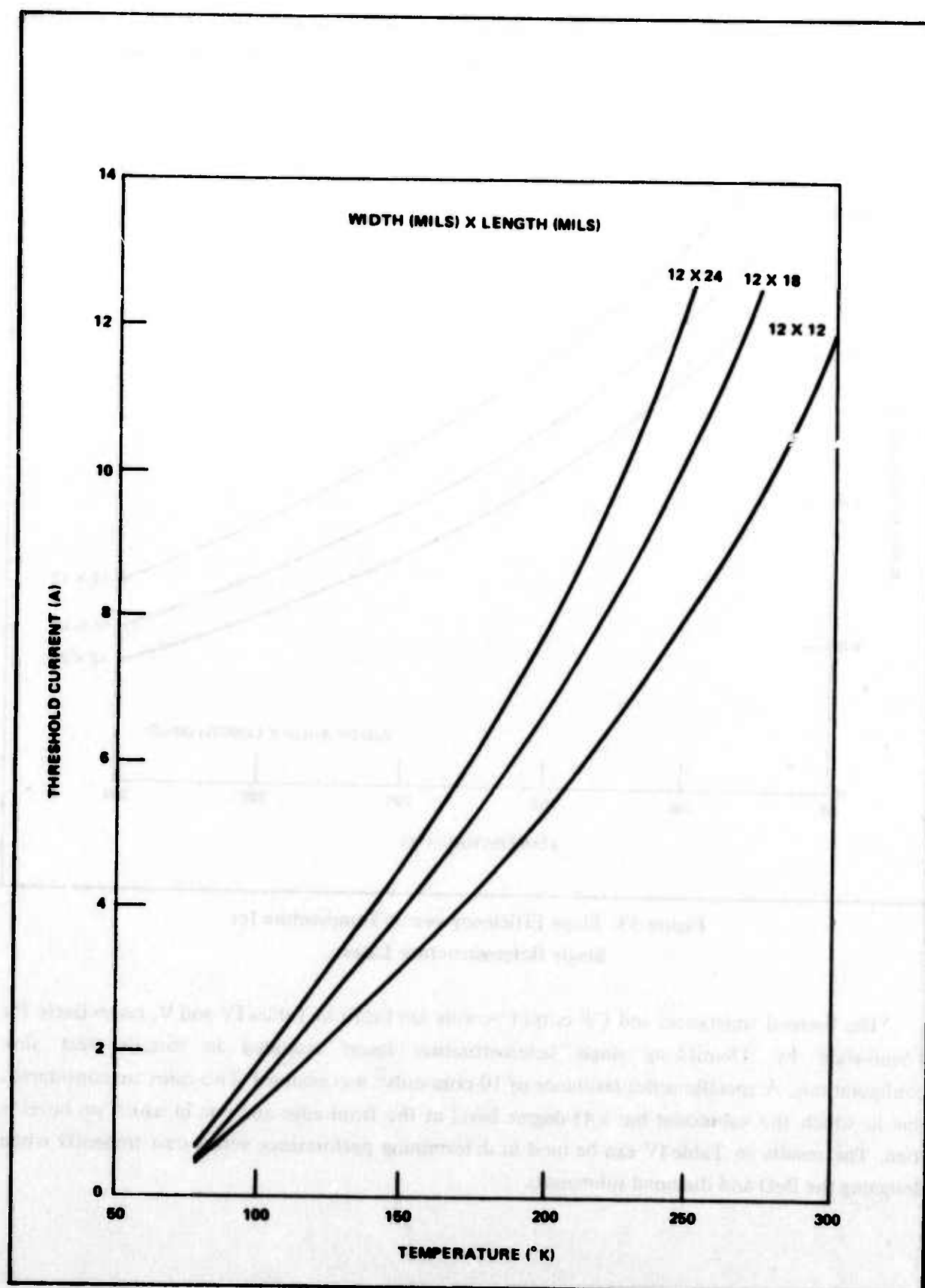


Figure 32. Threshold Current versus Temperature for Single Heterostructure Lasers

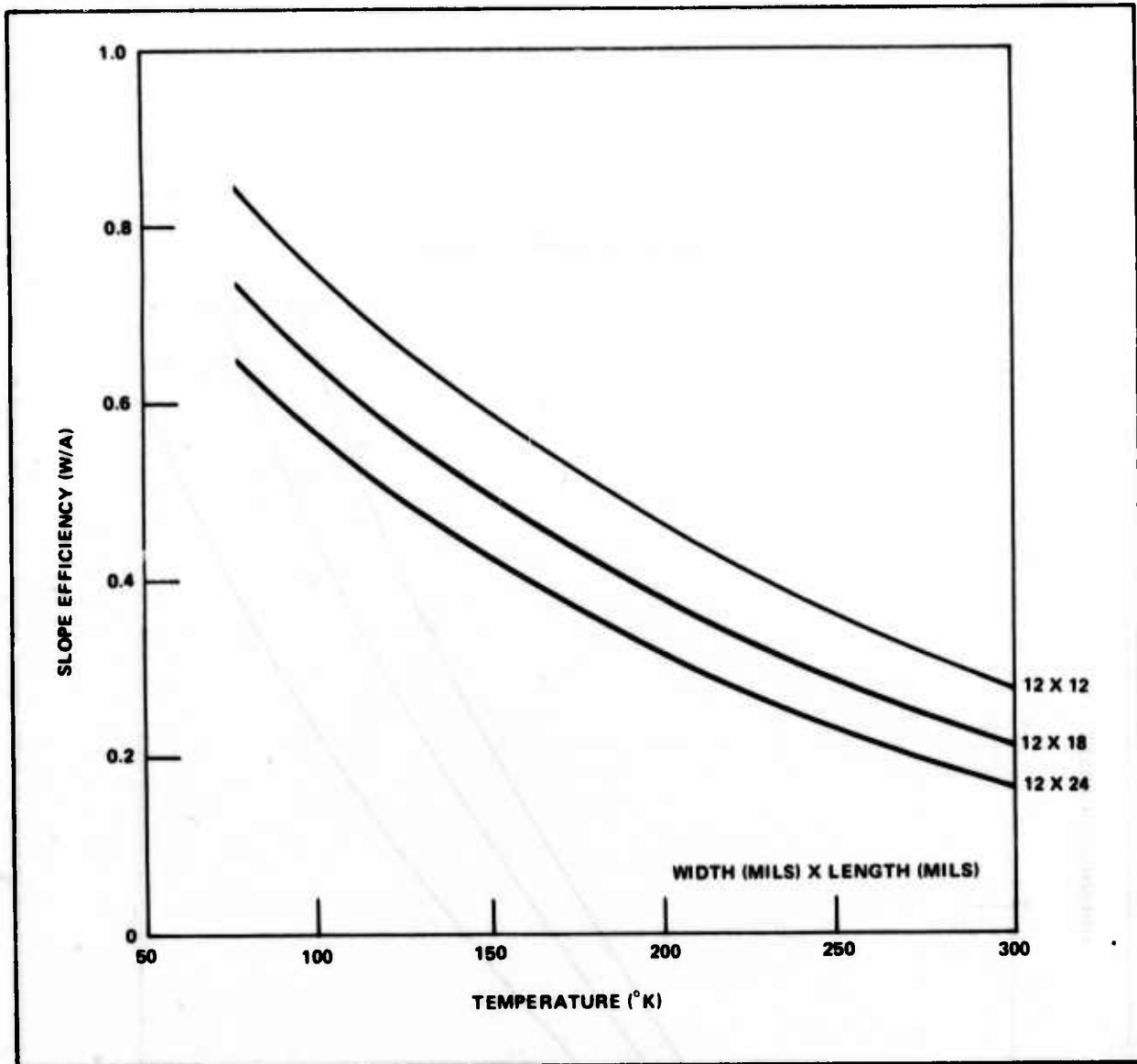


Figure 33. Slope Efficiency versus Temperature for Single Heterostructure Lasers

The thermal resistances and CW output powers are listed in Tables IV and V, respectively for 12-mil-wide by 18-mil-long single heterostructure lasers mounted in various heat sink configurations. A specific series resistance of 10 ohm-mils² was assumed. Two cases are considered: one in which the submount has a 45-degree bevel at the front edge and one in which no bevel is used. The results in Table IV can be used in determining performance versus cost tradeoffs when designing the BeO and diamond submounts.

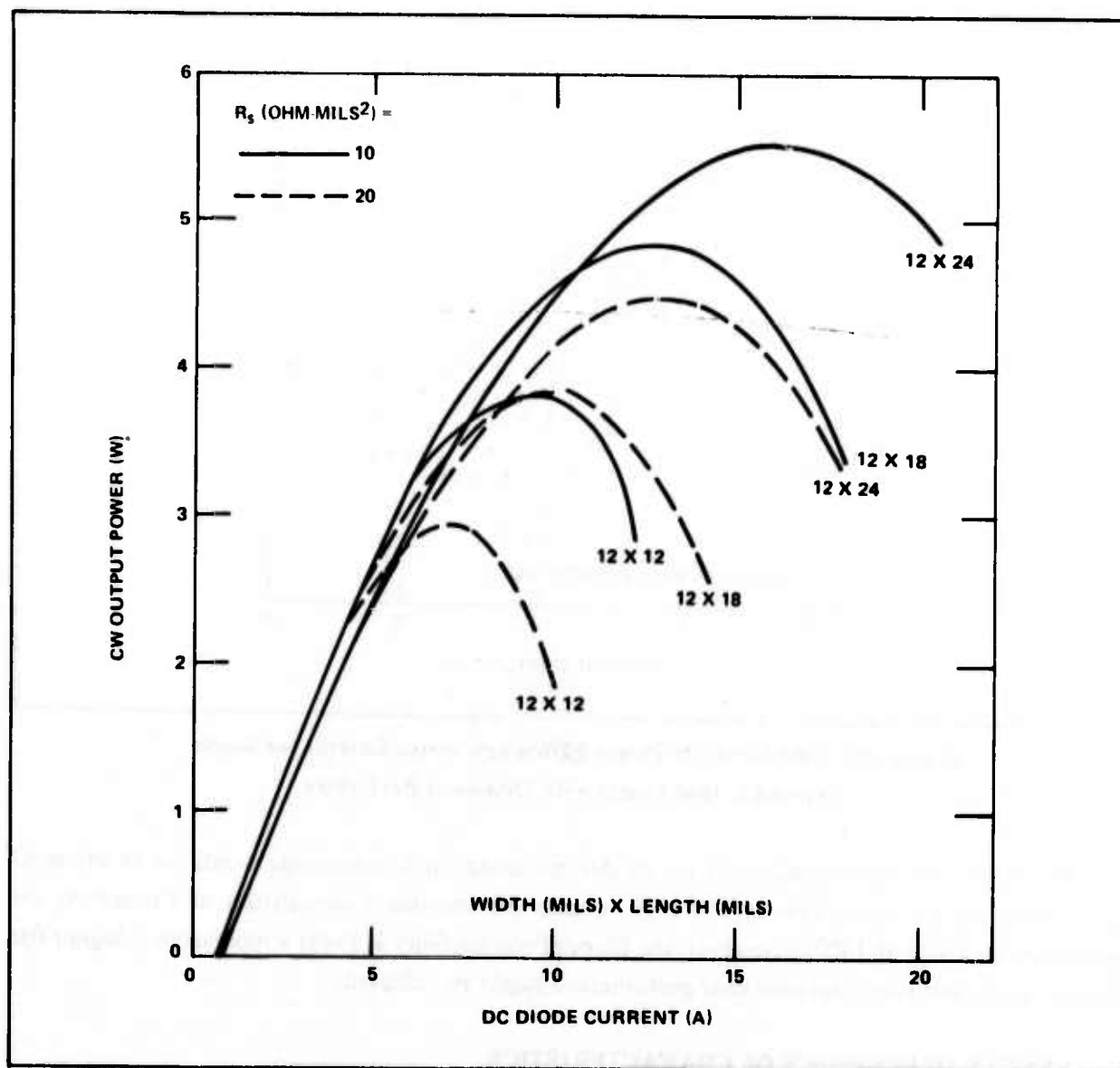


Figure 34. Calculated CW Output Power versus Current for Single Heterostructure Lasers with Diamond Heat Sinks

The results in Tables IV and V demonstrate the increased CW output powers expected by the use of high thermal conductivity submounts. Increasing the submount thickness increases the projected performance. The use of a bevel results in the greatest improvement when Cu heat sinks are used. Typically, a factor of 2 increase in CW output power is expected for a double-sided heatsink compared to a one-sided heat sink with a greater relative increase for Cu and a smaller relative increase for high thermal conductivity submount.

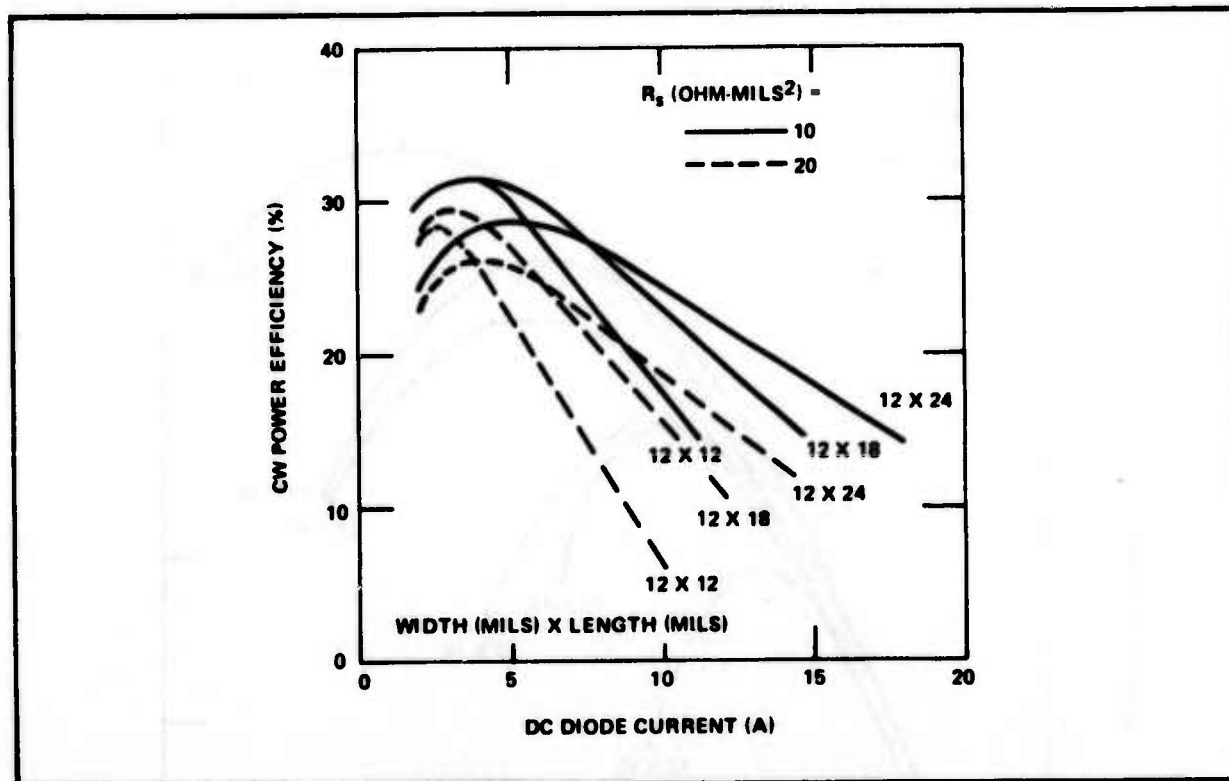


Figure 35. Calculated CW Power Efficiency versus Current for Single Heterostructure Lasers with Diamond Heat Sinks

The projected performance of laser diodes mounted on Si submounts would be identical to that shown for Cu submounts in Table III because the thermal conductivities of Cu and Si are essentially identical at 150° K. However, the thermal conductivity at lower temperature is higher for Si than for Cu and thus improved laser performance might be achieved.

6. LENGTH DEPENDENCE OF CHARACTERISTICS

The threshold current and slope efficiency are very dependent on the device design. Using the equations and parameters discussed in Section V.4, the expected laser performance has been calculated as a function of laser length for diodes 12 mils wide for 77° K and 300° K. The calculated values of threshold current density, threshold current, and slope efficiency are shown in Figures 39, 40, and 41 respectively. The ratio of the threshold current at 300° K to the threshold current at 77° K and the ratio of the slope efficiency at 77° K to the slope efficiency at 300° K are shown in Figure 42 as a function of the laser length. These figures enable a rapid comparison of experimental results with calculated values and enable the estimation of the 77° K laser performance from the 300° K laser performance.

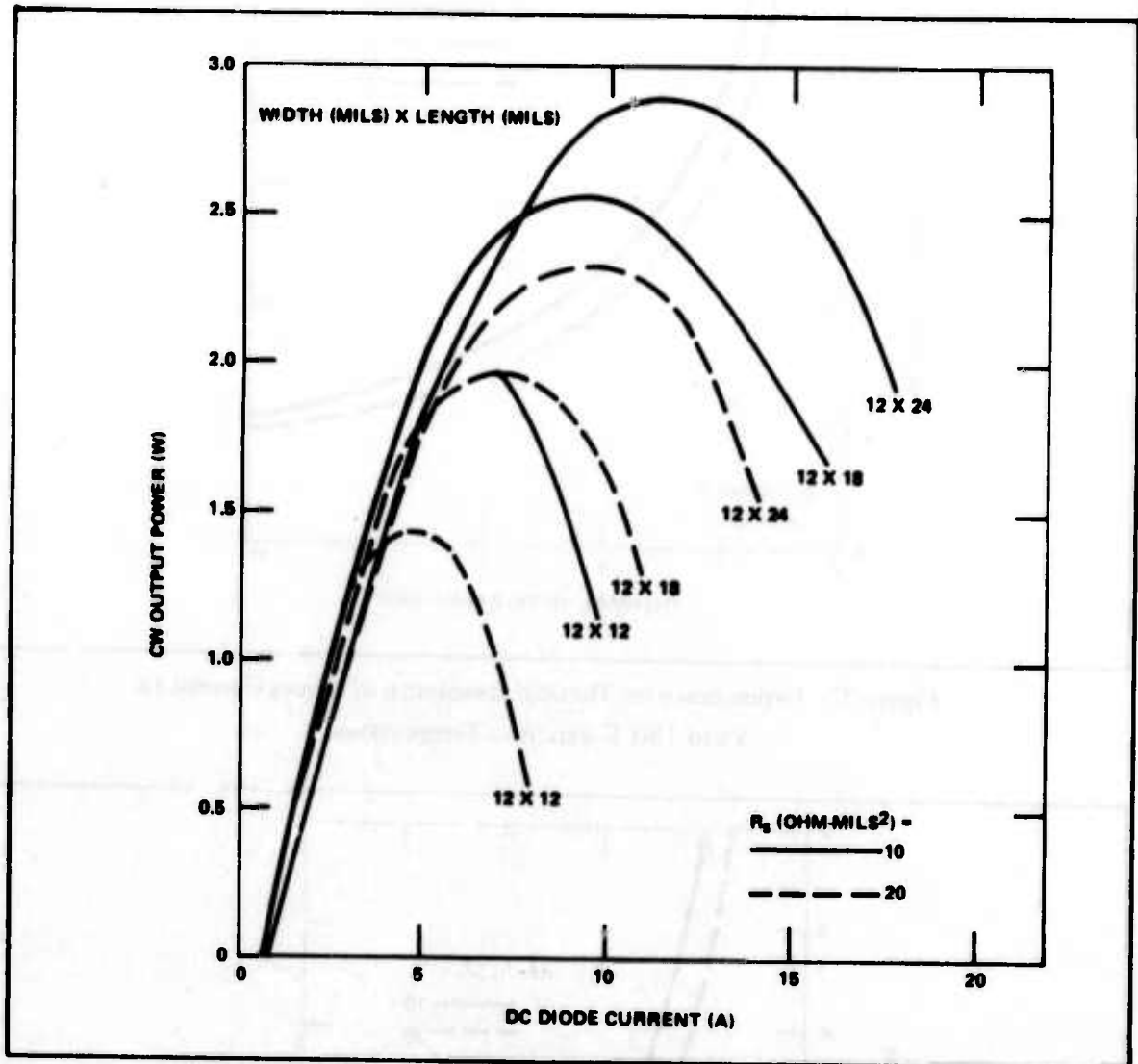


Figure 36. Calculated CW Output Power versus Current for Single Heterostructure Lasers Mounted Directly on Copper

The characteristics of the lasers from the good slices are in good agreement with the predicted values at 300° K. Usually the threshold current and slope efficiency do not change as much as predicted on cooling down to 77° K.

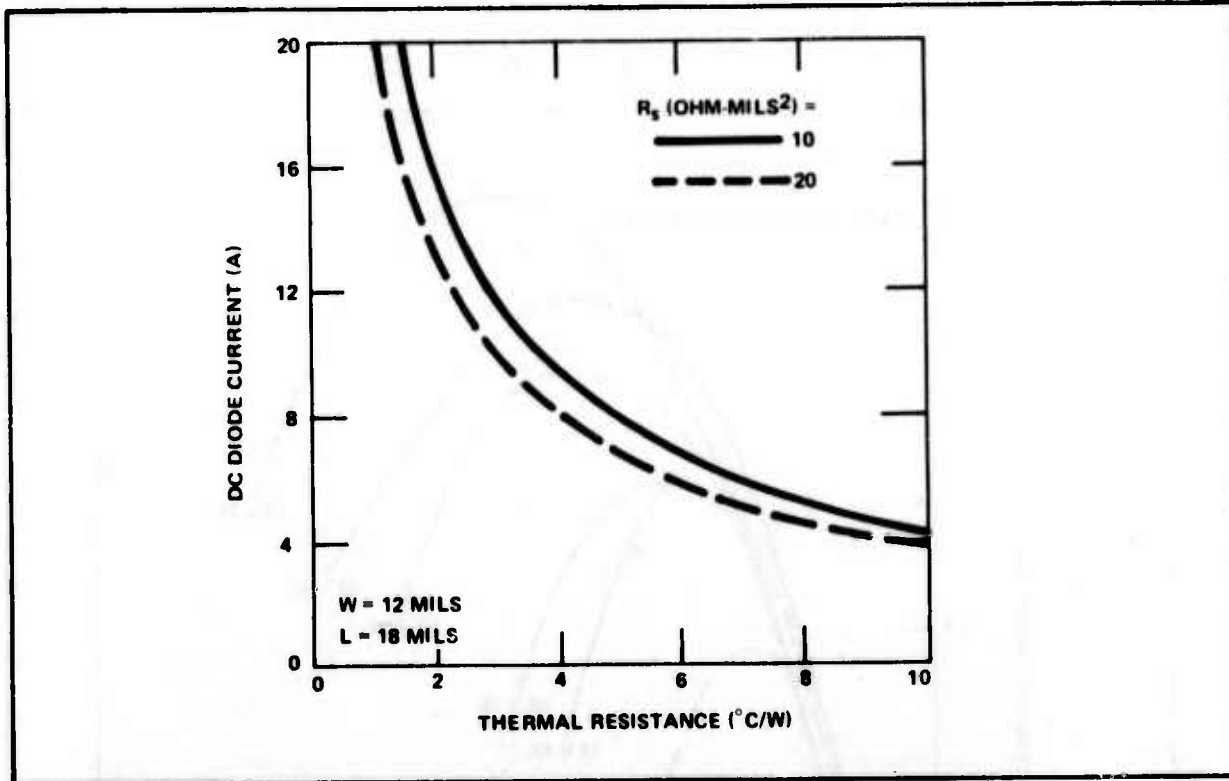


Figure 37. Dependence on Thermal Resistance of Direct Current to Yield 150° K Junction Temperature

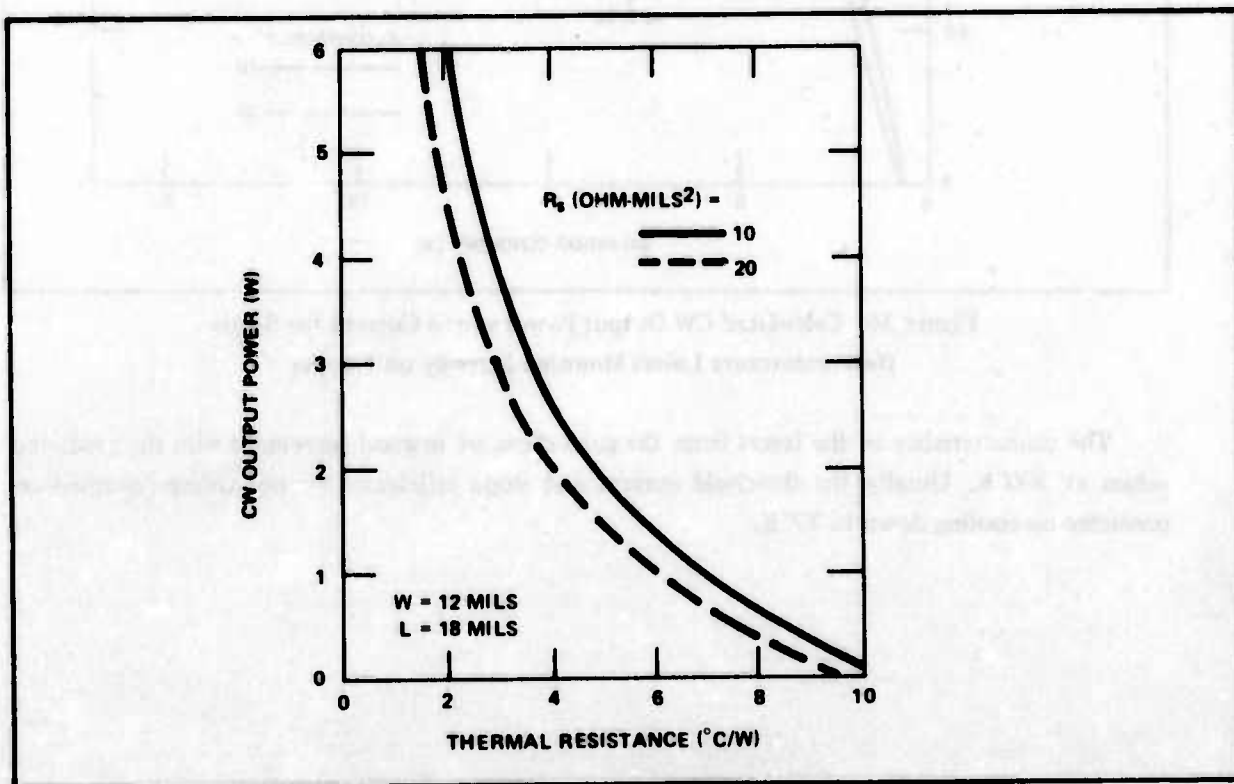


Figure 38. Calculated CW Output Power versus Thermal Resistance for Junction Temperature of 150° K

**TABLE IV. THERMAL RESISTANCE OF VARIOUS
HEAT SINK CONFIGURATIONS AT 150° K**

| Submount Thickness (mils) | Thermal Resistance (°C/W)* | | |
|----------------------------------|----------------------------|-----------|-----------|
| | 20 | 40 | 80 |
| Heat Sink Configuration** | | | |
| Cu Directly*** | | | |
| One-Sided | | | 7.00/5.90 |
| Double-Sided | | | 4.18/3.60 |
| Cu Submounts | | | |
| One-Sided | 7.60/6.63 | 7.20/6.27 | 7.06/6.05 |
| Double-Sided | 4.49/3.98 | 4.28/3.80 | 4.21/3.68 |
| BeO Submounts | | | |
| One-Sided | 5.70/5.09 | 4.96/4.47 | 4.55/4.12 |
| Double-Sided | 3.50/3.18 | 3.11/2.84 | 2.89/2.66 |
| Diamond Submounts | | | |
| One-Sided | 5.10/4.56 | 4.20/3.87 | 3.74/3.47 |
| Double-Sided | 3.18/2.89 | 2.70/2.52 | 2.45/2.30 |

*Values are for: No bevel/45° front bevel.

**For 12 mil wide X 18 mil long single heterostructure laser.

***No submount used.

**TABLE V. CALCULATED CW OUTPUT POWER OF VARIOUS
HEAT SINK CONFIGURATIONS AT 150° K**

| Submount Thickness (mils) | CW Output Power (W)* | | |
|----------------------------------|----------------------|-----------|-----------|
| | 20 | 40 | 80 |
| Heat Sink Configuration** | | | |
| Cu Directly*** | | | |
| One-Sided | | | 0.96/1.4 |
| Double-Sided | | | 2.56/3.09 |
| Cu Submounts | | | |
| One-Sided | 0.76/1.09 | 0.90/1.23 | 0.95/1.32 |
| Double-Sided | 2.25/2.73 | 2.46/2.88 | 2.50/3.00 |
| BeO Submounts | | | |
| One-Sided | 1.50/1.86 | 1.93/2.26 | 2.22/2.58 |
| Double-Sided | 3.23/3.64 | 3.74/4.16 | 4.08/4.48 |
| Diamond Submounts | | | |
| One-Sided | 1.84/2.23 | 2.51/2.82 | 2.94/3.25 |
| Double-Sided | 3.64/4.08 | 4.41/4.75 | 4.90/5.24 |

*Values are for: No bevel/45° front bevel.

**For 12 mil wide X 18 mil long single heterostructure laser.

***No submount is used.

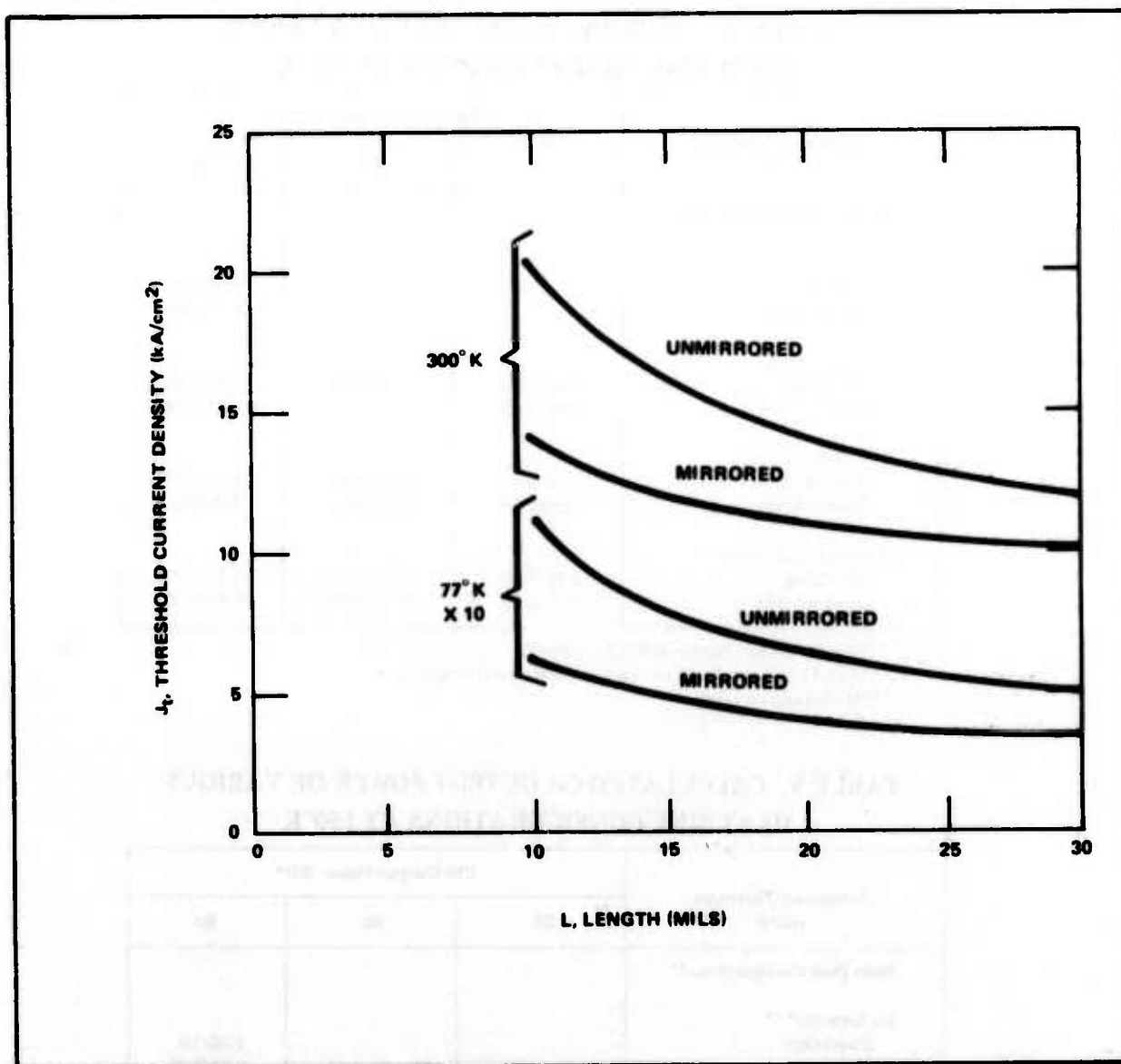


Figure 39. Calculated Threshold Current Density versus Length for Single Heterostructure Laser

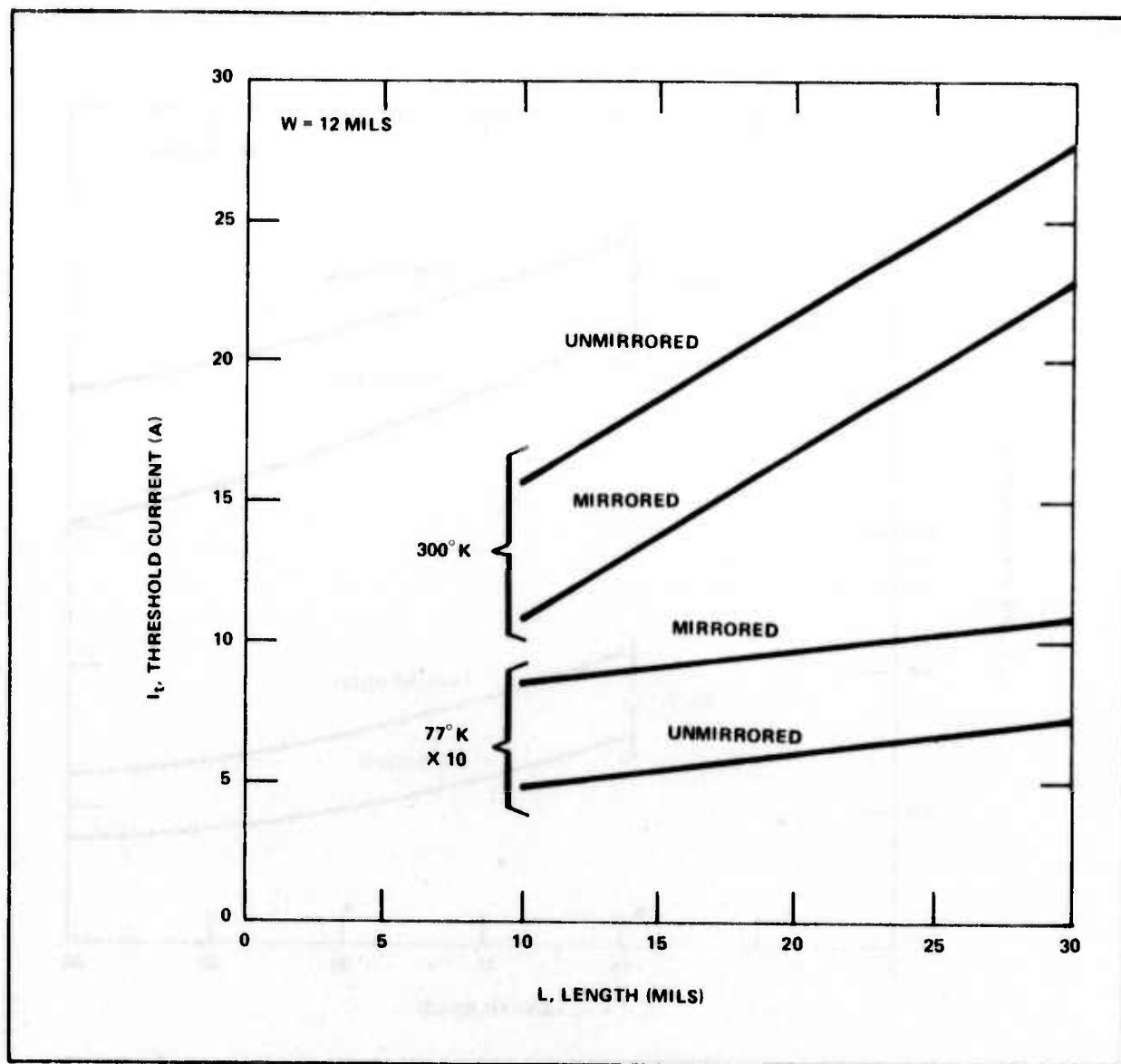


Figure 40. Calculated Threshold Current versus Length for Single Heterostructure Laser

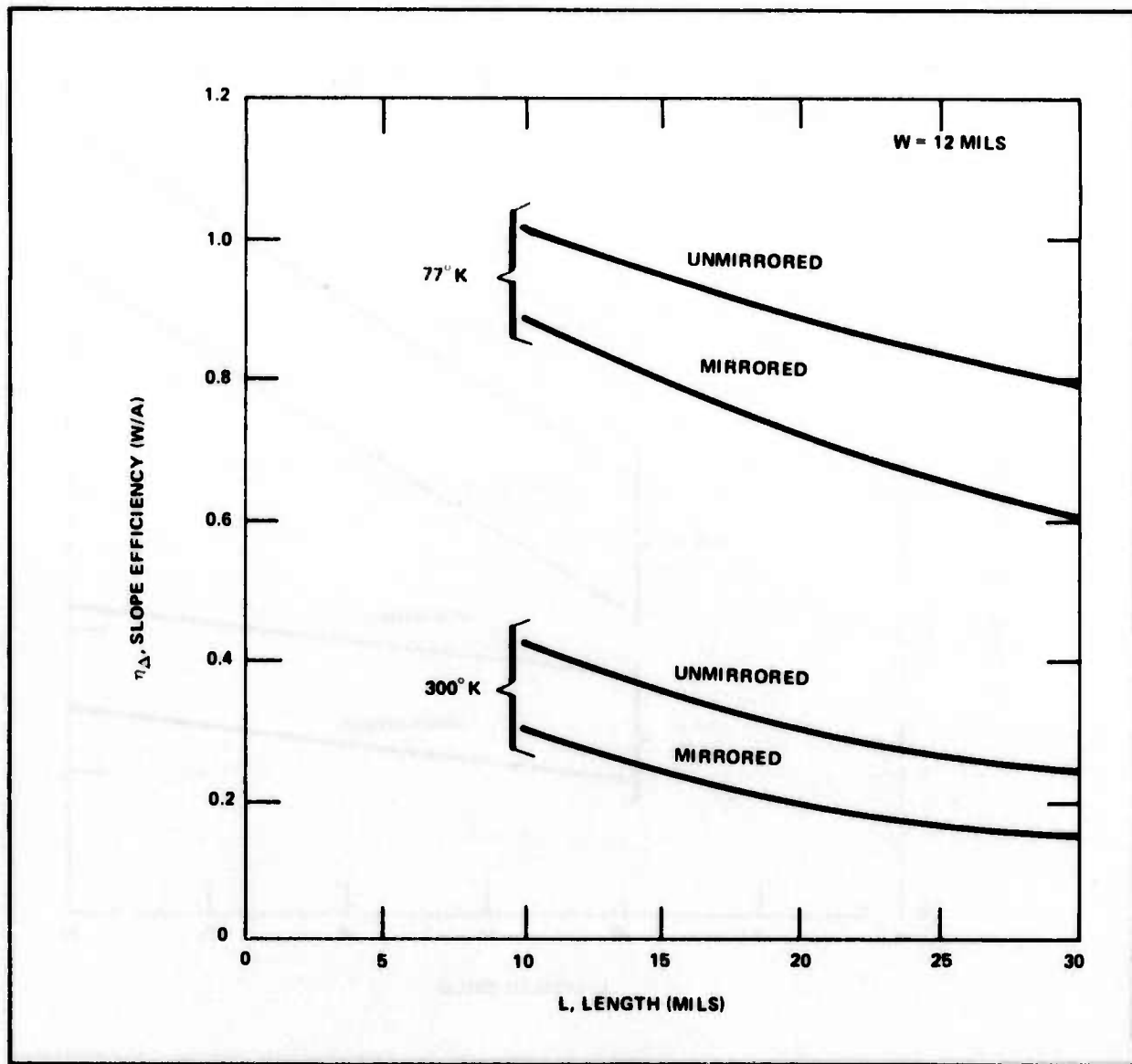


Figure 41. Calculated Slope Efficiency versus Length for Single Heterostructure Laser

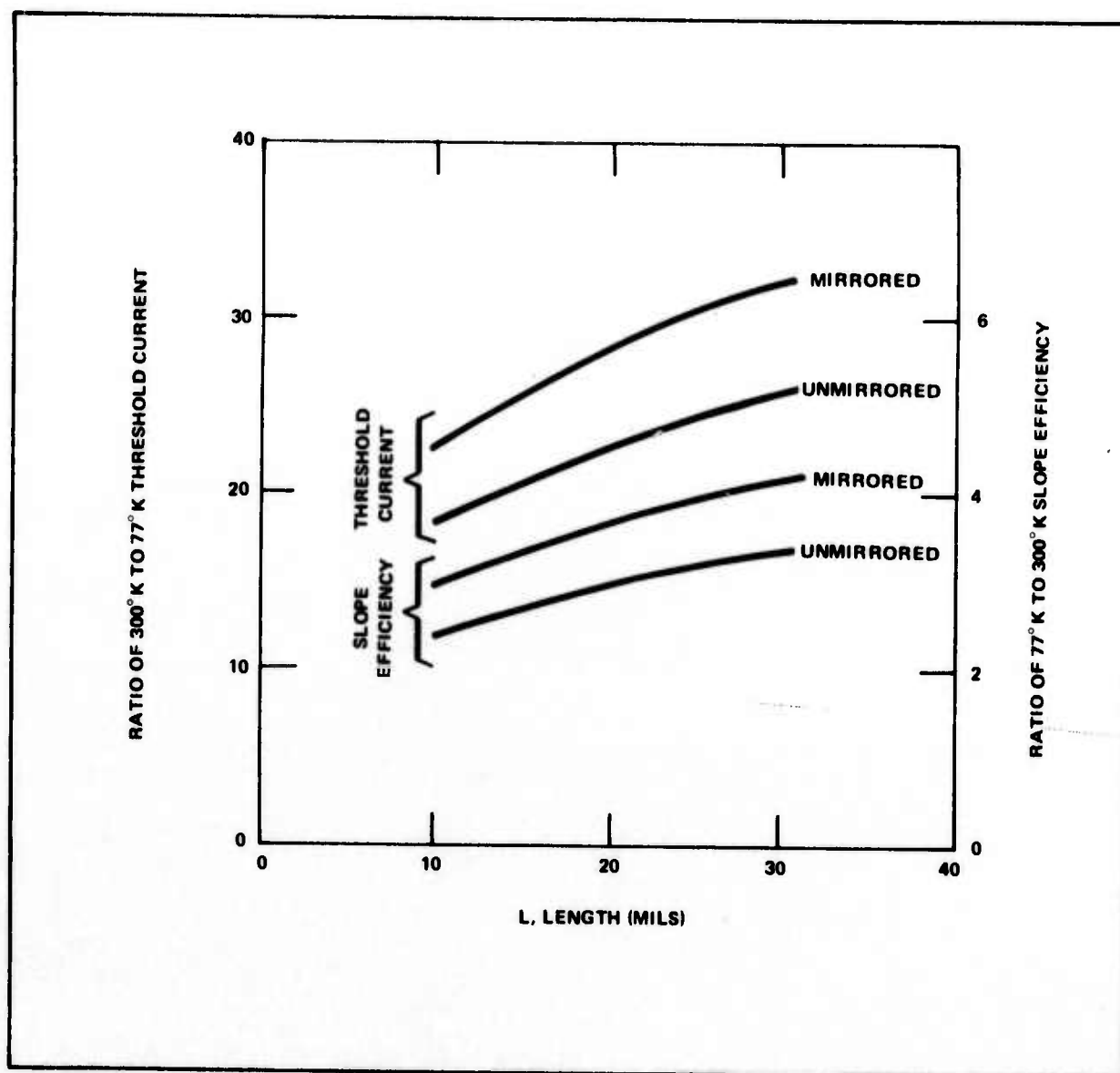


Figure 42. Comparison of Optical Parameters at 300°K and 77°K

SECTION VI

INTEGRAL GaAs LASER DIODE – BeO HEAT SINK DESIGN

1. INTRODUCTION

An objective of the program was to investigate new techniques for achieving improved CW laser diodes. The conventional approach of using a discrete GaAs laser diode mounted in a double-sided heat sink has been described in the previous sections. A small portion of the effort was also spent in investigating the feasibility of an entirely different approach. The alternate approach is an integral laser-heat sink design in which the laser diode is formed in GaAs epitaxial material grown directly on a single-crystal BeO substrate.

The liquid-phase epitaxial layers for the single heterostructure are grown on a GaAs-BeO composite substrate consisting of an N-type GaAs vapor-phase epitaxial layer grown on a single-crystal BeO crystal as shown in Figure 43. The GaAs-BeO composite substrates were obtained from Rockwell International. The potential advantage of this design is that the heat from the laser diode can spread over a larger area before any high thermal resistance interfaces are reached. The design should result in an overall decreased thermal resistance for the laser.

A sequence of processing steps to achieve the integral laser-heat sink devices is shown in Figure 44. The sides of the laser are defined by etching. A mesa structure is required to enable making electrical contact to the N-type material since BeO is electrically insulating. Both the N-type and P-type contacts are made on the top surface. The GaAs-BeO slice is then sawed into bars parallel to the mesa strips. Grooves would be cut perpendicular to the strips. The grooves would enable the mesa bars to be cleaved into discrete lasers.

Six GaAs-BeO composite substrates for this investigation were obtained from Rockwell International in two shipments of three each (plus one extra sample in last shipment to enable performance of additional experiments at TI). The metalorganic chemical vapor deposition process used for the growth of the GaAs vapor phase epitaxial layer is discussed in Section VI.2. The preparation and properties of the GaAs-BeO composite substrates are described in Section VI.3. The results of the liquid-phase epitaxial growth of the single heterostructure laser on the GaAs-BeO composite samples are given in Section VI.4.

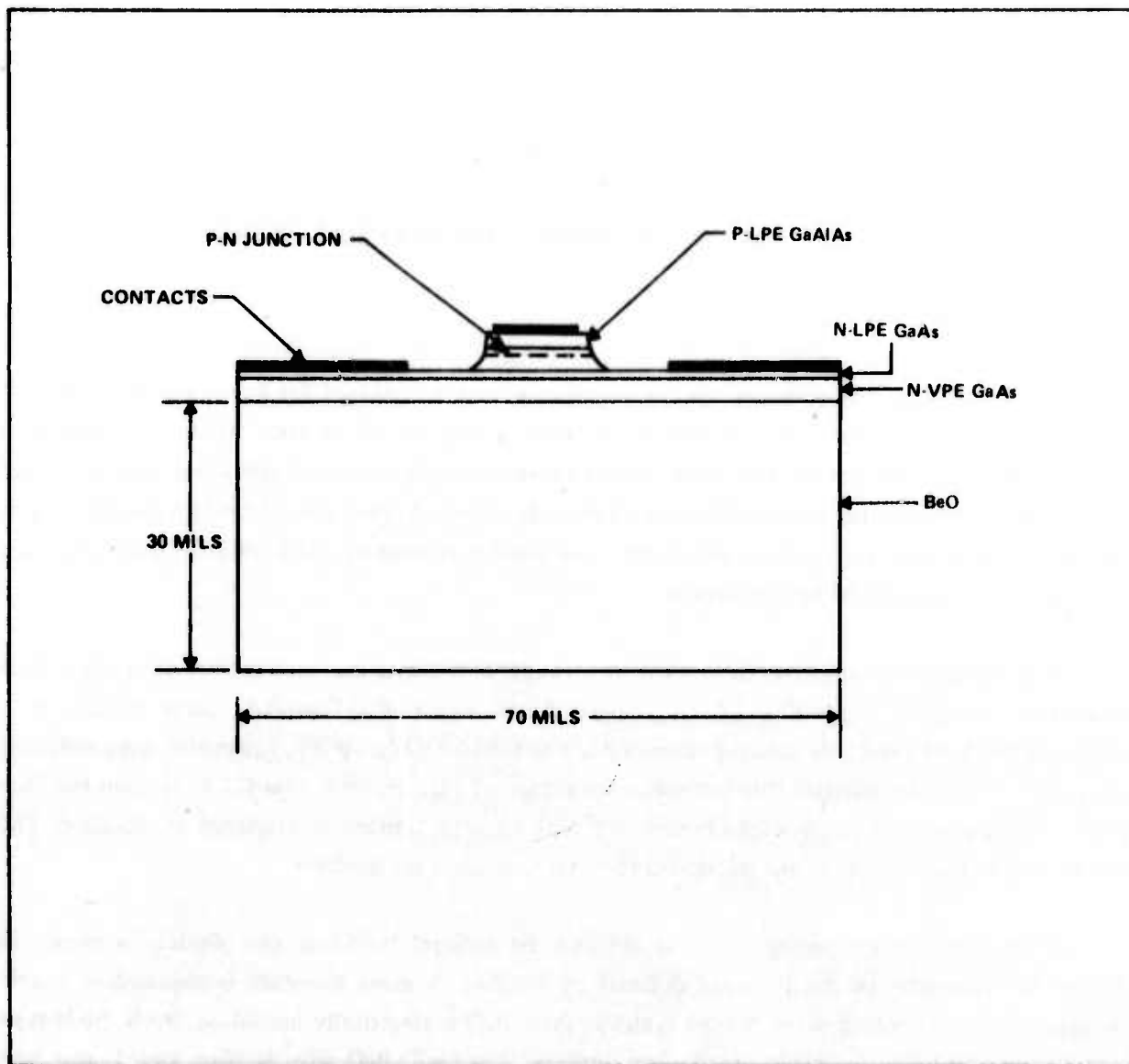


Figure 43. Integral GaAs Laser Diode-Heat Sink Design

The principal specifications for the GaAs-BeO composite substrates were as follows. The thickness would be 0.030 inch plus 0.005 or minus 0.0005 inch. The thickness variation across the slice would not exceed plus or minus 0.001 inch. The N-type epitaxial layer would have an orientation of (100) plus or minus one-half degree, a thickness of 15 to 20 micrometers, a doping concentration of $1 \text{ to } 4 \times 10^{18} \text{ cm}^{-3}$, and a mobility of greater than 1000 cm^2 per volt-second as measured by the van der Pauw technique. Each slice would have one edge sawed or a line scribed on the surface which is aligned with the (110) cleavage plane of the GaAs film.

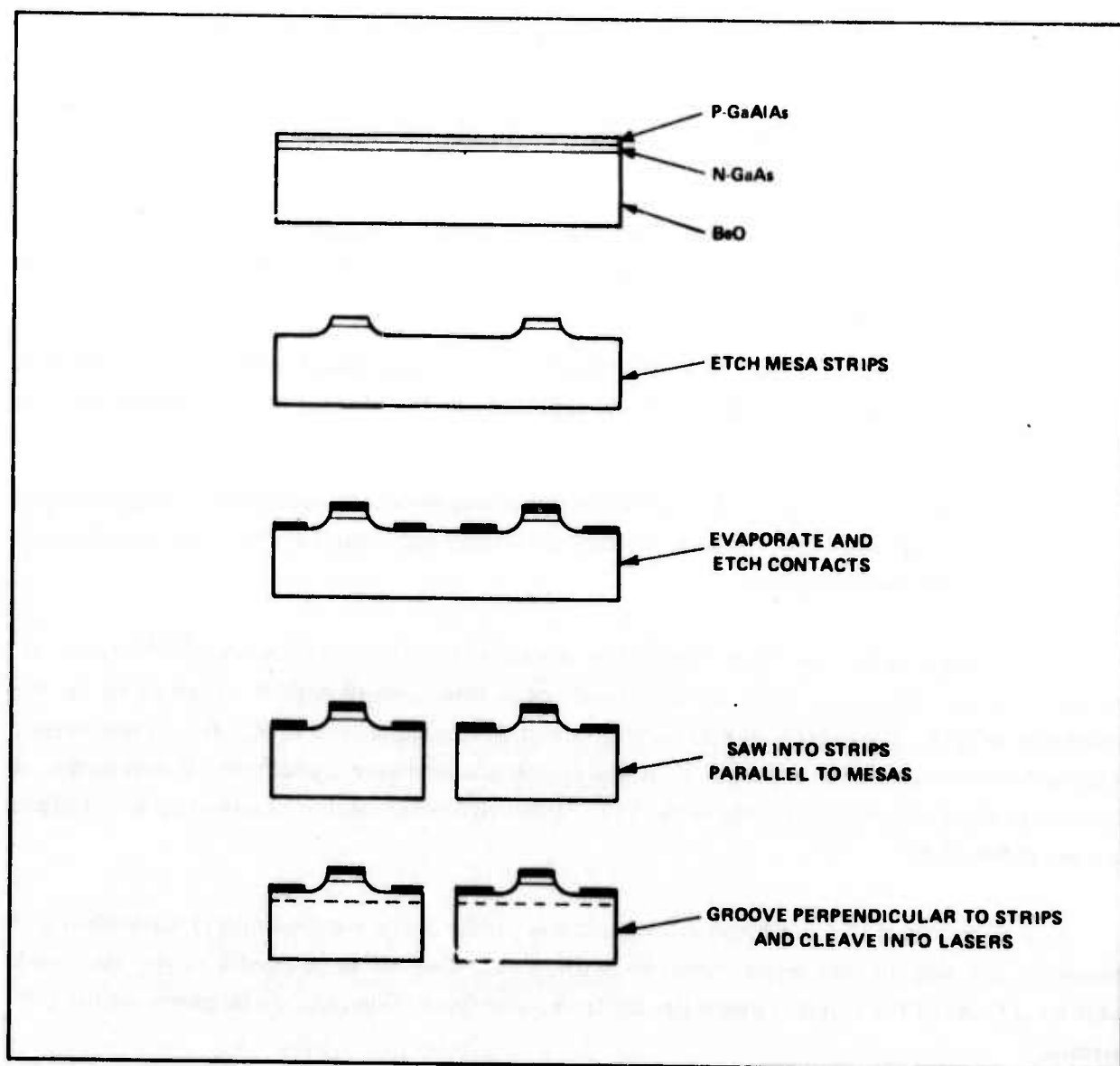


Figure 44. Processing Steps for Integral Laser-Heat Sink Design

2. GaAs METALORGANIC-CVD GROWTH PROCESS

The GaAs epitaxial layers were grown on single crystal BeO substrate by the metalorganic chemical vapor deposition process previously developed at Rockwell.³⁶ This process, which involves metalorganic-hydride reactions, can be used to form GaAs and many other III-V, II-VI, and IV-VI compound semiconductors³⁷ on a wide variety of substrates. Specific application of the technique to the GaAs/BeO system has been under study at Rockwell for the past four years, with support by government contract funds³⁸ as well as company funds.

The metalorganic-CVD method of GaAs film growth offers several distinct advantages over other types of CVD processes:

- 1) Only one hot-temperature region (specifically the substrate) is required, simplifying control problems
- 2) Film growth rates are controlled by simple flowmeter adjustments (at room temperature) which determine the concentrations of the reactants entering the deposition chamber
- 3) The reactants are free of halides, so a more abrupt and less contaminated film-substrate interface can be expected, in the absence of a competing etching reaction
- 4) The GaAs films can be doped directly during growth by introduction of appropriate compounds into the main reactant gas stream and control of their concentrations by flowmeter settings.

Good quality films have been obtained at Rockwell by this CVD technique.^{39,40} However, the GaAs characteristics required for laser diode operation coupled with the limitations on the properties of GaAs films grown on BeO substrates by this technique prior to the start of this project indicated that a composite approach to the problem was advisable. Specifically, it was proposed that the portion of the GaAs film to be used for the active junction region be grown by liquid-phase epitaxy (LPE) at TI.

In this approach the metalorganic-CVD process produces the required proper nucleation and complete covering of the oxide substrate with a thin film of single-crystal GaAs, on which additional GaAs of the requisite properties for laser diode fabrication can then be grown by the LPE method.

The apparatus used for preparation of the GaAs films was essentially like that previously used for GaAs film growth and described elsewhere.³⁶ The substrates were mounted on a horizontal pedestal (SiC-covered carbon) which was inductively heated and rotated during deposition in the vertical reactor chamber. Reported growth temperatures are uncorrected readings obtained by means of an infrared radiation thermometer viewing the surface of the pedestal and/or substrate through the quartz wall of the reactor tube.

Trimethylgallium (TMG), obtained from Texas Alkyls, Inc., and used as received from the vendor in a stainless-steel bubbler (except for initial purging with H_2 prior to use), was the source of Ga. Electronic-grade AsH_3 , obtained from 3H Corporation as 10 percent AsH_3 concentration in electronic-grade H_2 , was used as the source of As. The dopant gas used was H_2Se in electronic-grade

H_2 in a concentration of 975 ppm, obtained from Scientific Gas Products, to produce N-type Se-doped GaAs films. Pd-purified H_2 was used as the carrier gas, to carry all the reactants into the reactor chamber and the byproducts of the reactions out the exit (bottom) end of the chamber in this through-flow type of CVD process.

The BeO substrates used for this work were cut from crystals grown in Rockwell laboratories by the same flux-growth method used for the BeO heat-sink samples discussed in Section III.5. A diamond-impregnated ID saw or wire saw was used to slice the selected crystals into wafers which were then polished by methods previously developed at Rockwell. The substrates were cut and polished so that the surfaces to be used for GaAs deposition were nominally oriented in the $(11\bar{2}2)$ plane of the BeO. Further discussion of the precise substrate orientation is given later. Earlier work in the GaAs/BeO system at Rockwell showed that the $(11\bar{2}2)$ BeO plane produces (100)-oriented GaAs growth, the desired orientation for laser diode fabrication. The $(10\bar{1}0)$ BeO plane also produces (100) GaAs growth, but better results have consistently been obtained with the $(11\bar{2}2)$ orientation and this orientation also permits reuse of the substrate after removal of a deposited GaAs film, without repolishing being required.

The polished BeO substrates were typically prepared for use in a GaAs deposition experiment by the following standardized procedure:

- 1) Degreasing in hot trichloroethylene vapor
- 2) Washing (immersed) for 10 minutes in a hot hydrogen peroxide bath, four successive times (fresh bath each time)
- 3) Rinsing in liquid Freon TF until all evidence of hydrogen peroxide disappears
- 4) Blowing dry in twin jets of dry N_2 . The substrates were placed in the CVD reactor immediately after this cleaning procedure.

3. PREPARATION OF GaAs/BeO COMPOSITE SAMPLES

Because of the requirement for the crystallographic orientation of the epitaxial GaAs layers to be (100) to within ± 0.5 degree, some detailed x-ray analyses of the orientation relationship between the GaAs films and the $(11\bar{2}2)$ -oriented BeO substrate surfaces were carried out on a group of existing experimental samples prepared in earlier studies. The investigations showed that the nominal (100) GaAs/ $(11\bar{2}2)$ BeO epitaxial relationship in composites grown by the metalorganic CVD process appeared to involve a tilt of the (100) GaAs plane ~ 2.5 degrees away from exact parallelism with the $(11\bar{2}2)$ BeO plane.

Consequently, it was concluded that to obtain accurately-oriented (100) GaAs films it would be necessary to prepare (11 $\bar{2}$ 2)-oriented BeO substrates the surfaces of which would be ~ 2.5 degrees off the (11 $\bar{2}$ 2) plane (toward the (11 $\bar{2}$ 3) plane). This would require accurate initial slicing of the BeO wafers from the parent crystals and careful attention to maintaining the specified orientation throughout the lapping and polishing processes.

A group of BeO wafers, adequate in number to provide properly oriented substrates for the GaAs deposition experiments for the first group of three composite samples to be delivered, was sliced on the 1D diamond (275-325 grit) blade saw, using a blade 15 mils thick at the cutting edge. Two BeO crystals were used, and at least 10 useful wafers were obtained; the wafers were lapped and polished, using the standard procedures, for the subsequent deposition experiments.

In a series of deposition experiments directed toward achieving N-type GaAs films doped to concentrations from 1 to $4 \times 10^{18} \text{ cm}^{-3}$ it was found that the carrier concentrations actually achieved were in the range from 3.8 to $5.7 \times 10^{18} \text{ cm}^{-3}$. Films $10\text{-}20 \mu\text{m}$ thick exhibited mobilities of $1100\text{-}1200 \text{ cm}^2/\text{V-sec}$; these characteristics were also found in GaAs films grown under similar conditions on Al_2O_3 substrates. There was some indication that the flow rate of the H_2Se used as a source of Se dopant was sufficiently high to produce a near-saturation condition in the film; that is, only very slight variations in measured carrier concentration were observed for significant changes in H_2Se flow rates.

It was subsequently found that decreasing the H_2Se flow rate to approximately one-third of the range of values used in the above experiments resulted in GaAs films ($\sim 15 \mu\text{m}$ thick) with measured carrier concentrations of $1 \times 10^{18} \text{ cm}^{-3}$, mobilities $\sim 1800 \text{ cm}^2/\text{V-sec}$, and resistivities $\sim 3 \times 10^{-3} \text{ ohm-cm}$. Later GaAs growth experiments in this same reactor system indicated that a region of essentially linear dependence of carrier concentration on H_2Se flow rate (in a H_2 carrier gas) was encountered for flow rates below approximately 20 ccpm.

By mutual agreement between Rockwell and TI, three GaAs/BeO composite samples were selected from the total number available for the first shipment. Data sheets specifying various physical properties of the delivered samples were also supplied. The principal characteristics of these three composite samples are summarized in Table VI.

Despite the orientation observations described above, subsequent analysis of several additional GaAs/BeO samples prepared in the same experiments that produced the three delivered samples (Table VI) revealed further complication in the orientation relationship between film and substrate. In one case the (100) GaAs plane was found to be oriented $\sim 1/2$ degree away from the (11 $\bar{2}$ 2) BeO plane toward the (11 $\bar{2}$ 1) BeO plane, rather than $2\text{-}1/2$ degrees from the (11 $\bar{2}$ 2) toward the (11 $\bar{2}$ 3). This indicated an angle of ~ 3 degrees between the BeO substrate surface and the (100) GaAs film plane, along the zone defined by (11 $\bar{2}$ 1), (11 $\bar{2}$ 2), and (11 $\bar{2}$ 3). The situation is illustrated in Figure 45.

TABLE VI. PROPERTIES OF FIRST GROUP OF GaAs/BeO
COMPOSITE SAMPLES DELIVERED TO TI

| Sample Designation (GaAs/BeO) [†] | Total Sample Thickness (in.) | BeO Substrate Orientation | GaAs Film Properties | | | | | |
|---|---------------------------------|--|----------------------|---------|-----------------|--------------------------------------|--|-------------------------|
| | | | Thickness (μm) | Orient. | Type | Carrier Conc. (cm ⁻³) | Carrier Mobility** (cm ² /V-sec) | Resistivity (ohm-cm) |
| GaAs #2-20B-4/ BeO #AN238-1-6b | 0.0330 | ~2 1/2 deg off (11̄22) to-ward (1123) | 15.0 | (100)* | N (Se-doped) | 1 X 10 ¹⁸ | 1800 | 3.4 X 10 ⁻³ |
| GaAs #2-14A-4/ BeO #AN238-2-4 | 0.0330 | ~2 1/2 deg off (11̄22) to-ward (1123) | 15.8 | (100)* | N (Se-doped) | 4.1 X 10 ¹⁸ | 1180 | 1.3 X 10 ⁻³ |
| GaAs #2-14A-4/ BeO #AN238-2-7a | 0.0331 | ~2 1/2 deg off (11̄22) to-ward (1123) | 16.1 | (100)* | N (Se-doped) | 3.8 X 10 ¹⁸ | 1160 | 1.4 X 10 ⁻³ |

* See text for discussion

** Meas. by van der Pauw method.

[†] Designation of substrate orientation - " $\sim(11\bar{2}2)$ " - omitted from sample number for brevity.

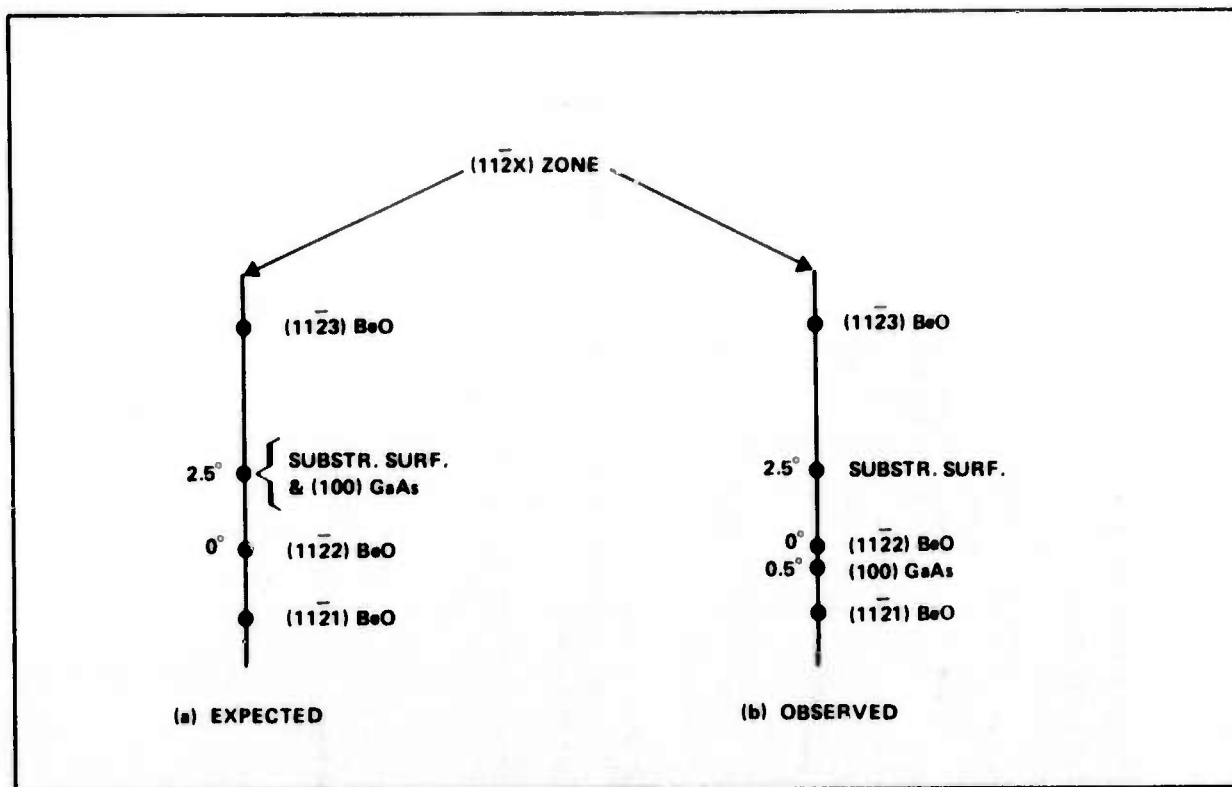


Figure 45. Expected and Observed Orientation Relationships Along $(11\bar{2}X)$ Zone

Three additional samples from the same group, each involving a BeO substrate having its front surface ~ 2.5 degrees off the $(11\bar{2}2)$ plane, produced similar results, shown in Figure 46. Thus, it appeared that the films prepared at the time of deposition of the three delivered samples exhibited an orientation in which the (100) plane was very nearly parallel to the $(11\bar{2}2)$ BeO plane, although a variability in this relationship of approximately $\pm 1/2$ degree was observed.

This variation in the GaAs/BeO orientation relationships appeared to be a real effect, but its cause is still not known. There is some precedent for such variable orientation relationships, within limited angular ranges, in other heteroepitaxial systems studied at Rockwell, however.

It is important to emphasize that the orientational uncertainties in question are along the $(11\bar{2}1)$ - $(11\bar{2}2)$ - $(11\bar{2}3)$ zone, and that the (100) GaAs plane lies on this zone to within the accuracy of measurement ($\leq 1/2$ degree). Furthermore, the (110) GaAs- $(10\bar{1}0)$ BeO cleavage planes are perpendicular to the above planes, so the above alignment uncertainty of the (100) GaAs plane along the zone does not affect alignment of the cleavage planes. Large transverse deviations of (100) GaAs from the above zone, if they occurred, would affect the perpendicularity of the cleavage planes to the nominal film-substrate interface. Since this was not observed it was concluded that the Fabry-Perot surfaces to be created by later cleavage during processing of the samples would have the required accuracy of orientation.

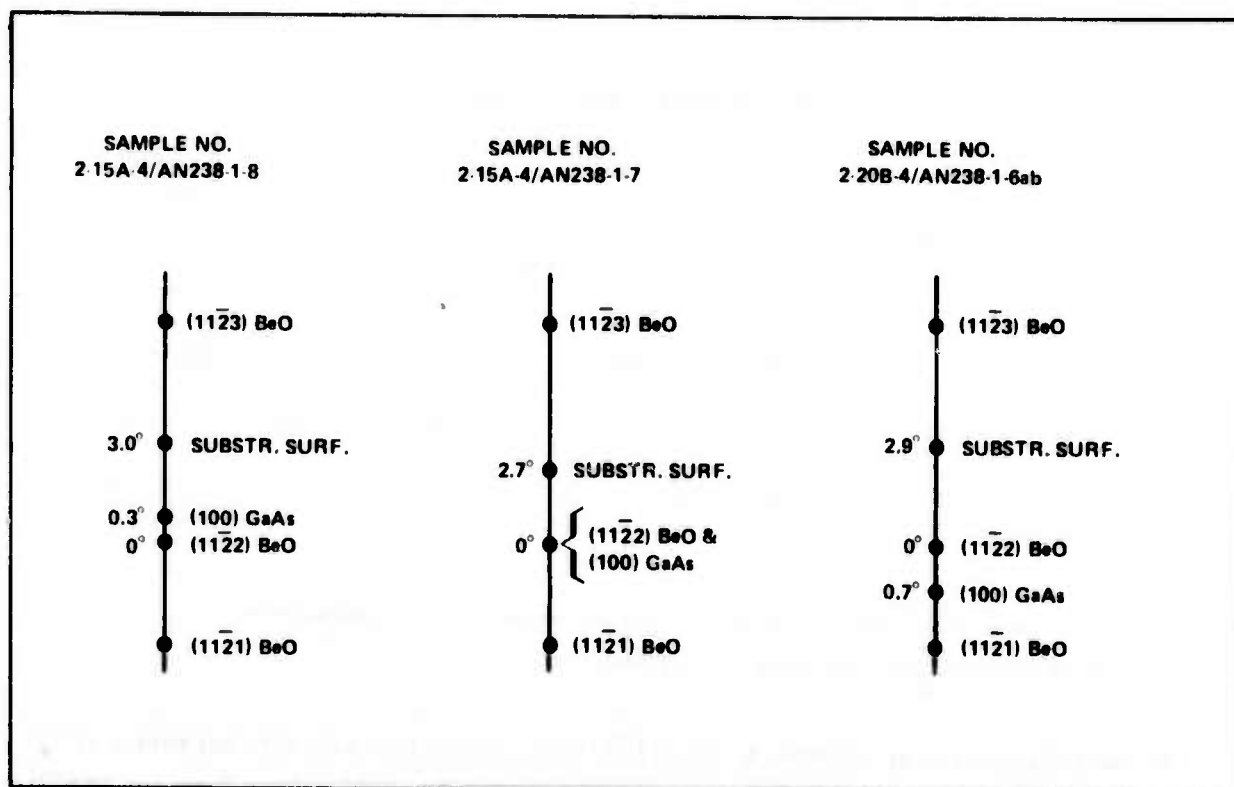


Figure 46. Additional Observed Orientation Relationships for GaAs/BeO

On the basis of the observed orientation relationships described above and the results obtained at TI in the first attempts to grow additional GaAs by LPE on the first three composite samples delivered by Rockwell, it was decided by mutual agreement that the three samples in the second group would involve BeO substrates accurately oriented (i.e., within $\pm 1/2$ degree) to the (1122) plane. The GaAs films grown on these substrates were to be polished prior to delivery, using the proprietary Rockwell process previously developed as a standard technique for preparing polished GaAs epitaxial films.

In the course of reaching this decision, however, it was also agreed that some BeO substrates with their surfaces $\sim 2-1/2$ degrees off the (1122) orientation would be included in the preliminary deposition experiments. Accordingly, in order to provide additional BeO substrate wafers for possible use in these experiments, TI returned two of the samples included in the first group of three delivered by Rockwell, Sample No. GaAs#2-14A-4/BeO#AN238-2~(1122)-4 and Sample No. GaAs#2-14A-4/BeO#AN238-2~(1122)-7a. Both samples had been used unsuccessful LPE GaAs growth experiments at TI and there was no further use for them at TI. The BeO substrates for those samples had growth surfaces oriented $\sim 2-1/2$ degrees off the (1122) plane toward the (1123) plane. The off-orientation substrates finally used in these experiments were selected from among the two returned samples and three other BeO wafers already available at Rockwell.

**TABLE VII. PROPERTIES OF GaAs FILMS GROWN BY METAL-ORGANIC
CVD ON BeO SUBSTRATES***

| Sample Designation (arbitrary) | Substrate Orientation [deg off (11 $\bar{2}$ 2)] | Deposition Temperature (°C) | Film Thickness (μ m) | Carrier Conc. (cm ⁻³) | Carrier Mobility (cm ² /V-sec) | Film Resistivity (ohm-cm) |
|--------------------------------|--|-----------------------------|---------------------------|-----------------------------------|---|---------------------------|
| A | <0.5 | 690 | 22.1 | 9.5 X 10 ¹⁷ | 1820 | 3.6 X 10 ⁻³ |
| B | ~3 ** | 690 | 22.1 | 7.8 X 10 ¹⁷ | 1530 | 5.2 X 10 ⁻³ |
| C | <0.5 | 690 | 22.1 | 1.1 X 10 ¹⁸ | 1830 | 3.2 X 10 ⁻³ |
| D | <0.5 | 690 | 22.1 | 1.0 X 10 ¹⁸ | 1950 | 3.2 X 10 ⁻³ |

* Films grown in deposition experiments prior to preparation of second set of samples delivered to TI.

** In a direction toward the (11 $\bar{2}$ 3) plane along the (11 $\bar{2}$ X) zone.

The substrates accurately oriented to the (11 $\bar{2}$ 2) BeO crystal plane were selected from a group of new wafers that were cut from BeO crystals recently removed from the growth furnaces. The 10 best-looking wafers, oriented to within $\pm 1/2$ degree of the (11 $\bar{2}$ 2) plane, were selected for polishing by the proprietary Rockwell process. Of the polished samples, several were then selected for use in preparing the epitaxial GaAs layers by CVD.

Results obtained on several composite GaAs/BeO samples prepared in preliminary experiments are given in Table VII. The data are approximate and were obtained on as-grown films, but it appeared that the required specifications had been achieved. The orientation of the GaAs on the accurately oriented substrates (samples A, C, D) was such that the (100) GaAs plane was within 1/2 to 1 degree of parallelism with the (11 $\bar{2}$ 2) BeO plane in the substrate.

Based on the above results several additional composite samples were prepared, and the three samples identified for delivery to TI were selected, together with one additional sample selected for inclusion in the shipment to provide TI personnel with additional opportunity for experimentation on the contract program.

Delivery of the samples was delayed by the accidental loss of several of the GaAs films during the final polishing process, just prior to shipment. A new set of samples was subsequently prepared, and from those were selected and processed the three that finally constituted the required shipment. The fourth sample (mentioned above) was one prepared with the first group that was being processed at the time of the polishing accident; it was not to be polished, however, and so was available for shipment in the as-grown condition.

The properties of the four samples constituting the second (and final) group shipped to TI are summarized in Table VIII. Data sheets of the properties of the samples and photographs of the samples were supplied at the time of delivery. A photograph of one of the as-received polished GaAs-BeO composite substrate (9-20A-4/AN262-1-4) is shown in Figure 47. The scribe line on the surface is for orientation alignment for processing.

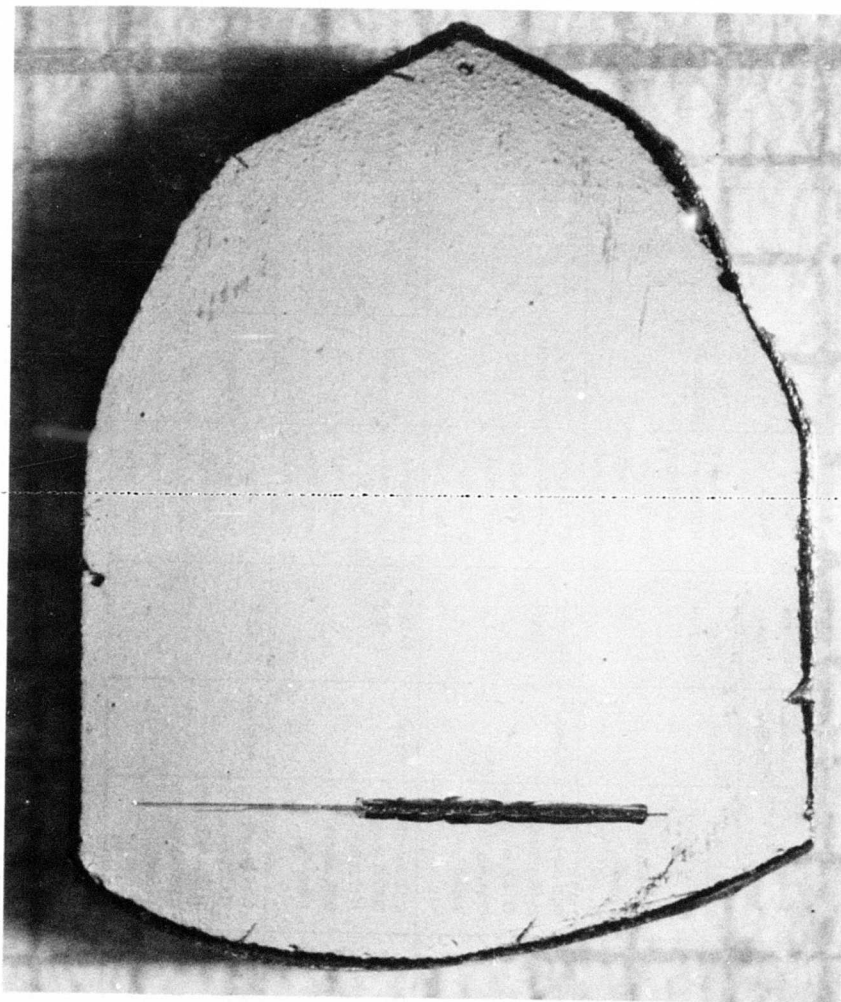


Figure 47. Polished GaAs-BeO Composite Substrate
(GaAs#9-20-A-4/BeO#AN262-1~(11 $\bar{2}2$)-4)

TABLE VIII. PROPERTIES OF SECOND GROUP OF GaAs/BeO
COMPOSITE SAMPLES DELIVERED TO TI

| Sample Design. ^a (GaAs/BeO) | Total Sample Thickness (in.) | BeO Substrate Surface Orient. | GaAs Film Properties | | | | | Carrier Mobility ^d (cm ² /V-sec) | Resistivity (ohm-cm) |
|--|------------------------------|--|----------------------|--------------------|--|-----------------|---|---|---|
| | | | Surface Condition | Thickness (μm) | Orientation of Surface | Type | Carrier Conc. (cm ⁻³) | | |
| #9-20A-4/ #AN262-1-4 (~680°C) ^f . | 0.0315c. | 0.03 deg off (11 $\bar{2}$ 2) toward (11 $\bar{2}$ 3) in zone ^b ; 0.26 deg tilt ⊥ zone ^b . | Polish | 18.3c. (~25) d. | 0.20 deg off (100); toward (11 $\bar{2}$ 3) BeO in zone ^b ; 0.34 deg tilt from (100) ⊥ zone ^b . | N (Se-doped) | 3.5 X 10 ¹⁸ d. | 1640 d. | 1.1 X 10 ⁻³ d. |
| #9-20A-4/ #AN262-2-2 (~680°C) ^f . | 0.0308c. | 0.32 deg off (11 $\bar{2}$ 2) toward (11 $\bar{2}$ 3) in zone ^b ; 0.94 deg tilt ⊥ zone ^b . | Polish | 18.8c. (~25) d. | 0.23 deg off (100); toward (11 $\bar{2}$ 3) BeO in zone ^b ; 0.94 deg tilt from (100) ⊥ zone ^b . | N (Se-doped) | 3.3 X 10 ¹⁸ d. | 1570 d. | 1.2 X 10 ⁻³ d. |
| #9-20A-4/ #AN262-3-5 (~680°C) ^f . | 0.0340c. | 0.16 deg off (11 $\bar{2}$ 2) toward (11 $\bar{2}$ 3) in zone ^b ; 0.36 deg tilt ⊥ zone ^b . | Polish | 19.8c. (~25) d. | 0.57 deg off (100); toward (11 $\bar{2}$ 3) BeO in zone ^b ; 0.57 deg tilt from (100) ⊥ zone ^b . | N (Se-doped) | 3.2 X 10 ¹⁸ c. (3.8 X 10 ¹⁸) d. | 1610 c. (1480) d. | 1.2 X 10 ⁻³ c. (1.1 X 10 ⁻³) d. |
| #9-11A-4/ #AN262-2-6 (Extra Sample) (~665°C) ^f . | 0.0336d. | 0.34 deg off (11 $\bar{2}$ 2) toward (11 $\bar{2}$ 3) in zone ^b ; 0.86 deg tilt ⊥ zone ^b . | As grown | 12.8d. | 0.46 deg off (100); toward (11 $\bar{2}$ 3) BeO in zone ^b ; 0.80 deg tilt from (100) ⊥ zone ^b . | N (Se-doped) | 1.7 X 10 ¹⁸ d. | 1530 d. | 2.4 X 10 ⁻³ d. |

a. Orientation designation in substrate identification — "(11 $\bar{2}$ 2)" — omitted from numbers for brevity.

b. Zone defined by (11 $\bar{2}$ 1), (11 $\bar{2}$ 2), (11 $\bar{2}$ 3),

c. After polishing.

d. As grown.

e. By van der Pauw method.

f. Growth temperature.

LIQUID-PHASE EPITAXIAL GROWTH

The growth of a multi-layer laser structure by the liquid-phase epitaxial process was attempted on all seven GaAs-BeO composite substrates obtained from Rockwell International. At the time of receipt of the first shipment of three GaAs-BeO composite substrates, a reproducible process for the growth of good single heterostructure lasers had not been developed. Therefore, on these samples, the growth of the large-optical-cavity laser structure was attempted using the process previously developed.¹⁸ Also, the accuracy of the orientation is not as critical for these layers as for the single heterostructure laser.

To ensure that uniform epitaxial layers could be grown on off-orientation substrates, the normal laser structure was grown on a regular GaAs substrate which was oriented 3 degrees from the (100). Good uniform epitaxial layers were grown with no evidence of a stepped type of growth. Since the GaAs-BeO composite substrates were much smaller than the GaAs substrates normally used, a washer-like spacer of 30-mil-thick high-purity graphite was used to fill the space around the substrate to prevent Ga transfer from one melt to the next. To determine if this modification affected the crystal growth, two small diameter 40-mil-thick GaAs substrates were used. Similar layers were obtained as for full-sized substrate.

An attempt at growth on sample AN238-2-7a resulted in a very severe etch-back of the GaAs vapor-phase epitaxial layer, in some spots etching back completely to the BeO substrate. One possible explanation for this was that the temperature at the solid-liquid interface might be increased due to the much higher thermal conductivity of the BeO compared to the normal GaAs substrate. This could cause the Ga melt near the interface to be slightly undersaturated and thus etch-back of the GaAs would occur instead of growth.

On the basis of this explanation, for the next sample (AN238-1-6b) the growth of the first layer was started at a 5-degree lower temperature (830°C) to ensure saturation. A much better growth occurred and continuous layers were achieved across the slice. The interface between the CVD GaAs layer and the LPE GaAs was relatively planar. However, the interface between the N-type GaAs layer and the P-type GaAlAs layer and the interface between the P-type GaAlAs layer and the P-type GaAs layer were very irregular. These interfaces had a step pattern consisting of many short straight segments at a tilt from the main plane of the layers. This suggested that one problem was the misorientation of the GaAs-BeO composite substrate.

Because of the improvement seen in the second run compared to the first run, oversaturation of the melts was increased further for the growth on the third sample (AN238-2-4). The result was a severe etch-back similar to that seen for the first attempt. The reason for this was not determined. Since this GaAs-BeO composite substrate was no longer useful, the GaAs layer was chemically removed and LPE growth directly on the BeO surface was attempted. Growth occurred on only a few small areas.

After the unsuccessful attempt at growth on the first composite substrate, it was decided to examine the quality of the CVD GaAs epitaxial layer in more detail. Laue x-ray patterns were determined on the other two samples from the first shipment. The much greater blurring of the GaAs points on the Laue for the GaAs-BeO sample as compared to a Laue on a normal GaAs substrate indicated that the CVD GaAs epitaxial layer was of poorer crystalline quality.

A reproducible growth process for single heterostructure lasers was established by the time the second shipment of GaAs-BeO composite substrates was received. Growth on the first sample (AN262-2-6) was made with two modifications: the growth temperature was reduced 5 degrees to ensure saturation (830°C) and a GaAs substrate was placed under the GaAs-BeO composite substrate to minimize the effect of the higher thermal conductivity of the BeO. Severe etch-back occurred again.

The CVD GaAs layers are grown at 690°C. Therefore, one conceivable explanation was that the CVD GaAs layers were being affected by the high temperatures used during the LPE growth cycle (855°C max). Therefore, for the next sample (AN262-2-2) an experiment was conducted in which the regular temperature-time cycle was followed except that the sample was removed from the furnace at the time at which growth of the first layer would normally occur. A vapor etching of the GaAs surface was apparent but was not sufficient to explain the severe etch-back observed for several LPE runs. The deterioration of the surface of the GaAs-BeO composite substrate was more noticeable than that of a normal GaAs substrate. This indicates poorer crystalline quality or greater concentration of defects.

The second sample (AN262-2-2) was reused for the growth of a single heterostructure laser. There were two principal differences for this run than for previous runs. First, this was the first GaAs-BeO composite substrate which had a polished surface when received from Rockwell. Second, this was the first attempt at growth on a composite substrate using the optimized growth procedure described in Section II.3. Growth started at 835°C. The boat was initially pushed into the furnace at 700°C. For all previous runs, the boat was pushed directly into the furnace at 855°C. The run resulted in the best LPE layers to that time. The interfaces were smooth but were wavy. The diffusion, however, was extremely irregular with the diffusion depth varying by a factor of two along the junction. The total thickness of the LPE layers was 18 mils.

The final two samples (AN262-1-4 and AN262-3-5) were also grown with the regular growth cycle for single heterostructure lasers except that the boat was initially put into the furnace at 600°C. Flat, planar interfaces were achieved between epitaxial layers. However, the zinc diffusion was very irregular. A photomicrograph of an angle-lapped cross section of the LPE layers is shown in Figure 48 for sample AN262-1-4. Each division is 0.6 μm . The total thickness of the LPE layers is 22 to 25 μm . The as-grown surface is much rougher than is usually obtained for LPE growth on

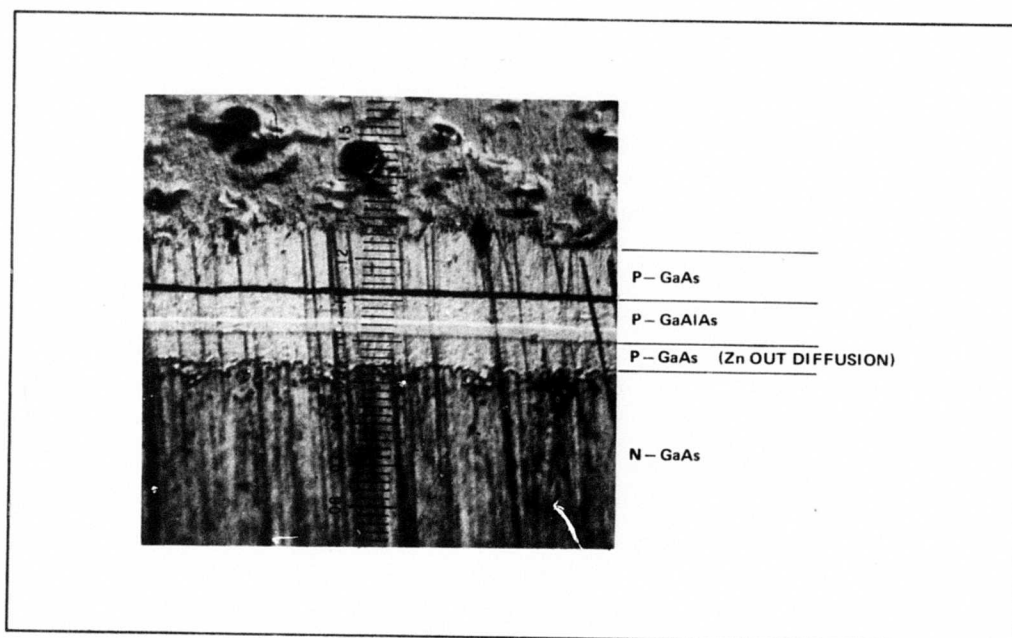


Figure 48. Cross Section of Liquid-Phase Epitaxial Layers on GaAs-BeO Composite Substrates

regular GaAs substrates. The apparent secondary band in the P-type GaAlAs layer results from the stain-etch solution used on the angle-lapped surface. The irregular zinc diffusion is another indication of the poor crystalline quality of the GaAs.

5. SUMMARY

Planar liquid-phase epitaxial layers are obtained on GaAs-BeO composite substrates if the CVD GaAs surface is accurately oriented, if the CVD GaAs surface is polished after growth, and if the substrates are initially placed into the furnace at 600°C to 700°C. The relatively poor crystalline quality of the initial CVD GaAs layer and of the resulting LPE layers causes the zinc diffusion to be very irregular, thus greatly decreasing the probability of achieving good laser performance. Reasonable laser performance might be achieved by using a separately grown P-type GaAs active region. Degradation of laser performance might be a problem for the integral laser-heat sink devices since recent studies on room temperature CW double heterostructure lasers emphasize the importance of high crystalline quality for long life lasers. None of the material grown during this program was processed into laser diodes because of the irregular diffusion and because of the effort required on the conventional approach.

SECTION VII

SUMMARY AND CONCLUSIONS

The objective of the program was to investigate techniques to improve the performance of CW laser diodes at 77°K. Work concentrated on the single heterostructure laser because its characteristics are much less temperature dependent than those of the conventional zinc-diffused homostructure. The lasers had an epitaxially grown N-type layer for good control of doping concentration. Thin P-type layers were used to reduce thermal resistance. The liquid-phase epitaxial growth procedure, the doping concentrations, and the active recombination region thickness were optimized to achieve single heterostructure lasers with low threshold currents, high slope efficiencies, and narrow emission beams.

An anomalous behavior was often observed at room temperature for single heterostructure lasers which were not grown with optimized layer characteristics. The lasing action was quenched above a critical current density. The behavior is attributed to the loss of optical confinement due to a reduction in the refractive index discontinuity at the P-N junction. This reduction is caused by a decrease of the refractive index in the active region as a result of the injected carriers.

The primary factor limiting the CW output power of injection lasers is removal of heat from the junction area. A major portion of the program concentrated on the design, assembly, and evaluation of the dewar and the double-sided heat sinks for efficient heat sinking of the laser diode. Intermediate submounts were used for improved control during assembly and to permit the use of high thermal conductivity materials to reduce thermal resistance.

The establishment of a suitable and reproducible assembly procedure for CW laser diodes to obtain good thermal characteristics without degrading the laser performance required more time than had originally been anticipated. However, solutions to the various difficulties were gradually developed and a suitable assembly process was established during the final period of the program.

The highest CW optical output power achieved was 690 milliwatts at 3A with a 13% power efficiency. This was obtained using a double-sided heat sink incorporating rectangular copper submounts. Subsequent evaluation of other lasers indicated that this laser with a thermal resistance of 4.6° K/W could have been safely driven to higher dc current levels and thus that the diode had the capability for even higher CW output powers.

The best thermal characteristics were achieved with a double-sided heat sink incorporating single-crystal BeO submounts. Due to the delay in the development of a good assembly procedure until late in the program, an adequate evaluation of the BeO approach was not completed. Because of the small number of available BeO submounts, copper submounts were used during most of the program while the gold and indium plating techniques and fabrication and assembly procedures were being developed.

A theoretical analysis of the single heterostructure laser mounted in a double-sided heat sink was performed to aid in optimizing the laser and heat sink design and to determine the expected values of thermal resistance and CW laser diode performance. The experimental values of the pulsed slope efficiency and threshold currents of the single heterostructure laser agreed well with the theoretical values. The lowest experimental values of thermal resistance also agreed well with the theoretical values. The theoretical analysis indicates that CW output powers of 2 to 3 watts can be achieved with copper submounts. However, output powers of greater than 4 watts require the use of higher thermal conductivity submount materials such as single-crystal BeO or diamond.

A portion of the program was devoted to investigating the feasibility of an alternate approach, an integral GaAs laser diode - BeO heat sink design in which the laser structure is grown directly on a single-crystal BeO substrate. GaAs-BeO composite substrates with a thin GaAs vapor-phase epitaxial layer were received from Rockwell International. The potential advantage of the design is decreased thermal resistance because heat from the laser can spread over a larger area before any high thermal resistance interfaces are reached.

Optimum conditions for the growth of uniform single heterostructure liquid-phase epitaxial layers on GaAs-BeO composite substrates were established. However, the material does not appear to be of sufficiently good quality to achieve high-performance lasers. Comparisons with regular GaAs substrates indicate that for the GaAs-BeO composite substrates the Laue X-ray pattern points are broader, vapor etching of the surface before growth in the furnace is more severe, the final surface after liquid-phase epitaxial growth is rougher, and a very nonuniform zinc outdiffusion occurs. Because of the lower quality and the greater growth complexity of the GaAs material and because of the increased complexity of device processing, the continued investigation of GaAs-BeO composite substrates for this application is not recommended at this time. However, as the quality of the GaAs improves, this approach may have definite advantages in other applications, such as integrated optics for high-speed optical communication using optical waveguides.

A large portion of the program was required to lay the basic groundwork for the effort, to design and obtain the required piece parts, and to develop the basic material, device, and assembly techniques. Improved results were continually achieved during the program as the processes were refined, as a better understanding was obtained of the limiting factors and as solutions were developed for the problems. The best CW laser diodes were achieved during the last period of the program. A continuation of the basic approaches developed in this program should result in CW laser diodes with optical output powers of greater than 2 W with the use of copper submounts and greater than 4 W with the use of diamond or single-crystal BeO submounts.

Now that a basic assembly process has been developed, immediate refinements which could be implemented to improve the CW laser performance are to increase the size of the laser and to use a 45-degree level on the submounts to reduce thermal resistance. Also, evaluation of the BeO submounts should be continued to achieve higher CW output powers. The size of the BeO submounts should be reduced for improved control during mounting of the laser. In the longer term, additional improvements in performance can be expected as other types of heterostructure lasers are developed which have characteristics even less temperature dependent than those of the single heterostructure laser. The use of high thermal conductivity submounts will continue to be required to minimize the overall thermal resistance and to minimize temperature gradients across the junction plane in order to achieve maximum CW performance.

REFERENCES

1. J. C. Marinace, *IBM Journal* **8**, 543 (1964).
2. G. C. Dousmanis, H. Nelson, and D. L. Staebler, *Appl. Phys. Letters* **5**, 174 (1964).
3. M. H. Pilkuhn and H. Rupprecht, *J. Appl. Phys.* **38**, 5 (1967).
4. R. O. Carlson, *J. Appl. Phys.* **38**, 661 (1967).
5. I. Hayashi, M. B. Panish, and P. Foy, *IEEE J. Quantum Electron.* **5**, 211 (1969).
6. M. B. Panish, I. Hayashi, and S. Sumski, *IEEE J. Quantum Electron.* **5**, 210 (1969).
7. H. Kressel and H. Nelson, *RCA Rev.* **30**, 106 (1969).
8. I. Hayashi and M. B. Panish, *J. Appl. Phys.* **41**, 150 (1970).
9. H. Kressel, H. Nelson, and F. Z. Hawrylo, *J. Appl. Phys.* **41**, 2019 (1970).
10. M. Ettenberg and H. Kressel, *J. Appl. Phys.* **43**, 1204 (1972).
11. M. B. Panish, I. Hayashi, and S. Sumski, *Appl. Phys. Lett.* **16**, 326 (1970).
12. I. Hayashi, M. B. Panish, P. W. Foy, and S. Sumski, *Appl. Phys. Lett.* **17**, 109 (1970).
13. J. E. Ripper, J. C. Dymont, L. A. D'Asaro, and T. L. Paoli, *Appl. Phys. Lett.* **18**, 155 (1971).
14. I. Hayashi, M. B. Panish, and F. K. Reinhart, *J. Appl. Phys.* **42**, 1929 (1971).
15. H. F. Lockwood, H. Kressel, H. S. Sommers, Jr., and F. Z. Hawrylo, *Appl. Phys. Letters*, **17**, 499 (1970).
16. H. Kressel, H. F. Lockwood, and F. Z. Hawrylo, *Appl. Phys. Letters* **18**, 43 (1971).

17. H. Kressel, H. F. Lockwood, and F. Z. Hawrylo, *J. Appl. Phys.* **43**, 561 (1972).
18. E. G. Dierschke, *High-Efficiency, Narrow-Beam-Angle, Large-Optical-Cavity Laser Diodes*, Final Report, Night Vision Laboratory Contract No. DAAK02-73-C-0110, Texas Instruments Incorporated, Dallas, Texas (July 1974).
19. M. Hegems and G. L. Pearson, *Proc. of the 1968 Symposium on GaAs* (The Institute of Physics and the Physical Society, London, 1969), p. 3.
20. Zh. I. Alferov, V. M. Andreyev, S. G. Konnikov, V. G. Nikitin, D. N. Tret' Yakov (*Proc. Internat. Conf. on the Phys. and Chem. of Semicond. Heterojunctions*, Hungary, October 11-17, 1970), p. 1, 93.
21. Final Engineering Report, "Production Engineering Measure for Low Radiant Power Infrared Sources," June 1974, Contract DAAB05-71-C-2602. Report to U.S. Army Electronics Command, Fort Monmouth, New Jersey, by RCA.
22. H. Kressel, "Semiconductor Lasers," *Lasers*, Vol. 3, edited by A. K. Levine and A. J. DeMaria (Marcel Dekker, Inc., New York, 1971), p. 72.
23. G. H. B. Thompson, P. R. Seway, G. D. Henshall, and J. E. A. Whiteway, *Electronics Letters* **10**, 456 (1974).
24. P. R. Selway, G. H. B. Thompson, G. D. Henshall, J. E. A. Whiteway, *Electronics Letters* **10**, 453 (1974).
25. H. T. Minden and R. Premo, *J. Appl. Phys.* **45**, 4520 (1974).
26. S. Grundorfer, M. J. Adams, and B. Thomas, "H-Pulsing: A Transient Effect in GaAs/GaAlAs Injection Lasers," IEEE International Semiconductor Laser Conference, Atlanta, Georgia, November 18-20, 1974.
27. H. A. Wheeler, *IEEE Trans. on Microwave Theory and Techniques* **MTT-13**, No. 2, 172 (1965).
28. S. B. Austerman, *J. Nucl. Mat.* **14**, 225 (1964).

29. Report AFML-TR-72-175, "Manufacturing Methods for Production of Single Crystal Beryllium Oxide," 27 September 1972. Report to Air Force Materials Laboratory, Air Force Systems Command, Wright-Patterson Air Force Base, Ohio, by Rockwell International, Electronics Research Division, Anaheim, California.
30. G. A. Slack and S. B. Austerman, *J. Appl. Phys.* **42**, 4713 (1971).
31. C. H. Gooch, *Gallium Arsenide Lasers* (John Wiley and Sons, New York, 1969).
32. M. A. Afromowitz, *J. Appl. Phys.* **44**, 1292 (1973).
33. L. Balents, R. Gold, F. Kamp, *Proc. Elect. Comp. Conf.*, May 1969, p. 15.
34. D. J. Dean, *Proc. Inter. Nepcon*, 1972, p. 206.
35. G. K. Baxter, *Proc. Inter. Nepcon*, 1972, February 1972, p. 29.
36. H. M. Manasevit and W. I. Simpson, *J. Electrochem. Soc.* **116**, 1725 (1969).
37. See, e.g., H. M. Manasevit, *J. Cryst. Growth* **13/14**, 306 (1972).
38. Much of the GaAs/BeO technology has been developed under contract to the Naval Air Systems Command under contract numbers N00019-70-C-0080 (1970-71), N00019-71-C-0334 (1971-72), and N00019-72-C-0459 (1972-73).
39. J. M. Owens, *Proc. IEEE* **58**, 930 (1970).
40. "GaAs on Beryllia Substrates for Application to Microwave Generation," Final Engineering Report, 1 May 1972 to 30 April 1973, for NASC Contract No. N00019-72-C-0459. Prepared by Rockwell International Corporation for Naval Air Systems Command, Code AIR-52022.